RETURN TO
J82
THE JOHN CRERAR
JUN 23 1948
LIBRARY

JOURNAL OF THE AERONAUTICAL SCIENCES

VOLUME 15 JUNE, 1948 NUMBER 6

CONTENTS

Interference Between Wing and Body at Supersonic Speeds—Theory and Numerical Application ..... CARLO FERRARI 317

Problem Types in the Theory of Perfectly Plastic Materials ..... W. PRAGER 337

Harmonic and Transient Motion of a Swept Wing in Supersonic Flow ..... JOHN W. MILES 343

Buckling of a Column with Elastic Supports ..... T. H. LIN AND K. S. CHING 347

Machmeters for High-Speed Flight Research ..... HERBERT SCHAEFER 351

An Improved Schlieren Apparatus ... FRANK W. BARRY AND GILBERT M. EDELMAN 364

A Note on Flight Flutter Testing ... ROBERT ROSENBAUM AND ROBERT H. SCANLAN 366

Stability of an Oscillating Airfoil in Supersonic Airflow ..... M. V. BARTON 371

Letter to the Editor 341

Published by the
INSTITUTE OF THE AERONAUTICAL SCIENCES, INC.

JOURNAL OF THE AERONAUTICAL SCIENCES

Editor: HUGH L. DRYDEN, *Director of Aeronautical Research, N.A.C.A.*

Associate Editor: ROBERT R. DEXTER *Associate Editor:* BERNEICE H. JARCK

The Institute of the Aeronautical Sciences publishes monthly the JOURNAL OF THE AERONAUTICAL SCIENCES and the AERONAUTICAL ENGINEERING REVIEW.

The JOURNAL OF THE AERONAUTICAL SCIENCES prints papers of scientific and technical interest to Institute members and subscribers. In general, it provides an opportunity for specialists to publish articles disclosing new knowledge and new applications in the field of the aeronautical sciences. The JOURNAL restricts itself to the aeronautical aspects of advances in science and engineering, and papers printed have either been submitted directly to the JOURNAL or have been previously presented at a meeting of the Institute.

The AERONAUTICAL ENGINEERING REVIEW keeps members and subscribers informed regarding the contents of new books and current periodicals in the field of aeronautics. It reviews new developments in the aircraft industry and reports on progress from house organs and catalogs published by aircraft and engine manufacturers and other companies engaged in aeronautical activities. It publishes papers on applied engineering and aircraft production. News of Institute activities is published in the REVIEW.

Statements and opinions expressed in the JOURNAL are to be understood as individual expressions of the authors and not those of the Institute.

SUBSCRIPTION RATES

Journal of the Aeronautical Sciences
Published Monthly

United States and Possessions		Foreign Countries Including Canada (American Currency Rates)	
1 Year	$12.00	1 Year	$13.00
Single Copies	1.50	Single Copies	1.50

Aeronautical Engineering Review
Published Monthly

United States and Possessions		Foreign Countries Including Canada (American Currency Rates)	
1 Year	$3.00	1 Year	$3.50
Single Copies	0.50	Single Copies	0.50

Notices of change of address should be sent to the Institute at least 30 days prior to actual change of address.

Manuscripts for publication, proofs, and all correspondence should be addressed to the Editorial Office of the JOURNAL.

Correspondence regarding subscriptions may be addressed to Publication Office, 20th and Northampton Sts., Easton, Pa., or to the Editorial Office of the JOURNAL OF THE AERONAUTICAL SCIENCES, 2 East 64th Street, New York 21, New York.

Copyright, 1948, by the Institute of the Aeronautical Sciences, Inc.

Entered as Second Class Matter at the Post Office, Easton, Pa., May 1, 1937. Acceptance for mailing at a special rate of Postage provided for in the Act of August 24, 1912. Authorized April 29, 1937.

IN

JOHN K

SMITH J
C. L. J
R. P. L
EARL D

S. PAUL

BENNET

E. E. A
REX B.
LAWREN
WILLIAM
W. A. M
VICTOR

WALTER
FRANK V
RALPH S
KENNETH
R. H. FL
R. PAUL

JOHN C. A
JOHN N. B
FRANK O.
E. U. CON

H. H. ARN
FRANK W.
SIR GEOFF
JAMES H. I
DONALD W
HUGH L. D

E. E. ALDR
HART O. B
W. A. M. B
E. L. CORD
DONALD W.
SHERMAN M

IRA H. ABB
JOHN D. AK
E. E. ALDRI
HARRY G. A
KARL ARNST
J. L. ATWOO
PAUL S. BA
RALPH S. BA
P. R. BASSE
WELLWOOD
REX B. BEI
G. M. BELLA
DON R. BER
HENRY A. B
WILLIAM BO
GEORGE W.
LYMAN J. BR
W. G. BROM
WILLIAM G.
CHARLES P.
KENNETH CA
CHARLES H.
ALLAN CHIL
FRANKLIN R.
CHARLES H.
KARL T. CO
EMERSON W.
JOHN W. CR
RALPH S. DA
LUIS DE FLO
SMITH J. DE
J. P. DEN HA
WALTER S. D
C. S. DRAPE
IVAN H. DRI
WILLIAM K.
C. L. EGTVE
FREDERIC FL

INSTITUTE of the AERONAUTICAL SCIENCES

President
JOHN K. NORTHROP

Vice-Presidents
SMITH J. DE FRANCE
C. L. JOHNSON
R. P. LANSING
EARL D. OSBORN

Director
S. PAUL JOHNSTON

Executive Vice-President
BENNETT H. HORCHLER

Past-Presidents
J. C. HUNSAKER
CHARLES L. LAWRANCE
DONALD W. DOUGLAS
GLENN L. MARTIN
CLARK B. MILLIKAN
T. P. WRIGHT
GEORGE W. LEWIS
JAMES H. DOOLITTLE
FRANK W. CALDWELL
HALL L. HIBBARD
HUGH L. DRYDEN
R. H. FLEET
CHARLES H. COLVIN
ARTHUR E. RAYMOND
P. R. BASSETT

Secretary
ROBERT R. DEXTER

Treasurer
SHERMAN M. FAIRCHILD

Controller
JOSEPH J. MAITAN

Counsel
ALLAN D. EMIL

COUNCIL

E. E. ALDRIN
REX B. BEISEL
LAWRENCE D. BELL
WILLIAM BOLLAY
W. A. M. BURDEN
VICTOR E. CARBONARA
FRANK O. CARROLL
CHARLES H. COLVIN
JAMES H. DOOLITTLE
C. C. FURNAS
LEROY R. GRUMMAN
J. A. HERLIHY
JEROME LEDERER
JOHN C. LESLIE
JACK MASON
C. KENNETH RAZAK
L. B. RICHARDSON
RUSSELL G. ROBINSON
GEORGE S. SCHAIRER
ERNEST G. STOUT
A. J. THIEBLOT

ADVISORY COMMITTEE

WALTER BEECH
FRANK W. CALDWELL
RALPH S. DAMON
KENNETH S. M. DAVIDSON
R. H. FLEET
R. PAUL HARRINGTON
R. M. HAZEN
HALL L. HIBBARD
J. C. HUNSAKER
TH. VON KÁRMÁN
THOMAS A. KNOWLES
I. M. LADDON
GROVER LOENING
GLENN L. MARTIN
CLARK B. MILLIKAN
THOMAS A. MORGAN
ARTHUR E. RAYMOND
F. W. REICHELDERFER
LAURANCE S. ROCKEFELLER
T. CLAUDE RYAN
ELMER A. SPERRY, JR.
EDWARD P. WARNER
BURDETTE S. WRIGHT
T. P. WRIGHT

HONORARY MEMBERS

JOHN C. ADAMS
JOHN N. BROWN
FRANK O. CARROLL
E. U. CONDON
L. C. CRAIGIE
HARRY F. GUGGENHEIM
HENRY G. HOUGHTON
GEORGE C. KENNEY
GEORGE B. PEGRAM
E. M. POWERS
J. LAURENCE PRITCHARD
F. W. REICHELDERFER
CARL SPAATZ

HONORARY FELLOWS

H. H. ARNOLD
FRANK W. CALDWELL
SIR GEOFFREY DE HAVILLAND
JAMES H. DOOLITTLE
DONALD W. DOUGLAS
HUGH L. DRYDEN
W. F. DURAND
SIR RICHARD FAIREY
SIR ROY FEDDEN
J. C. HUNSAKER
SIR MELVILL JONES
GEORGE W. LEWIS
GLENN L. MARTIN
GEORGE J. MEAD
SIR FREDERICK HANDLEY PAGE
D. R. PYE
IGOR I. SIKORSKY
SIR GEOFFREY TAYLOR
TH. VON KÁRMÁN
EDWARD P. WARNER
T. P. WRIGHT

BENEFACTORS

E. E. ALDRIN
HART O. BERG (Deceased)
W. A. M. BURDEN
E. L. CORD
DONALD W. DOUGLAS
SHERMAN M FAIRCHILD
SIR RICHARD FAIREY
R. H. FLEET
FLORENCE GUGGENHEIM (Deceased)
C. D. HANSCOM
JOHN P. V. HEINMULLER
ALEXANDER KLEMIN
PAUL KOLLSMAN
BELLA C. LANDAUER
WILLIAM LANDAUER
GROVER LOENING
EDMUND C. LYNCH (Deceased)
F. W. MAGIN
GLENN L. MARTIN
GEORGE J. MEAD
S. A. REED (Deceased)
LAURANCE S. ROCKEFELLER
EDWARD P. WARNER

AMERICAN FELLOWS

IRA H. ABBOTT
JOHN D. ACKERMAN
E. E. ALDRIN
HARRY G. ARMSTRONG
KARL ARNSTEIN
J. L. ATWOOD
PAUL S. BAKER
RALPH S. BARNABY
P. R. BASSETT
WELLWOOD E. BEALL
REX B. BEISEL
G. M. BELLANCA
DON R. BERLIN
HENRY A. BERLINER
WILLIAM BOLLAY
GEORGE W. BRADY
LYMAN J. BRIGGS
W. G. BROMBACHER
WILLIAM G. BROWN
CHARLES P. BURGESS
KENNETH CAMPBELL
CHARLES H. CHATFIELD
ALLAN CHILTON
FRANKLIN R. COLLBOHM
CHARLES H. COLVIN
KARL T. COMPTON
EMERSON W. CONLON
JOHN W. CROWLEY, JR.
RALPH S. DAMON
LUIS DE FLOREZ
SMITH J. DE FRANCE
J. P. DEN HARTOG
WALTER S. DIEHL
C. S. DRAPER
IVAN H. DRIGGS
WILLIAM K. EBEL
C. L. EGTVEDT
FREDERIC FLADER
CHARLES FROESCH
JACK FRYE
GARLAND FULTON
LESTER D. GARDNER
RICHARD C. GAZLEY
MICHAEL E. GLUHAREFF
MELVIN N. GOUGH
LEROY R. GRUMMAN
HAROLD R. HARRIS
R. M. HAZEN
ALBERT F. HEGENBERGER
EDWARD H. HEINEMANN
S. D. HERON
HALL L. HIBBARD
L. S. HOBBS
PAUL E. HOVGAARD
WILLIAM HOVGAARD
ROBERT INSLEY
EASTMAN N. JACOBS
C. L. JOHNSON
S. PAUL JOHNSTON
ALEXANDER KARTVELI
PAUL H. KEMMER
CARLETON KEMPER
J. H. KINDELBERGER
OTTO E. KIRCHNER
ARTHUR L. KLEIN
ALEXANDER KLEMIN
W. B. KLEMPERER
PAUL KOLLSMAN
OTTO C. KOPPEN
B. V. KORVIN-KROUKOVSKY
S. M. KRAUS
ARNOLD M. KUETHE
I. M. LADDON
E. S. LAND
CHARLES L. LAWRANCE
JEROME LEDERER
JOHN G. LEE
JOHN C. LESLIE
CHARLES A. LINDBERGH
WILLIAM LITTLEWOOD
GROVER LOENING
ALBERT E. LOMBARD
F. A. LOUDEN
W. RANDOLPH LOVELACE, II
EUGENE E. LUNDQUIST
R. D. MACCART
JOHN R. MARKHAM
ERLE MARTIN
WM. H. MCAVOY
C. J. MCCARTHY
J. S. MCDONNELL
CLARK B. MILLIKAN
ROBERT J. MINSHALL
JOSEPH S. NEWELL
ALFRED S. NILES
JOHN K. NORTHROP
ARTHUR NUTT
SHATSWELL OBER
ROBERT R. OSBORN
W. BAILEY OSWALD
GEORGE A. PAGE, JR.
F. W. PAWLOWSKI
F. W. PENNOYER, JR.
A. A. PRIESTER
ARTHUR E. RAYMOND
F. W. REICHELDERFER
ELLIOTT G. REID
H. J. E. REID
H. C. RICHARDSON
L. B. RICHARDSON
RUSSELL G. ROBINSON
LEONARD B. ROOT
C. E. ROSENDAHL
ADDISON M. ROTHROCK
W. R. SEARS
WILLIAM T. SCHWENDLER
FRANCIS R. SHANLEY
JAMES M. SHOEMAKER
MAC SHORT
IGOR ALEXIS SIKORSKY
ABE SILVERSTEIN
SELDEN B. SPANGLER
ELMER A. SPERRY, JR.
JOHN STACK
ROBERT M. STANLEY
WILLIAM B. STOUT
HARRY A. SUTTON
C. FAYETTE TAYLOR
EDWARD S. TAYLOR
PHILIP B. TAYLOR
TH. THEODORSEN
T. E. TILLINGHAST
S. TIMOSHENKO
L. B. TUCKERMAN
RALPH H. UPSON
J. PARKER VAN ZANDT
J. G. VINCENT
RICHARD VON MISES
FRANK L. WATTENDORF
P. V. H. WEEMS
FRED E. WEICK
R. D. WEYBRBACHER
JOHN B. WHEATLEY
ANDREW V. WILLGOOS
DONALD H. WOOD
ROBERT J. WOODS
JOHN E. YOUNGER
ALBERT F. ZAHM
STEPHEN J. ZAND

Corporate Members

of the

Institute of the Aeronautical Sciences

Academy of Aeronautics, Inc.
Casey Jones School of Aeronautics

Aero Insurance Underwriters

Aerojet Engineering Corporation

Aeroproducts Division, General Motors Corporation

Aeroquip Corporation

Agawam Aircraft Products, Inc.

Airborne Instruments Laboratory, Inc.

Airchox Company Division, Joyce Aviation, Inc.

Aircraft Radio Corporation

AiResearch Manufacturing Company, Division of The Garrett Corporation

Allis-Chalmers Manufacturing Company

Allison Division, General Motors Corporation

Aluminum Company of America

American Airlines System

American Bosch Corporation

American Overseas Airlines, Inc.
Iceland Airport Corporation (Subsidiary)

American Phenolic Corporation

Associated Aviation Underwriters

Atlas Supply Company

Baker Steel & Tube Company

Beech Aircraft Corporation

Bell Aircraft Corporation

Bendix Aviation Corporation
Bendix International Division
Bendix Products Division
Bendix Radio Corporation
Eclipse-Pioneer Division
Friez Instrument Division
Pacific Division
Scintilla Magneto Company

The BG Corporation

Boeing Airplane Company
Seattle Division
Wichita Division

Breeze Corporations, Inc.
Aircraft Standard Parts Company, Inc.
Aldrich Company
Anderson Stove Company, Inc.
Federal Laboratories, Inc.
Foundry Service, Inc.

Cal-Aero Technical Institute, A Division of Grand Central Airport Company

Cessna Aircraft Company

Chandler-Evans Division, Niles-Bement-Pond Company

Chase Aircraft Company, Inc.

Chase National Bank of the City of New York

The Cleveland Graphite Bronze Company

The Cleveland Pneumatic Tool Company
Automotive-Aircraft Division

Clifford Manufacturing Company, Division of Standard-Thomson Corporation

Consolidated Vultee Aircraft Corporation
Fort Worth Division
Stinson Aircraft Division

Continental Motors Corporation

Curtiss-Wright Corporation
Airplane Division
Propeller Division
Wright Aeronautical Corporation Division

Doak Aircraft Company, Inc.

Douglas Aircraft Company, Inc.
El Segundo Plant
Long Beach Plant
Santa Monica Plant

The Dow Chemical Company

Dzus Fastener Company, Inc.

Eastern Air Lines, Inc.

Eaton Manufacturing Company
Dynamatic Corporation (Subsidiary)
Eaton-Wilcox-Rich Ltd. (Subsidiary)

Thomas A. Edison, Incorporated, Instrument Division

Edo Corporation

Electrol Incorporated

Ethyl Corporation

Fairchild Camera & Instrument Corporation
Fairchild Aerial Surveys, Inc.

Fairchild Engine and Airplane Corporation
Al-Fin Division
Fairchild Aircraft Division
Fairchild Personal Planes Division
Fairchild Pilotless Plane Division
NEPA Division
Ranger Aircraft Engines Division
Stratos Corporation (Subsidiary)

Federal Telephone and Radio Corporation
Federal Electric Manufacturing Company, Ltd.
Federal Telecommunication Laboratories, Inc. (Partial Subsidiary)
General Aviation Equipment Company, Inc.
General Electric Company
Aircraft Gas Turbine Division
Aviation Divisions
General Tire and Rubber Company of California, Research and Development Division
The B. F. Goodrich Company
The Goodyear Tire & Rubber Company
Goodyear Aircraft Corporation
Grumman Aircraft Engineering Corporation
W. &. L. E. Gurley
The International Nickel Company, Inc.
Irving Air Chute Company, Inc.
Jack & Heintz Precision Industries, Inc.
Johns-Manville Sales Corporation
Walter Kidde & Company, Inc.
Kollsman Instrument Division, Square D Company
Lavelle Aircraft Corporation
Lear Incorporated
Link Aviation, Inc.
The Liquidometer Corporation
Lockheed Aircraft Corporation
Airquipment Company (Subsidiary)
Lockheed Air Terminal (Subsidiary)
Lockheed Aircraft Overseas Corporation (Subsidiary)
Lockheed Aircraft Service, Inc. (Subsidiary)
Longines-Wittnauer Watch Company, Inc.
The Glenn L. Martin Company
GLM Chemical Division
Rotawings Division
Warren McArthur Corporation
McDonnell Aircraft Corporation
Minneapolis-Honeywell Regulator Company
Brown Instrument Company (Subsidiary)
Moore Drop Forging Company
National City Bank of New York
National Credit Office, Inc.
North American Aviation, Inc.
North American Aviation, Inc., of Texas
Northrop Aircraft, Inc.
Northwest Airlines, Inc.
Owens-Corning Fiberglas Corporation
Pan American World Airways System
The Parker Appliance Company
Pesco Products Division, Borg-Warner Corporation
Phillips Petroleum Company
Pure Oil Company
Radioplane Company
Republic Aviation Corporation
A. V. Roe Canada Limited
John A. Roebling's Sons Company
Rohr Aircraft Corporation
Ryan Aeronautical Company
Shell Oil Company, Inc.
Simmonds Aerocessories, Inc.
Socony-Vacuum Oil Company, Inc.
Solar Aircraft Company
Sperry Gyroscope Company Division of The Sperry Corporation
Square D Company
Standard Oil Company of California
Standard Oil Company (Indiana)
Standard Oil Company of New Jersey
The Texas Company
Thompson Products, Inc.
Tinnerman Products, Inc.
Union Carbide and Carbon Corporation
Bakelite Corporation
Electro Metallurgical Company
Haynes Stellite Company
The Linde Air Products Company
National Carbon Company, Inc.
United Air Lines, Inc.
United Aircraft Corporation
Chance Vought Aircraft Division
Hamilton Standard Propellers Division
Pratt & Whitney Aircraft Division
Sikorsky Aircraft Division
United Aircraft Export Corporation
United Aircraft Service Corporation
United States Aviation Underwriters, Inc.
United States Rubber Company
Dominion Rubber Company, Ltd.
Vickers, Inc.
Warner Aircraft Corporation
The Weatherhead Company
Angola, Indiana Division
Columbia Products Division
Houma Division
The Weatherhead Company of Canada (Subsidiary)
Westinghouse Electric Corporation
Aviation Gas Turbine Division
Industrial Electronics Division
Marine & Aviation Sales Department
Small Motor Division, Aviation Sales
Weston Electrical Instrument Corporation
Wyman-Gordon Company
Young Radiator Company

EDITORIAL COMMITTEE

HUGH L. DRYDEN, *Chairman*

Aerodynamics

Francis Clauser
Howard Emmons
R. Paul Harrington
R. T. Jones
W. B. Klemperer
Otto C. Koppen
John G. Lee
H. P. Liepmann
C. C. Lin
H. F. Ludloff
John R. Markham
Clark B. Millikan
Shatswell Ober
W. Bailey Oswald
Allen E. Puckett
Elliott G. Reid
H. J. E. Reid
Russell Robinson
L. E. Root
G. B. Schubauer
W. R. Sears
John Stack
Th. von Kármán
Richard von Mises

Air Transport

A. W. Dallas
Charles Froesch
J. A. Herlihy
Otto E. Kirchner
John C. Leslie

Aircraft Design

W. E. Beall
Rex B. Beisel
W. K. Ebel
Hall L. Hibbard
C. L. Johnson
I. M. Laddon
C. J. McCarthy
Fred E. Weick
Robert J. Woods

Physiologic Problems

H. G. Armstrong
Louis H. Bauer
Eugene Du Bois
W. Randolph Lovelace, II
Ross A. McFarland
A. D. Tuttle

Aircraft Propulsion

George W. Brady
Frank W. Caldwell
L. S. Hobbs
E. E. Johnson
Joseph Keenan
R. P. Kroon
Arthur Nutt
Hans Reissner
Abe Silverstein
C. Fayette Taylor
E. S. Taylor
P. Taylor

Structures and Materials

W. B. Bleakney
E. W. Conlon
J. P. Den Hartog
L. H. Donnell
E. C. Hartmann
N. J. Hoff
E. E. Lundquist
C. F. Nagel, Jr.
J. S. Newell
Alfred S. Niles
W. Ramberg
E. Reissner
F. R. Shanley
H. W. Sibert
C. R. Strang
S. Timoshenko
H. S. Tsien
Chi-Teh Wang

Meteorology

C. F. Brooks
D. M. Little
E. J. Minser
F. W. Reichelderfer
H. C. Willett

Fuels and Oils

A. L. Beall
J. H. Doolittle
Graham Edgar
R. T. Goodwin
S. D. Heron
A. M. Rothrock

Instruments

Allan G. Binnie
W. G. Brombacher
J. Callahan
Charles H. Colvin
C. S. Draper
O. E. Esval
David W. Moore
W. A. Reichel
C. F. Savage
O. Hugo Schuck
R. Sylvander

Rotating Wing Aircraft

Robert Coleman
K. H. Hohenemser
G. Horvay
Alexander Klemin
Ralph McClarren
R. H. Miller
R. H. Prewitt
Igor I. Sikorsky
Robert A. Wolf

Vibration and Flutter

Lee Arnold
M. A. Biot
William Bollay
Chieh-Chien Chang
J. P. Den Hartog
Manfred Rauscher

Flight Testing

W. K. Ebel
R. R. Gilruth
Melvin N. Gough
Robert Stanley
E. A. Stout

I.A.S. REPRESENTATIVES TO OTHER ORGANIZATIONS

Aircraft Industries Association of America, Inc.—CHARLES MARCUS

American Association for the Advancement of Science—J. C. HUNSAKER

American Society of Mechanical Engineers—CHARLES H. COLVIN

American Standards Association—P. R. BASSETT

Engineering Society of Detroit—DONALD C. HUNT, GEORGE TWENEY

Greater New York Safety Council—WILLIAM LITTLEWOOD

Daniel Guggenheim Medal Board of Award—CHARLES H. COLVIN, GROVER LOENING, S. PAUL JOHNSTON

Institute of Radio Engineers—L. M. HULL

Manufacturers Aircraft Association—ARTHUR E. RAYMOND

National Aeronautic Association—WILLIAM R. ENYART

National Fire Protection Association—E. E. ALDRIN

National Research Council Engineering Division—HUGH L. DRYDEN

National Safety Council—JEROME LEDERER

New York Museum of Science and Industry—LESTER D. GARDNER

Society of Automotive Engineers—STEPHEN J. ZAND

JOURNAL OF THE AERONAUTICAL SCIENCES

VOLUME 15 JUNE, 1948 NUMBER 6

Interference Between Wing and Body at Supersonic Speeds—Theory and Numerical Application*

CARLO FERRARI†

Cornell Aeronautical Laboratory

ABSTRACT

The supersonic flow past a body of revolution with pointed nose and carrying a wing is treated. The flow at infinity is uniform at a small angle of attack with respect to both the axis of the body and the chord of the wing and parallel to the plane of symmetry of the body-wing combination. The wing profile is assumed to be that of a flat plate. All perturbations on the uniform stream are assumed to be so small that it is legitimate to linearize the equation of motion.

The following are determined:

(1) Interference of the wing on the streamlined body, assuming that the induced field generated by the wing is that which would exist around the wing if it were placed in the uniform stream alone.

(2) Interference of the body on the wing, neglecting the distortion of the field around the body due to the presence of the wing.

A detailed numerical example serves to show that the interference effect of the wing upon the body is about half as great as the effect of the body upon the wing when the lift increments are compared, but the moment increment on the body is nearly two and a half times as large as the increment experienced by the wing. An optimum angle of wing setting for least drag is also determined.

INTRODUCTION

THE DEVELOPMENT OF A THEORY of wing-body interference is importunate because the effects of such interaction upon the aerodynamics of a supersonic configuration are apt to overshadow completely the behavior that would be predicted on the basis of individual treatment of the body and lifting surfaces as though they were isolated in the impinging stream. Empirical data indicate that large discrepancies exist between experiment and the simplified theory which accounts solely for the aerodynamics of the isolated components acting alone. Not only do the interference phenomena markedly alter the lift, drag, and moment of the combination of body and lifting surface, but, of course, the downwash excited by the same changes of the flow in the region of the wing-body juncture also profoundly affects the behavior of the stabilizing and control surfaces in general.

The subsequent discussion is a step in the delineation of the mechanisms at play in the generation of interference effects. It is based on the assumptions of a perfect fluid and of the existence of a velocity potential (nonrotational field). In addition, the method of small perturbations (and, consequently, small angles of attack) imposes further restrictions. The latter confining hypothesis may be removed by use of the method of characteristics to solve the same problem as treated here. This approach has also been investigated by the author, and the results are expected to be made available through the JOURNAL OF THE AERONAUTICAL SCIENCES at a later date. There are many other phases of this problem to be solved in addition to the analysis presented now, but the principal basic effects are clearly delimited for the simplified configuration studied. Thus these interactions are eminently worth consideration in order to arrive at a more lucid interpretation of the aerodynamics of supersonic aircraft.

SYMBOLS

Only those of most importance are included here.

$\Phi^{(1)}$ = potential function for the perturbed flow around the isolated body arising from the impingement of the longitudinal stream upon the body alone

$\Phi^{(2)}$ = potential function for the perturbed flow around the isolated body arising from the impingement

Received January 30, 1948.

* Italian manuscript submitted to Cornell Aeronautical Laboratory, March 4, 1947. The numerical application was accomplished under Navy BuOrd sponsorship.

† Member of C.A.L. consulting staff. Professor, Laboratorio di Aeronautica, Politecnico di Torino.

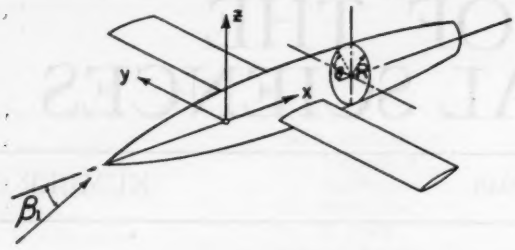

FIG. 1. Designation of coordinate axes.

of the transverse component of the stream upon the body alone

$\Phi^{(3)}$ = potential function for the perturbation field generated around the body from the influence of the wing

Φ = potential function for the combined effect of the above three factors in producing a perturbation field about the body in the presence of the wing; the velocity field described by this potential must be added to the undisturbed velocity, $\vec{V}_0$, as well as to the velocities generated by the isolated wing, in order to obtain the final flow about the wing-body combination

Φ' = potential function of the perturbed field around the wing from the interference effect of the body

(x, y, z) = coordinates relative to a system of orthogonal Cartesian axes oriented as shown in Fig. 1; the x-axis is aligned along the axis of the body and is directed in the same sense as the velocity of the undisturbed stream; the z-axis is normal to the x-axis and lies in the plane of symmetry and is directed in the sense of positive lift; the y-axis is normal to the plane of symmetry (along the wing span) and directed in conformity with a right-handed system; the origin is situated in accordance with the construction noted in Fig. 2 for the determination of the perturbations about the body, but it is shifted to the wing leading edge in Section B

(x, r, θ) = cylindrical coordinates; the initial side of the angle is in the direction of the positive y-axis; the terminal side sweeps out a positive angle when it is rotated clockwise (looking in the direction of the positive x-axis)

b = semispan of the wing

l = wing chord

R = radius of any right cross section of the streamlined body

(ξ, η, ζ) = nondimensional coordinates defined as

$$\xi = x/b, \quad \eta = y/b, \quad \zeta = z/b$$

$\vec{V}_0$ = velocity of the undisturbed stream

β_1 = angle between $\vec{V}_0$ and the x-axis

V_0 = V_∞ = magnitude of the velocity in the undisturbed stream

β_2 = angle between $\vec{V}_0$ and the wing chord

C = C_∞ = velocity of sound in the undisturbed stream

M = $M_\infty = V_0/C$ = Mach Number of the undisturbed stream

α = $\sqrt{M^2 - 1}$ = cotangent of the Mach angle

ρ = ρ_∞ = corresponding value of the density in the undisturbed stream

p = p_∞ = corresponding value of the pressure in the undisturbed stream

V_l = limiting velocity (for nondimensionalizing purposes)

c_m = C_∞/V_l, $v_\infty = V_\infty/V_l$

λ = distance between the tip of the nose of the body and the parallel (circumference of a section normal to the body axis) at which the leading edge of the wing joins the body (see Fig. 7)

ξ^* = x/λ, $\eta^* = y/\lambda$, $\zeta^* = z/\lambda$

(A) INTERFERENCE EFFECT OF THE WING UPON THE BODY

(A-1) *General Equations*

With the hypothesis of small perturbations the linearized differential equation defining the potential Φ of the perturbed field around the streamlined body is, in cylindrical coordinates (x, r, θ),

$$\frac{\partial^2\Phi}{\partial r^2} + \frac{1}{r}\frac{\partial\Phi}{\partial r} + \frac{1}{r^2}\frac{\partial^2\Phi}{\partial\theta^2} = \alpha^2\frac{\partial^2\Phi}{\partial x^2} \tag{1}$$

One must determine a solution of Eq. (1), satisfying the condition that the derivative of Φ in the direction of the exterior normal to the meridian line of the body be equal and opposite to the component along this normal of the velocity vector for the stream flowing around the body-wing configuration, without interference effects. This component is the sum of: (a) the similarly situated component of the undisturbed (i.e., free stream) velocity about the streamlined body, which may be set equal to $V_0(-\dot{R} + \beta_1 \sin\theta)$ since the slenderness of the body is such as to make $\dot{R}$ of the same order of magnitude as β_1, and where $\dot{R} = dR/dx$; and (b) the similarly situated component of the perturbation velocity generated by the wing, acting alone. This component may be expressed in the form

$$V_{nb} = V_0\sum_m F_m(x/R)\sin m\theta \tag{2}$$

The determination of the functions $F_m(x/R)$ will be indicated in Section A-3.

If, therefore, one assumes $\Phi = \Phi^{(1)} + \Phi^{(2)} + \Phi^{(3)}$; in which $\Phi^{(1)}$ is the potential of the perturbation field corresponding to the longitudinal component of the stream, $V_0\cos\beta_1 \cong V_0$; $\Phi^{(2)}$ is the potential of the perturbation field corresponding to the transverse component of the stream, $V_0\sin\beta_1 \cong V_0\beta_1$; and $\Phi^{(3)}$ represents the potential of the perturbation field due to the interference effect of the wing; then $\Phi^{(1)}$ and $\Phi^{(2)}$ are determined, as is well known, following the methods expounded by Kármán and Moore,[1] Ferrari,[2] and Tsien.[3]

(A-2) *Determination of the Potential* $\Phi^{(3)}$

For the determination of $\Phi^{(3)}$ let

$$\Phi^{(3)} = V_0\sum_m \Phi_m{}^{(3)}(x, r)r^m \sin m\theta \tag{3}$$

Substituting Eq. (3) in Eq. (1), it is found that each of the functions $\Phi_m{}^{(3)}$ must satisfy the equation

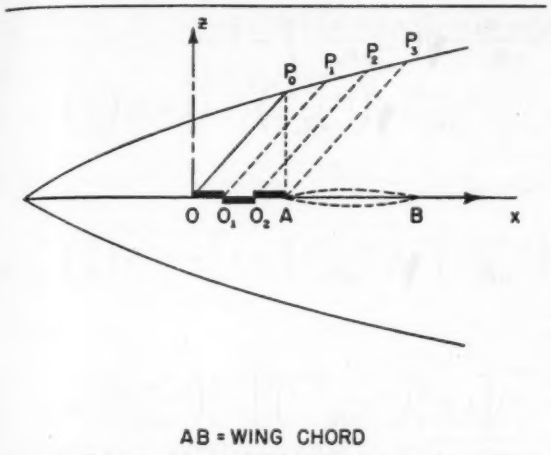

AB = WING CHORD

FIG. 2. Scheme of interval division for the stepwise evaluations.

$$\frac{\partial^2 \Phi_m^{(3)}}{\partial r^2} + \left(\frac{2m+1}{r}\right)\left(\frac{\partial \Phi_m^{(3)}}{\partial r}\right) = \alpha^2 \frac{\partial^2 \Phi_m^{(3)}}{\partial x^2} \qquad (4)$$

Now the solution of Eq. (4) is[4]

$$\Phi_m^{(3)} = \left(\frac{1}{r}\frac{\partial}{\partial r}\right)^m \Phi_0^{(3)} \qquad (5)$$

where

$$\Phi_0^{(3)} = \int_{\text{arcosh } x/\alpha r}^{0} f(x - \alpha r \cosh u)\, du \qquad (6)$$

and the origin of the coordinates is at the point on the x-axis at which all harmonic components of the perturbation begin to arise (Fig. 2). Thus,

$$\left.\begin{aligned} r\Phi_1^{(3)} &= \\ &-\alpha \int_{\text{arcosh } x/\alpha r}^{0} f_1(x - \alpha r \cosh u) \cosh u\, du \\ r^2\Phi_2^{(3)} &= \\ &\alpha^2 \int_{\text{arcosh } x/\alpha r}^{0} f_2(x - \alpha r \cosh u) \cosh^2 u\, du \end{aligned}\right\} \qquad (7)$$

etc.

The arbitrary functions f_1, f_2, etc., must be calculated in such a way as to satisfy the boundary conditions, and therefore

$$\left.\begin{aligned} \left[\frac{\partial}{\partial r}(r\Phi_1^{(3)})\right]_{r=R} &= \alpha^2 \int_{\text{arcosh } x/\alpha R}^{0} \dot{f}_1(x - \alpha R \cosh u) \cosh^2 u\, du = -F_1\left(\frac{x}{R}\right) \\ \left[\frac{\partial}{\partial r}(r^2\Phi_2^{(3)})\right]_{r=R} &= -\alpha^3 \int_{\text{arcosh } x/\alpha R}^{0} \dot{f}_2(x - \alpha R \cosh u) \cosh^3 u\, du = -F_2\left(\frac{x}{R}\right) \\ &\text{etc.} \end{aligned}\right\} \qquad (8)$$

in which $\dot{f}$ is the derivative of f with respect to the parameter on which it depends.

The solution of the integral Eqs. (8) is performed most simply by following the procedure given by von Kármán.[1] The interval of integration is subdivided into smaller partial intervals, in each of which the individual $\dot{f}$ are considered constant.

Consider then the points P_1, P_2, etc., on the meridian line, which are the intersections of this meridian with the straight lines: $x - x_i' = \alpha r$, where x_i' is the abscissa of the right end of each of the above-mentioned small intervals. The condition is imposed that Eqs. (8) be satisfied at the points P_i (Fig. 2). Then at the point P_1 with coordinates (x_1, R_1), one obtains

$$\left.\begin{aligned} &\frac{1}{2}\alpha^2 K_1^{(1)}\left(\text{arcosh}\frac{x_1}{\alpha R_1} + \frac{x_1}{\alpha R_1}\sqrt{\frac{x_1^2}{\alpha^2 R_1^2} - 1}\right) = F_1\left(\frac{x_1}{R_1}\right) \\ &\text{where } K_1^{(1)} \text{ is the constant value of } \dot{f}_1 \text{ in the first small interval} \\ &\frac{1}{3}\alpha^3 K_2^{(1)}\left(2\sqrt{\frac{x_1^2}{\alpha^2 R_1^2} - 1} + \frac{x_1^2}{\alpha^2 R_1^2}\sqrt{\frac{x_1^2}{\alpha^2 R_1^2} - 1}\right) = -F_2\left(\frac{x_1}{R_1}\right) \\ &\text{where } K_2^{(1)} \text{ is the constant value of } \dot{f}_2 \text{ in the first small interval} \\ &\frac{1}{4}\alpha^4 K_3^{(1)}\left[\frac{3}{2}\text{arcosh}\frac{x_1}{\alpha R_1} + \frac{3}{2}\frac{x_1}{\alpha R_1}\sqrt{\frac{x_1^2}{\alpha^2 R_1^2} - 1}\left(1 + \frac{2}{3}\frac{x_1^2}{\alpha^2 R_1^2}\right)\right] = F_3\left(\frac{x_1}{R_1}\right) \\ &\text{with analogous significance for } K_3^{(1)}, \text{ etc.} \end{aligned}\right\} \qquad (8')$$

The value of $K_1^{(1)}$ can be calculated immediately from the first of the set of Eqs. (8′); $K_2^{(1)}$ from the second; and the rest in like manner.

In general, if x_{i-1}', x_i' are the abscissas of the left and right ends of the ith interval, respectively, and $K_k^{(i)}$ is the constant value of $\dot{f}_k$ in that interval, then one has, at the point P_n with coordinates (x_n, R_n):

$$\left.\begin{aligned}
&\frac{1}{2}\alpha^2\sum_{i=1}^{n}K_1^{(i)}\left[\operatorname{arcosh}\frac{x_n-x_{i-1}'}{\alpha R_n}-\operatorname{arcosh}\frac{x_n-x_i'}{\alpha R_n}+\frac{x_n-x_{i-1}'}{\alpha R_n}\sqrt{\left(\frac{x_n-x_{i-1}'}{\alpha R_n}\right)^2-1}-\right.\\
&\qquad\left.\frac{x_n-x_i'}{\alpha R_n}\sqrt{\left(\frac{x_n-x_i'}{\alpha R_n}\right)^2-1}\right]=F_1\left(\frac{x_n}{R_n}\right)\\
&\frac{\alpha^3}{3}\sum_{i=1}^{n}K_2^{(i)}\left[2\sqrt{\left(\frac{x_n-x_{i-1}'}{\alpha R_n}\right)^2-1}-2\sqrt{\left(\frac{x_n-x_i'}{\alpha R_n}\right)^2-1}+\right.\\
&\qquad\left.\left(\frac{x_n-x_{i-1}'}{\alpha R_n}\right)^2\sqrt{\left(\frac{x_n-x_{i-1}'}{\alpha R_n}\right)^2-1}-\left(\frac{x_n-x_i'}{\alpha R_n}\right)^2\sqrt{\left(\frac{x_n-x_i'}{\alpha R_n}\right)^2-1}\right]=-F_2\left(\frac{x_n}{R_n}\right)\\
&\frac{\alpha^4}{4}\sum_{i=1}^{n}K_3^{(i)}\left\{\frac{3}{2}\left(\operatorname{arcosh}\frac{x_n-x_{i-1}'}{\alpha R_n}-\operatorname{arcosh}\frac{x_n-x_i'}{\alpha R_n}\right)+\right.\\
&\qquad\frac{3}{2}\left(\frac{x_n-x_{i-1}'}{\alpha R_n}\right)\sqrt{\left(\frac{x_n-x_{i-1}'}{\alpha R_n}\right)^2-1}\left[1+\frac{2}{3}\left(\frac{x_n-x_{i-1}'}{\alpha R_n}\right)^2\right]-\frac{3}{2}\left(\frac{x_n-x_i'}{\alpha R_n}\right)\times\\
&\qquad\left.\sqrt{\left(\frac{x_n-x_i'}{\alpha R_n}\right)^2-1}\left[1+\frac{2}{3}\left(\frac{x_n-x_i'}{\alpha R_n}\right)^2\right]\right\}=F_3\left(\frac{x_n}{R_n}\right)\\
&\text{etc}
\end{aligned}\right\}\qquad(9)$$

From these equations the constants $K_h^{(i)}$ can be determined successively, provided the F_h are known. It is important to note that for the purpose of calculating the lift and moment of the body—not the local pressures—it is necessary and sufficient to compute only $\Phi_1^{(3)}$ and therefore only the constants $K_1^{(i)}$.

(A-3) *Determination of the Harmonic Components of the Perturbed Velocity Induced by the Wing*

The problem is thus reduced to the determination of the velocity normal to the body, induced by the wing—that is, to the calculation of the harmonic components of this velocity, according to Eq. (2). For this calculation we let the wing be a flat plate and assume that the field induced by it is the same as it would be if the body were absent. Under this condition it is known that V_{nb} reduces to

$$V_{nb} = -\beta_2 V_0 \sin\theta \qquad (10)$$

in the region included between the planes that pass through the leading and trailing edges of the wing and are inclined by the Mach angle with respect to V_0, while $V_{nb} = 0$ outside of this region (Fig. 3). Consequently,

$$\left.\begin{aligned}
&F_1 = -\beta_2; \qquad F_m = 0 \quad \text{if } m > 1\\
&\text{for } \alpha(R_0 + R_1^*) \le x \le \alpha R_0 + l
\end{aligned}\right\}\qquad(11)$$

where R_0 and R_1^* have the meaning indicated in Fig. 3 and l is the wing chord.

For $0 \le x \le \alpha R_0$ we have $F_m = 0$ regardless of m, and for $\alpha R_0 \le x \le \alpha(R_0 + R_1^*)$ the graph defining the variation of V_{nb} for a cross section is shown in Fig. 4.

Letting

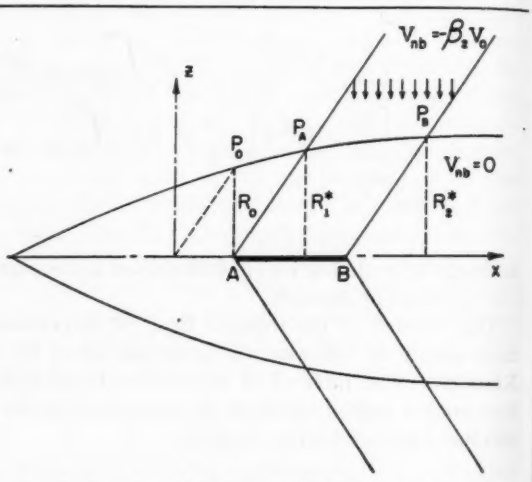

FIG. 3. Regions in which the wing-induced normal velocities take on different formulations.

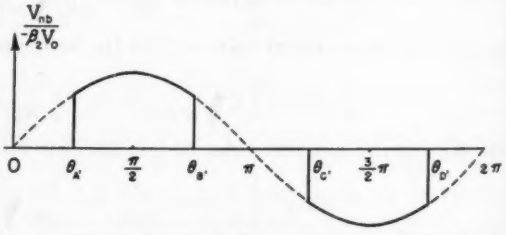

FIG. 4. Wing-induced velocity normal to body in the region immediately aft of wing leading edge.

$$\left.\begin{aligned}
&\theta_A = \arcsin\frac{x-\alpha R_0}{\alpha R}; \qquad \theta_B = \pi - \theta_A\\
&\theta_C = \pi + \theta_A; \qquad \theta_D = 2\pi - \theta_A
\end{aligned}\right\}\qquad(12)$$

one obtains, therefore, for a general function

$$F_m = -\frac{\beta_2}{\pi}\left[\int_0^{\theta_A} \sin\theta \sin m\theta\, d\theta + \int_{\theta_B}^{\theta_C} \sin\theta \sin m\theta\, d\theta + \int_{\theta_D}^{2\pi} \sin\theta \sin m\theta\, d\theta\right]$$

then

$$\left.\begin{aligned} F_1 &= -\frac{\beta_2}{\pi}\left[\int_0^{\theta_A} \sin^2\theta\, d\theta + \int_{\theta_B}^{\theta_C} \sin^2\theta\, d\theta + \int_{\theta_D}^{2\pi} \sin^2\theta\, d\theta\right] = \frac{-\beta_2}{\pi}\left[2\theta_A - \sin 2\theta_A\right], \quad \text{for } m = 1 \\ F_m &= -\frac{2}{\pi}\beta_2\left[\frac{\sin(m-1)\theta_A}{m-1} - \frac{\sin(m+1)\theta_A}{m+1}\right], \quad \text{for } m \text{ odd and} > 1 \\ &= 0, \quad \text{for } m \text{ even} \end{aligned}\right\} \quad (13)$$

Finally, for

$$(\alpha R_0 + l) \leq x \leq \alpha(R_0 + R_2^*) + l$$

(see Fig. 3) the curve defining the law of variation of V_{nb} for any cross section is shown in Fig. 5.

Putting

$$\left.\begin{aligned} \theta_{A'} &= \arcsin(x - \alpha R_0 - l)/\alpha R; \qquad \theta_{B'} = \pi - \theta_{A'} \\ \theta_{C'} &= \pi + \theta_{A'}; \qquad \theta_{D'} = 2\pi - \theta_{A'} \end{aligned}\right\} \quad (14)$$

one obtains

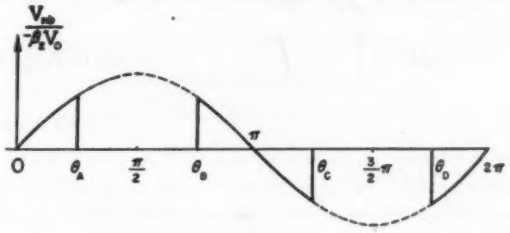

FIG. 5. Wing-induced velocity normal to body in the region immediately aft of wing trailing edge.

$$\left.\begin{aligned} F_1 &= \frac{-\beta_2}{\pi}\left[\int_{\theta_{A'}}^{\theta_{B'}} \sin^2\theta\, d\theta + \int_{\theta_{C'}}^{\theta_{D'}} \sin^2\theta\, d\theta\right] = \frac{-\beta_2}{\pi}\left[\pi - 2\theta_{A'} + \sin 2\theta_{A'}\right], \quad \text{for } m = 1 \\ F_m &= \frac{-\beta_2}{\pi}\left[\int_{\theta_{A'}}^{\theta_{B'}} \sin\theta \sin m\theta\, d\theta + \int_{\theta_{C'}}^{\theta_{D'}} \sin\theta \sin m\theta\, d\theta\right] \\ &= \frac{+2\beta_2}{\pi}\left[\frac{\sin(m-1)\theta_{A'}}{m-1} - \frac{\sin(m+1)\theta_{A'}}{m+1}\right], \quad \text{if } m \text{ is odd and} > 1 \\ &= 0, \quad \text{if } m \text{ is even} \end{aligned}\right\} \quad (15)$$

In the event that the body diameter is so large that $l < \alpha R_1^*$, then Fig. 3 no longer applies, and a new formulation for the V_{nb} is required in the interval

$$\alpha R_0 + l \leq x \leq \alpha(R_0 + R_1^*)$$

The above-given equations must be replaced by

$$F_1 = \frac{-\beta_2}{\pi}\left[2(\theta_A - \theta_{A'}) - (\sin 2\theta_A - \sin 2\theta_{A'})\right], \quad \text{for } m = 1$$

$$F_m = \frac{-2\beta_2}{\pi}\left[\frac{\sin(m-1)\theta_A - \sin(m-1)\theta_{A'}}{m-1} - \frac{\sin(m+1)\theta_A - \sin(m+1)\theta_{A'}}{m+1}\right], \quad \text{for } m \text{ odd and} > 1$$

$$= 0, \quad \text{for } m \text{ even}$$

and Eqs. (13) and (15) apply to the regions

$$\alpha R_0 \leq x \leq \alpha R_0 + l$$

and

$$\alpha(R_0 + R_1^*) \leq x \leq \alpha(R_0 + R_2^*) + l$$

respectively.

(A-4) *Determination of the Influence of the Wing on the Lift and Moment of the Body*

In order to calculate the overall interference effect of the wing upon the body—i.e., the variation of the resultant of the pressures acting on the surface of the latter, not the local pressures—the evaluation may proceed from the approximate solution of the first equation of Eqs. (8). The approximation is obtained for the limiting case wherein the radius of the body tends to zero; this evaluation is valid because only f_1 is of importance as far as the overall lift and moment are concerned, as pointed out above.

Now, if we let $x' = x - \alpha R \cosh u$, the middle expression in the first equation of Eqs. (8) reduces to

$$-\frac{1}{R^2}\int_0^{x-\alpha R} f_1(x')\frac{(x-x')^2}{\sqrt{(x-x')^2 - \alpha^2 R^2}}\,dx' \cong -\frac{1}{R^2}\int_0^x f_1(x')(x-x')\,dx'$$

if one takes the limiting value of the integral as $R \to 0$.' Setting this expression equal to the right-hand side of the first equation of Eqs. (8) and differentiating with respect to x, one obtains

$$f_1(x) = (d/dx)[R^2F_1(x/R)] \tag{16}$$

On the other hand, the variation of lift of an element dx of the body, produced by the velocities normal to it that are generated by the wing, is given by

$$\frac{d}{dx}(\Delta_1 L_b) = \rho V_0 R \int_0^{2\pi} \frac{\partial \Phi^{(3)}}{\partial x} \sin\theta \, d\theta = \rho V_0^2 \pi R \frac{\partial (R\Phi_1^{(3)})}{\partial x}$$

$$= \rho \pi R V_0^2 \left[-\alpha \int_{\text{arcosh } x/\alpha R}^{0} \dot{f}_1(x - \alpha R \cosh u) \times \cosh u \, du \right]$$

$$= \rho V_0^2 \pi f_1(x)$$

again with the hypothesis that R tends to zero. The overall change of lift due to the field of normal velocities is then, taking into account Eq. (16):

$$\Delta_1 L_b = \rho V_0^2 \pi \int_0^{\infty} f_1(x)\, dx = \rho V_0^2 \pi \int_0^{\infty} \frac{d}{dx}\left[R^2 F_1\left(\frac{x}{R}\right)\right] dx = 0$$

because $F_1(x/R)$ is continuous in the interval and zero at its ends. Moreover, since the change of lift due to the velocity components along x, induced on the body by the wing, is given by

$$\Delta_2 L_b = \frac{2\rho V_0^2}{\alpha} \int_0^{\pi} \int_0^{\infty} R\beta_2(x, \theta) \sin\theta \, d\theta \, dx$$

and, by making use of the relations already given in Eqs. (11), (12), and (14) for determining when $\beta_2(x, \theta)$ is zero or equal to a constant, β_2, one perceives that

$$\Delta_2 L_b = \left(\frac{-2\rho V_0^2}{\alpha}\right)\beta_2 \left\{ \int_{\alpha R_0}^{\alpha(R_0 + R_1^*)} 2R\left[\sqrt{1 - \left(\frac{x - \alpha R_0}{\alpha R}\right)^2} - 1\right] dx - \int_{\alpha(R_0 + R_1^*)}^{\alpha R_0 + l} R\, dx - \int_{\alpha R_0 + l}^{\alpha(R_0 + R_2^*) + l} 2R\sqrt{1 - \left(\frac{x - \alpha R_0 - l}{\alpha R}\right)^2} dx \right\}$$

Even if R is finite but constant, this expression reduces to

$$\Delta_2 L_b = (4/\alpha)(1/2)\rho V_0^2 \beta_2 2Rl = \Delta L_b \tag{17}$$

so that this change is equal to the lift of a portion of wing which has just the same extent as the wing area covered by the body. When R is extremely small, it is necessary to observe simply that

$$d(\Delta_2 L_b)/dx = (4/\alpha)\rho V_0^2 \beta_2 R$$

for x lying between the abscissa $x_0 = \alpha R_0$ (of the leading edge) and the abscissa $x_0 + l$ (of the trailing edge), while $d(\Delta_2 L_b)/dx = 0$ for x outside the interval. Consequently, the overall change of lift of the body is

$$\Delta L_b = \Delta_2 L_b = (4/\alpha)\rho V_0^2 \beta_2 \int_{x_0}^{x_0 + l} R\, dx \tag{17'}$$

With the same approximation we may obtain the changes in the moment, about the y-axis, of the aerodynamic forces acting on the body as a result of the interference effect of the wing. This change is given by

$$\Delta_1 M_y = -\rho V_0^2 \pi \int_0^{\infty} x \left(\frac{d}{dx}\right)\left[R^2 F_1\left(\frac{x}{R}\right)\right] dx$$

Under the hypothesis, generally quite legitimate, that R may be considered constant for that portion of the body influenced by the wing, one gets

$$\Delta_1 M_y = -\rho V_0^2 \pi R^2 l \beta_2 \tag{18}$$

The amount of moment change, $\Delta_2 M_y$, due to the longitudinal velocity induced directly by the wing, may again be obtained simply in terms of a finite R, provided it is constant in the region

$$\alpha R_0 \leq R \leq \alpha(R_0 + R_2^*) + l$$

Proceeding as in the case for Eq. (17), it is found that

$$\Delta_2 M_y = -\left(\frac{4}{\alpha}\right)\beta_2 \left(\frac{1}{2}\right)\rho V_0^2 R l \left(l \mp \frac{\alpha R \pi}{2}\right)$$

and this moment is likewise, when R becomes very small, exactly equal to the moment that would arise from an isolated portion of wing, the spanwise extent of which is $2R$.

(B) Interference Effect of the Body on the Wing

(B-1) *Condition That Interference Be Nil*

The perturbation potential field for an isolated body, considered immersed in a uniform stream of velocity V_0, is

$$\Phi^{(1)} + \Phi^{(2)} = V_0 \left[\int_{\text{arcosh } x/\alpha r}^{0} f(x - \alpha r \cosh u)\, du - \alpha \sin\theta \int_{\text{arcosh } x/\alpha r}^{0} g(x - \alpha r \cosh u) \cosh u \, du \right] \tag{19}$$

At any point of the (x, y)-plane, the velocity, corresponding to this potential, has a component normal to that plane given by

$$\left(\frac{1}{r}\frac{\partial\Phi^{(2)}}{\partial\theta}\right)_{\theta=0} =$$

$$-\frac{\alpha}{y}V_0\int_{\operatorname{arcosh} x/\alpha y}^{0} g(x-\alpha y\cosh u)\cosh u\,du \quad (20)$$

wherein one may set, at least in first approximation,[4]

$$g(x) = (\beta_1/\pi)(dS/dx)$$

where S is the area of a general cross section of the body.

Within the degree of approximation consistent with the linearized theory, the condition for the nonexistence of body interference effects on the wing, when the latter is at a given angle of attack, β_2, is that the slope of the wing profile at each point in the plane of the wing [considered to be close to the (x, y)-plane] be

$$\frac{dz}{dx} = -\frac{\alpha}{y}\int_{\operatorname{arcosh} x/\alpha y}^{0} g(x-\alpha y\cosh u)\cosh u\,du \quad (21)$$

Under this restriction, certainly, the velocity induced by the body has a zero component normal to the wing profile.

(B-2) *Condition of Non-Zero Interference—General Equations*

If points along the chord line of the profile do not satisfy condition (21), the velocity component normal to the wing [that is, to the (x, y)-plane, since the wing is considered to be close to the (x, y)-plane], at each point of its surface, may be expressed in the form

$$\frac{V_{nw}}{V_0} = \sum_m G_m\left(\frac{x}{b}\right)\cos\frac{2\pi m y}{4b} = \sum_m G_m(\xi)\cos\frac{\pi}{2}m\eta \quad (22)$$

Here the origin of coordinates is at the leading edge of the profile which lies in the (x, z)-plane, and the functions $G_m(\xi)$ can be determined from Eq. (20) as indicated in Section B-5. In order to satisfy the boundary condition relative to the wing, it is necessary to superimpose on potential field (19) a new set of velocities with a corresponding potential that is expressed as

$$\Phi' = V_0 b\sum_m \Phi_m'(\xi,\zeta)\cos(\pi m\eta/2) \quad (23)$$

and which is defined by the following conditions: (a) it must satisfy

$$(\partial^2\Phi'/\partial\eta^2) + (\partial^2\Phi'/\partial\zeta^2) = \alpha^2(\partial^2\Phi'/\partial\xi^2) \quad (24)$$

everywhere; (b) while in the plane of the wing with $\zeta = 0$, it is required that

$$\left(\frac{1}{bV_0}\right)\left(\frac{\partial\Phi'}{\partial\zeta}\right) = -\frac{V_{nw}}{V_0} = -\sum_m G_m(\xi)\cos\frac{\pi m\eta}{2} \quad (25)$$

By substitution of the potential (23) into Eq. (24), one obtains

$$-\sum_m k^2\Phi_m'\cos\frac{\pi m\eta}{2} + \sum_m \frac{\partial^2\Phi_m'}{\partial\zeta^2}\cos\frac{\pi m\eta}{2} = \alpha^2\sum_m\frac{\partial^2\Phi_m'}{\partial\xi^2}\cos\frac{\pi m\eta}{2}$$

where $k = \pi m/2$; so that it is apparent any Φ_m' must satisfy the equation

$$(\partial^2\Phi_m'/\partial\zeta^2) - \alpha^2(\partial^2\Phi_m'/\partial\xi^2) = k^2\Phi_m' \quad (26)$$

while Eqs. (23) and (25) give, on the plane of the wing $\zeta = 0$,

$$\partial\Phi_m'/\partial\zeta = -G_m(\xi) \quad (27)$$

Now Eq. (26), with condition (27), is formally analogous to the so-called telegraph equation[5] (in its reduced form) and, in consequence, can be solved by means of the corresponding Riemann functions. In order to give the procedure a more well-rounded development than was done under Section A, however, the solution of Eq. (26) that satisfies condition (27) can be found as follows:

(B-3) *Determination of the Potential* Φ_m'

(B-3-1) Construction of the Potential from Elemental Sources, and Related Doublet Distribution.—We now consider Φ_m' as being a function of η also, and satisfying the equation

$$\frac{\partial^2\Phi_m'}{\partial\eta^2} + \frac{\partial^2\Phi_m'}{\partial\zeta^2} - \alpha^2\frac{\partial^2\Phi_m'}{\partial\xi^2} - k^2\Phi_m' = 0 \quad (28)$$

A particular integral of Eq. (28) is immediately seen to be

$$\Phi_m' = [\cos(k/\alpha)r]/r \quad (29)$$

in which now $r = \sqrt{\xi^2 - \alpha^2(\eta^2+\zeta^2)}$. The function Φ_m', as defined by Eq. (29), is called the potential of the source that is located at the origin of coordinates. If the source, instead of being at the origin, were located at the point with coordinates,

$$\xi = \xi', \qquad \eta = \eta', \qquad \zeta = 0$$

the corresponding potential would still be expressed by Eq. (29), in which now, however,

$$r = \sqrt{(\xi-\xi')^2 - \alpha^2[(\eta-\eta')^2+\zeta^2]}$$

Consider further a uniform distribution of sources on the semiplane (ξ, η), $(\xi > 0)$ extending from $\eta' = -\infty$ to $\eta' = +\infty$; the intensity of source in the element $d\xi'\,d\eta'$ is $h(\xi)d\xi'd\eta'$. The potential of the source distribution will still satisfy Eq. (28), since it is a linear combination of particular solutions of this equation. Consequently, we have:

$$\Phi_m' = \int_{-\infty}^{\infty} d\eta' \int_0^{\xi-\alpha[(\eta-\eta')^2+\zeta^2]^{1/2}} \frac{h(\xi')\cos(k/\alpha)\sqrt{(\xi-\xi')^2-\alpha^2[(\eta-\eta')^2+\zeta^2]}}{\sqrt{(\xi-\xi')^2-\alpha^2[(\eta-\eta')^2+\zeta^2]}}\,d\xi'$$

$$= \int_0^{\xi-\alpha|\zeta|} h(\xi')d\xi' \int_{\eta-[(\xi-\xi')^2-\alpha^2\zeta^2]^{1/2}(1/\alpha)}^{\eta+[(\xi-\xi')^2-\alpha^2\zeta^2]^{1/2}(1/\alpha)} \frac{\cos(k/\alpha)\sqrt{(\xi-\xi')^2-\alpha^2[(\eta-\eta')^2+\zeta^2]}}{\sqrt{(\xi-\xi')^2-\alpha^2[(\eta-\eta')^2+\zeta^2]}}\,d\eta' \qquad (30)$$

Making the transformation

$$\eta - \eta_i = (1/\alpha)\sqrt{(\xi-\xi')^2-\alpha^2\zeta^2}\cos\varphi$$

and since

$$-d\eta' = -(1/\alpha)\sqrt{(\xi-\xi')^2-\alpha^2\zeta^2}\sin\varphi\,d\varphi$$

$$\sqrt{(\xi-\xi')^2-\alpha^2[(\eta-\eta')^2+\zeta^2]} =$$

$$\sqrt{(\xi-\xi')^2-\alpha^2\zeta^2}\sqrt{1-\frac{\alpha^2(\eta-\eta')^2}{(\xi-\xi')^2-\alpha^2\zeta^2}} =$$

$$\sqrt{(\xi-\xi')^2-\alpha^2\zeta^2}\sin\varphi$$

one arrives at

$$\Phi_m' = \frac{1}{\alpha}\int_0^{\xi-\alpha|\zeta|} h(\xi')d\xi' \times \int_0^{\pi} \cos\left[\frac{k}{\alpha}\sqrt{(\xi-\xi')^2-\alpha^2\zeta^2}\sin\varphi\right]d\psi$$

$$= \frac{\pi}{\alpha}\int_0^{\xi-\alpha|\zeta|} h(\xi')J_0\left[\frac{k}{\alpha}\sqrt{(\xi-\xi')^2-\alpha^2\zeta^2}\right]d\xi' \qquad (31)$$

where J_0 is the cylindrical Bessel function of zero order. This result satisfies Eq. (28), and therefore, since it does not contain η, it also satisfies Eq. (26).

Corresponding to this potential for the source distribution there will exist a potential for a doublet distribution,[6] with axis in the direction of ζ and lying in the plane (ξ, η), of the form:

$$\Phi_m' = \frac{\pi}{\alpha}\frac{\partial}{\partial\zeta}\int_0^{\xi-\alpha|\zeta|} h(\xi')J_0\left[\frac{k}{\alpha}\sqrt{(\xi-\xi')^2-\alpha^2\zeta^2}\right]d\xi'$$

$$= \pm\pi h[\xi-\alpha|\zeta|] + \pi k\zeta\int_0^{\xi-\alpha|\zeta|} h(\xi')J_1\left[\frac{k}{\alpha}\sqrt{(\xi-\xi')^2-\alpha^2\zeta^2}\right]\frac{d\xi'}{\sqrt{(\xi-\xi')^2-\alpha^2\zeta^2}} \qquad (32)$$

where J_1 is the cylindrical Bessel function of the first order and where the minus or plus sign should be used according to whether ζ is greater or less than zero, respectively. It is seen from Eq. (32) that the derivative of Φ_m' with respect to ζ is continuous at the plane $\zeta = 0$, while that with respect to ξ is discontinuous and has the value

$$(\partial\Phi_m'/\partial\xi)_{\zeta=0^+} = -(\partial\Phi_m'/\partial\xi)_{\zeta=0^-}$$

In what follows we shall consider the perturbed flow in the semiplane $\zeta > 0$; the remark just made above enables one to determine the flow in the other semiplane when that in the first is known. It is assumed that Φ_m', defined by Eq. (23), is to be expressed by Eq. (32), into which it transcribes when $h(\xi')$ is replaced by $h_m(\xi')$.

(*B-3-2*) *Application of the Boundary Condition.*—The function $h_m(\xi')$ *a priori* arbitrary, must be determined so as to satisfy Eq. (27). In order to calculate $\partial\Phi_m'/\partial\zeta$, it is convenient, as usual, to put $\xi' = \xi - \alpha\zeta\cosh u$, with the result that

$$\frac{\partial\Phi_m'}{\partial\zeta} = \pi\alpha\dot{h}_m(\xi-\alpha\zeta) - \pi k\int_{\operatorname{arcosh}\xi/\alpha\zeta}^{0} h_m(\xi-\alpha\zeta\cosh u)J_1(k\zeta\sinh u)\,du +$$

$$\pi k\zeta\alpha\int_{\operatorname{arcosh}\xi/\alpha\zeta}^{0} \dot{h}_m(\xi-\alpha\zeta\cosh u)\cosh u\,J_1(k\zeta\sinh u)\,du - \pi k^2\zeta\int_{\operatorname{arcosh}\xi/\alpha\zeta}^{0} h_m(\xi-\alpha\zeta\cosh u)\times$$

$$\dot{J}_1(k\zeta\sinh u)\sinh u\,du$$

$$\frac{\partial \Phi_m'}{\partial \zeta} = \pi\alpha \dot{h}_m(\xi - \alpha\zeta) + \pi k \int_0^{\xi-\alpha\zeta} h_m(\xi') J_1\left[\frac{k}{\alpha}\sqrt{(\xi-\xi')^2 - \alpha^2\zeta^2}\right] \frac{d\xi'}{\sqrt{(\xi-\xi')^2 - \alpha^2\zeta^2}} -$$
$$\pi k \int_0^{\xi-\alpha\zeta} \dot{h}_m(\xi')(\xi-\xi') J_1\left[\frac{k}{\alpha}\sqrt{(\xi-\xi')^2 - \alpha^2\zeta^2}\right] \frac{d\xi'}{\sqrt{(\xi-\xi')^2 - \alpha^2\zeta^2}} +$$
$$\frac{\pi k^2}{\alpha} \int_0^{\xi-\alpha\zeta} h_m(\xi') \dot{J}_1\left[\frac{k}{\alpha}\sqrt{(\xi-\xi')^2 - \alpha^2\zeta^2}\right] d\xi'$$

where $\dot{h}_m$ and $\dot{J}_1$ are, respectively, the derivatives of h_m and of J_1 with respect to their corresponding parameters.

On the plane of the wing, for which $\zeta = 0$, one has

$$\left(\frac{\partial \Phi_m'}{\partial \zeta}\right)_{\zeta=0} = \pi\alpha \dot{h}_m(\xi) + \frac{\pi k^2}{\alpha} \int_0^{\xi} h_m(\xi') J_1\left[k\left(\frac{\xi-\xi'}{\alpha}\right)\right] d\xi' \Big/ k\left(\frac{\xi-\xi'}{\alpha}\right) -$$
$$\pi k \int_0^{\xi} \dot{h}_m(\xi') J_1\left[k\,\frac{\xi-\xi'}{\alpha}\right] d\xi' + \frac{\pi k^2}{\alpha} \int_0^{\xi} h_m(\xi') \dot{J}_1\left[k\left(\frac{\xi-\xi'}{\alpha}\right)\right] d\xi'$$

but $J_1(\theta)/\theta + \dot{J}_1(\theta) = J_0(\theta)$ and therefore

$$\left(\frac{\partial \Phi_m'}{\partial \zeta}\right)_{\zeta=0} = \pi\alpha \dot{h}_m(\xi) + \pi\,\frac{k^2}{\alpha} \int_0^{\xi} h_m(\xi') J_0\left[k\left(\frac{\xi-\xi'}{\alpha}\right)\right] d\xi' -$$
$$\pi k \int^{\xi} \dot{h}_m(\xi') J_1\left[k\left(\frac{\xi-\xi'}{\alpha}\right)\right] d\xi' = -G_m(\xi) \quad (33)$$

(B-3-3) Stepwise Procedure for Evaluation of the Doublet Distribution.—Equation (33) can be solved simply by following a procedure analogous to that followed in Section B-2. If the interval 0 to l/b (where l is the length of the wing chord) is divided into parts, in each of which $h_m(\xi')$ is assumed to vary linearly, then

$$h_m(\xi') = H_m^{(1)} \xi'$$

in the first small interval,

$$h_m(\xi') = H_m^{(1)} \Delta_1 + H_m^{(2)}(\xi' - \Delta_1)$$

in the second small interval,

$$h_m(\xi') = H_m^{(1)} \Delta_1 + H_m^{(2)} \Delta_2 + H_m^{(3)}(\xi' - \Delta_1 - \Delta_2)$$

in the third, and so on.

If, for the sake of simplicity, the lengths of the intervals are all set equal to Δ, then one has in the ith small interval that

$$h_m(\xi') = \Delta \sum_i H_m^{(i-1)} + H_m^{(i)}[\xi' - (i-1)\Delta]$$

On the other hand,

$$\int_0^{\xi} \xi' J_0\left[\frac{k}{\alpha}\left(\xi - \xi'\right)\right] d\xi' = \frac{\alpha^2}{k^2} \int_0^{\xi} \frac{k}{\alpha}\left(\xi - \xi'\right) J_0\left[k\left(\frac{\xi-\xi'}{\alpha}\right)\right] d\left[k\left(\frac{\xi-\xi'}{\alpha}\right)\right] -$$
$$\frac{\alpha}{k}\,\xi \int_0^{\xi} J_0\left[k\left(\frac{\xi-\xi'}{\alpha}\right)\right] d\left[k\left(\frac{\xi-\xi'}{\alpha}\right)\right]$$
$$= -\frac{\alpha}{k}\,\xi J_1\left(\frac{k\xi}{\alpha}\right) + 2\,\frac{\alpha}{k}\,\xi \sum_{n=0}^{n=\infty} J_{2n+1}\left(\frac{k\xi}{\alpha}\right)$$

and

$$\int_0^{\xi} J_1\left[k\left(\frac{\xi-\xi'}{\alpha}\right)\right] d\xi' = -\frac{\alpha}{k} \int_0^{\xi} J_1\left[k\left(\frac{\xi-\xi'}{\alpha}\right)\right] d\left[k\left(\frac{\xi-\xi'}{\alpha}\right)\right]$$
$$= \frac{\alpha}{k}\left[1 - J_0\left(\frac{k}{\alpha}\,\xi\right)\right]$$

Therefore, imposing the condition that Eq. (33) be satisfied at the point $\xi = \Delta$, corresponding to the right-hand end of the first small interval, one obtains:

$$H_m^{(1)}\left[\pi\alpha J_0\left(\frac{k}{\alpha}\Delta\right) + \pi k \Delta J_1\left(\frac{k}{\alpha}\Delta\right) + 2\pi k \Delta \sum_{n=1}^{\infty} J_{2n+1}\left(\frac{k\Delta}{\alpha}\right)\right] = -G_m(\Delta) \quad (34)$$

whence $H_m^{(1)}$ can be determined.

Analogously, imposing the condition that Eq. (33) be satisfied at the point $\xi = 2\Delta$, corresponding to the right-hand end of the second small interval, and since

$$\int_0^{\xi} h_m(\xi')J_0\left[k\left(\frac{\xi-\xi'}{\alpha}\right)\right]d\xi' = H_m{}^{(1)}\int_0^{\Delta}\xi' J_0 d\xi' + H_m{}^{(1)}\Delta\int^{\xi} J_0\, d\xi' + H_m{}^{(2)}\int^{\xi}(\xi'-\Delta)J_0\, d\xi'$$

while

$$\int_0^{\Delta}\xi' J_0\, d\xi' = \frac{\alpha^2}{k^2}\left\{\frac{k}{\alpha}\left(\xi-\Delta\right)J_1\left[k\left(\frac{\xi-\Delta}{\alpha}\right)\right] - k\frac{\xi}{\alpha}J_1\left(k\frac{\xi}{\alpha}\right)\right\} - \frac{2\alpha\xi}{k}\left\{\sum_{n=0}^{\infty}J_{2n+1}\left[k\left(\frac{\xi-\Delta}{\alpha}\right)\right] - \sum_{n=0}^{\infty}J_{2n+1}\left(\frac{k\xi}{\alpha}\right)\right\}$$

and

$$\int_{\Delta}^{\xi} J_0\, d\xi' = \frac{2\alpha}{k}\sum_{n=0}^{\infty}J_{2n+1}\left[\frac{k}{\alpha}\left(\xi-\Delta\right)\right]$$

and

$$\int_{\Delta}^{\xi}(\xi'-\Delta)J_0\left[k\left(\frac{\xi-\xi'}{\alpha}\right)\right]d\xi' = -\frac{\alpha}{k}\left(\xi-\Delta\right)J_1\left[\frac{k}{\alpha}\left(\xi-\Delta\right)\right] - 2\frac{\alpha}{k}\left(\Delta-\xi\right)\sum_{n=0}^{\infty}J_{2n+1}\left[k\left(\frac{\xi-\Delta}{\alpha}\right)\right]$$

and lastly

$$\int_0^{\xi}\dot{h}_m(\xi')J_1\, d\xi' = H_m{}^{(1)}\int_0^{\Delta}J_1\, d\xi' + H_m{}^{(2)}\int_{\Delta}^{\xi}J_1\, d\xi'$$
$$= H_m{}^{(1)}\frac{\alpha}{k}\left\{J_0\left[k\left(\frac{\xi-\Delta}{\alpha}\right)\right] - J_0\left(\frac{k\xi}{\alpha}\right)\right\} + H_m{}^{(2)}\frac{\alpha}{k}\left\{1 - J_0\left[k\left(\frac{\xi-\Delta}{\alpha}\right)\right]\right\}$$

then there evolves, for $\xi = 2\Delta$:

$$H_m{}^{(1)}\pi\left\{k\Delta\left[-J_1\left(\frac{k}{\alpha}\Delta\right) - 2\sum_1^{\infty}J_{2n+1}\left(\frac{k\Delta}{\alpha}\right) + 2J_1\left(\frac{2k\Delta}{\alpha}\right) + 4\sum_1^{\infty}J_{2n+1}\left(\frac{2k\Delta}{\alpha}\right)\right] - \alpha\left[J_0\left(\frac{k\Delta}{\alpha}\right) - J_0\left(\frac{2k\Delta}{\alpha}\right)\right]\right\} +$$
$$H_m{}^{(2)}\pi\left\{\alpha J_0\left(\frac{k\Delta}{\alpha}\right) + k\Delta\left[J_1\left(\frac{k\Delta}{\alpha}\right) + 2\sum_1^{\infty}J_{2n+1}\left(\frac{k\Delta}{\alpha}\right)\right]\right\} = -G_m(2\Delta)$$

or, taking into account Eq. (34),

$$H_m{}^{(1)}\pi\left\{2k\Delta J_1\left(\frac{2k\Delta}{\alpha}\right) + 4k\Delta\sum_1^{\infty}J_{2n+1}\left(\frac{2k\Delta}{\alpha}\right) + \alpha J_0\left(\frac{2k\Delta}{\alpha}\right)\right\} +$$
$$H_m{}^{(2)}\pi\left\{\alpha J_0\left(\frac{k\Delta}{\alpha}\right) + k\Delta\left[J_1\left(\frac{k\Delta}{\alpha}\right) + 2\sum_1^{\infty}J_{2n+1}\left(\frac{k\Delta}{\alpha}\right)\right]\right\} = -G_m(\Delta) - G_m(2\Delta) \quad (35)$$

for which $H_m{}^{(2)}$ is determined. Similarly one obtains

$$H_m{}^{(1)}\pi\left[3k\Delta J_1\left(\frac{3k\Delta}{\alpha}\right) + 6k\Delta\sum_1^{\infty}J_{2n+1}\left(\frac{3k\Delta}{\alpha}\right) + \alpha J_0\left(\frac{3k\Delta}{\alpha}\right)\right] + H_m{}^{(2)}\pi\left[2k\Delta J_1\left(\frac{2k\Delta}{\alpha}\right) +\right.$$
$$\left. 4k\Delta\sum_1^{\infty}J_{2n+1}\left(\frac{2k\Delta}{\alpha}\right) + \alpha J_0\left(\frac{2k\Delta}{\alpha}\right)\right] + H_m{}^{(3)}\pi\left[k\Delta J_1\left(\frac{k\Delta}{\alpha}\right) + 2k\Delta\sum_1^{\infty}J_{2n+1}\left(\frac{k\Delta}{\alpha}\right) + \alpha J_0\left(\frac{k\Delta}{\alpha}\right)\right] =$$
$$-G_m(\Delta) - G_m(2\Delta) - G_m(3\Delta) \quad (36)$$

which gives $H_m{}^{(3)}$, and so forth.

(B-4) *Solution of the Problem in the Limiting Case of an Infinitesimally Narrow Chord Wing*

An approximate solution of Eq. (33) can be obtained by taking as the solution of that equation the one corresponding to the case of an infinitesimally narrow chord wing. Indeed, substituting in Eq. (33) for J_0 and J_1 their limit values, when their argument tends to zero, Eq. (33) reduces to

$$\pi\alpha\dot{h}_m(\xi) + \pi(k^2/2\alpha)\int_0^{\xi}h_m(\xi')d\xi' = -G_m(\xi) \quad (33')$$

In order to derive this Eq. (33′) from Eq. (33) and for the purpose of demonstrating within what limits the substitution of Eq. (33′) for Eq. (33) is legitimate, the following detailed procedure is subjoined:

The familiar expressions for the Bessel functions are:

$$J_0\{k[(\xi-\xi')/\alpha]\} = 1 - \{(k^2/2^2)[(\xi-\xi')/\alpha]^2\} + \ldots$$

and

$$J_1\left[k\left(\frac{\xi-\xi'}{\alpha}\right)\right]=\frac{k}{2}\left(\frac{\xi-\xi'}{\alpha}\right)\left[1-\left(\frac{k^2}{2(4)}\right)\left(\frac{\xi-\xi'}{\alpha}\right)^2+\dots\right]$$

These series are uniformly convergent in every finite interval; hence, the integral of each series in Eq. (33) may be replaced by the following series of integrals:

$$\int_0^\xi h_m(\xi')J_0\left[k\left(\frac{\xi-\xi'}{\alpha}\right)\right]d\xi'=\int_0^\xi h_m(\xi')\,d\xi'-\frac{k^2}{2^2}\int_0^\xi h_m(\xi')\left(\frac{\xi-\xi'}{\alpha}\right)^2 d\xi'+\dots$$

and

$$\int_0^\xi \dot{h}_m(\xi')J_1\left[k\left(\frac{\xi-\xi'}{\alpha}\right)\right]d\xi'=\frac{k}{2}\int_0^\xi \dot{h}_m(\xi')\left(\frac{\xi-\xi'}{\alpha}\right)d\xi'-\left(\frac{k}{2}\right)\left[\frac{k^2}{2(4)}\right]\int^\xi \dot{h}_m(\xi')\left(\frac{\xi-\xi'}{\alpha}\right)^3+\dots$$

Now let $\xi = x/b = (x/l)(l/b) = (l/b)\mathrm{X}$ and $\xi' = (l/b)\mathrm{X}'$; then

$$\int_0^\xi h_m(\xi')J_0\left[k\left(\frac{\xi-\xi'}{\alpha}\right)\right]d\xi'=\frac{l}{b}\int_0^{\mathrm{X}} h_m(\mathrm{X}')\,d\mathrm{X}'-\frac{k^2}{2^2}\left(\frac{l^2}{b^2\alpha^2}\right)\left(\frac{l}{b}\right)\int_0^{\mathrm{X}} h_m(\mathrm{X}')(\mathrm{X}-\mathrm{X}')^2\,d\mathrm{X}'+\dots$$

$$=\frac{l}{b}\left[\int_0^{\mathrm{X}} h_m(\mathrm{X}')\,d\mathrm{X}'\right]\left[1+\mathrm{O}\left(\frac{k^2l^2}{4b^2\alpha^2}\right)\right]$$

where $\mathrm{O}(k^2l^2/4b^2\alpha^2)$ is an infinitesimal of the same order as $k^2l^2/4b^2\alpha^2$. Analogously,

$$\int_0^\xi \dot{h}_m(\xi')J_1\left[k\left(\frac{\xi-\xi'}{\alpha}\right)\right]d\xi'=\frac{k}{2}\left(\frac{l}{b\alpha}\right)\int_0^{\mathrm{X}} \dot{h}_m(\mathrm{X}')(\mathrm{X}-\mathrm{X}')\,d\mathrm{X}'-$$

$$\frac{k}{2}\left(\frac{k^2}{2(4)}\right)\left(\frac{l^3}{b^3\alpha^3}\right)\int_0^{\mathrm{X}} \dot{h}_m(\mathrm{X}')(\mathrm{X}-\mathrm{X}')^3\,d\mathrm{X}'+\dots$$

$$=\frac{kl}{2b\alpha}\left[\int^{\mathrm{X}} \dot{h}_m(\mathrm{X}')(\mathrm{X}-\mathrm{X}')\,d\mathrm{X}'\right]\left[1+\mathrm{O}\left(\frac{k^2l^2}{4b^2\alpha^2}\right)\right]$$

Therefore we have,

$$\frac{\pi k^2}{\alpha}\int_0^\xi h_m(\xi')J_0\left[k\left(\frac{\xi-\xi'}{\alpha}\right)\right]d\xi'-\pi k\int^\xi \dot{h}_m(\xi')J_1\left[k\left(\frac{\xi-\xi'}{\alpha}\right)\right]d\xi'=\frac{\pi k^2 l}{b\alpha}\left[\int^{\mathrm{X}} h_m(\mathrm{X}')\,d\mathrm{X}'\right]\times$$

$$\left[1+\mathrm{O}\left(\frac{k^2l^2}{4b^2\alpha^2}\right)\right]-\frac{\pi k^2 l}{2b\alpha}\left[\int_0^{\mathrm{X}} h_m(\mathrm{X}')\,d\mathrm{X}'\right]\left[1+\mathrm{O}\left(\frac{k^2l^2}{4b^2\alpha^2}\right)\right]=\frac{\pi k^2 l}{2b\alpha}\left[\int_0^{\mathrm{X}} h_m(\mathrm{X}')\,d\mathrm{X}'\right]\left[1+\mathrm{O}\left(\frac{k^2l^2}{4b^2\alpha^2}\right)\right]$$

If one assumes, accordingly, that $kl/2b\alpha$ is an infinitesimal of the first order, it is legitimate to neglect the term $\mathrm{O}(k^2l^2/4b^2\alpha^2)$, and Eq. (33) becomes Eq. (33′).

It follows, because of the above discussion, that in the case of a given wing chord for which $l/b \ll 1$ the approximation supplied by means of Eq. (33′) improves as α becomes larger and as k (that is, m) becomes smaller. For large values of m the approximating Eq. (33′) can still give a close estimate of the value of $h_m(\xi)$ only at the points P of the wing which are in proximity to the leading edge, O; they must be so situated that, if l is set equal to OP, then

$$k^2l^2/4b^2\alpha^2 = (k^2\overline{OP}^2/4b^2\alpha^2) \ll 1$$

Now consider the approximating Eq. (33′) further. By differentiating it with respect to ξ, we obtain

$$\pi\alpha\ddot{h}_m(\xi)+\pi(k^2/2\alpha)h_m(\xi)=-\dot{G}_m(\xi) \tag{37}$$

while at the same time it must be true that

$$h_m(0)=0;\ \dot{h}_m(0)=-(1/\pi\alpha)G_m(0) \tag{38}$$

One deduces that the solution of Eq. (37), which satisfies the conditions (38), is given by

$$h_m(\xi)=\frac{\sqrt{2}}{\pi k}\left[\cos\left(\frac{k\xi}{\sqrt{2}\alpha}\right)\int^\xi \dot{G}_m(\xi)\sin\left(\frac{k\xi}{\sqrt{2}\alpha}\right)d\xi-\right.$$

$$\left.\sin\left(\frac{k\xi}{\sqrt{2}\alpha}\right)\int_0^\xi \dot{G}_m(\xi)\cos\left(\frac{k\xi}{\sqrt{2}\alpha}\right)d\xi-G_m(0)\sin\left(\frac{k\xi}{\sqrt{2}\alpha}\right)\right] \tag{39}$$

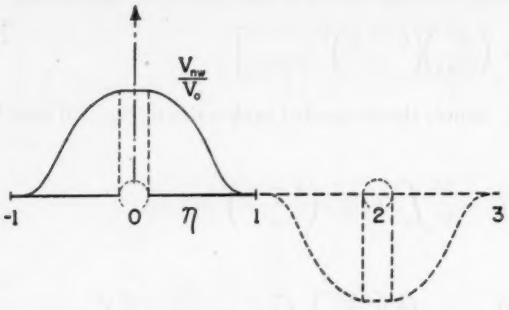

FIG. 6. Antisymmetrical extension of body-induced velocity distribution.

(B-5) *Determination of the Harmonic Components of the Perturbed Velocity Induced by the Body*

The solution of the problem is thus reduced to the determination of the functions $G_m(\xi)$ which represent the amplitudes of the harmonic components of the velocity, perturbed by the body, at the wing. The calculation of these functions, when the potential of the perturbation field induced by the body is known, can be performed in the following manner. Once the graph of the normal perturbation velocities V_{nw}/V_0 has been determined along the span of the wing for a given value of ξ, by means of Eq. (20), it will be possible in general to approximate the function defining V_{nw}/V_0 with η as parameter (for η varying in the interval from -1 to $+1$) by a trigonometric polynomial of period 4 and consisting of n terms.

If the graph of the function V_{nw}/V_0 is extended antisymmetrically (Fig. 6) outside the interval $-1 \leq \eta \leq 1$, only the terms that contain odd values of m will be different from zero (that is, $m = 2n$).

If $(V_{nw}/V_0)_{0,h}$, $(V_{nw}/V_0)_{i,h}$ are the values of V_{nw}/V_0, respectively, at the points

$$(\eta = 0; \quad \xi = \xi_h)$$

and

$$\left[\eta = \frac{i}{n} \text{ for } (i = 1, 2, \ldots, 2n); \qquad \xi = \xi_h\right]$$

then the value of $G_m(\xi_h)$ can be calculated from the formula of Clairaut de la Vallée Poussin:[7]

$$G_m(\xi_h) = \frac{1}{n}\sum_{i=1}^{2n-1}\left(\frac{V_{nw}}{V_0}\right)_{i,h}\cos\frac{mi\pi}{2n} + \left[\frac{\left(\frac{V_{nw}}{V_0}\right)_{0,h} + (-1)^m\left(\frac{V_{nw}}{V_0}\right)_{2n,h}}{2n}\right], \quad \text{for } m = 1, 3, \ldots, 2n-1 \quad (40)$$

(B-6) *Calculation of the Changes of Lift and Drag of the Wing Caused by Interference Effects of the Body*

The component along ξ of the perturbation velocity corresponding to the interference effect of the body on the wing is, at the plane of the wing, the sum of: (a) a component corresponding to the potential $\Phi^{(1)}$ and given by

$$u_1 = V_0 \int_{\operatorname{arcosh} x/\alpha y}^{0} f(x - \alpha y \cosh u)\, du$$

where the abscissa x must be measured from the apex of the nose of the body; (b) a component corresponding to the potential Φ' just determined; it is given by

$$u_2 = \partial\Phi'/\partial x = V_0 \sum_m \cos(\pi m\eta/2)\left(\frac{\partial \Phi_m'}{\partial \xi}\right)_{\xi=0} = -V_0\pi \sum_m \cos(\pi m\eta/2)\dot{h}_m(\xi)$$

for the upper surface of the wing, and has the same value but of opposite sign for the lower surface of the wing.

It follows that the pressure change on an element $b^2 d\xi\, d\eta$ of the wing surface is equal to $\Delta p_d = -\rho V_0 \times (u_1 + u_2)$ for the upper surface and $\Delta p_v = -\rho V_0 \times (u_1 - u_2)$ for the lower surface, where ρ is the density of the fluid. Thus the change of lift on such an element which is caused by interference from the body is:

$$d^2\Delta L = b^2 d\xi d\eta(\Delta p_v - \Delta p_d) = 2\rho V_0 u_2 b^2 d\xi\, d\eta = -2\rho V_0^2 \pi b^2 \sum_m \cos\frac{\pi m\eta}{2}\,\dot{h}_m(\xi)\, d\xi\, d\eta$$

At the wing tip, for $\eta = \pm 1$, and m being odd, one always has $d^2\Delta L = 0$. Moreover,

$$\frac{d\Delta L}{d\eta} = -2\rho V_0^2 \pi b^2 \sum_m \cos\frac{\pi m\eta}{2}\, h_m\left(\frac{l}{b}\right)$$

The overall change of lift is therefore

$$\Delta L = -2\rho V_0^2 b^2 \pi \sum_m h_m(l/b) \int_{-1}^{1} \cos(\pi m\eta/2)\, d\eta = 8\rho V_0^2\, b^2 \sum_m (-1)^{(m+1)/2}\left[\frac{h_m(l/b)}{m}\right] \quad (41)$$

In order to keep the wing lift unchanged, it is thus necessary to change the wing incidence an amount $\Delta\beta_2$ given by

$$\Delta\beta_2 = \frac{\Delta L \alpha}{8bl(1/2)\rho V_0^2} = \alpha\frac{\Delta L}{4bl\rho V_0^2}$$

Hence, the increment of wave drag (induced drag), for the same lift, is

$$\Delta D = \Delta\beta_2 L_w = \alpha\left(\frac{\Delta L}{4bl\rho V_0^2}\right)L_w = 2\,\alpha\,\frac{b}{l}\sum_m (-1)^{(m+1)/2}\left[\frac{h_m(l/b)}{m}\right]L_w$$

where L_w is the wing lift. Therefore, the increment of drag coefficient is given by

$$\Delta C_D = 2\alpha\,(b/l)C_L \sum_m (-1)^{(m+1)/2}\,[h_m(l/b)]/m \quad (42)$$

in which C_L is the lift coefficient of the wing.

(C) Numerical Application to Determine the Interference of Wing upon the Body

(C-0) *Description of the Wing-Body Configuration and the Conditions of the Free Stream*

A numerical application has been carried through for the case of a wing-body configuration having the following properties:

Assume the origin of coordinates to be at the tip of the nose of the body, and let λ be the distance between the tip of the nose of the body and the diametral cross section at which the leading edge of the wing joins the body (see Fig. 7). In terms of the nondimensional coordinates $\xi^* = x/\lambda$, $\eta^* = y/\lambda$, and $\zeta^* = z/\lambda$, the body contour is delimited by means of the relations:

$$\eta^* = {}^2/_{10}\xi^* - {}^1/_{10}\xi^{*2}, \text{ in the interval } 0 \leq \xi^* \leq 1 \quad (43)$$

$$\eta^* = 0.1 = R_0/\lambda, \qquad \text{for } 1 \leq \xi^* \leq 1.3 \quad (43')$$

$$\eta^* = 0.068 + 0.049\xi^* - 0.01886\xi^{*2}, \qquad \text{for } 1.3 \leq \xi^* \leq 1.75 \quad (43'')$$

The wing is rectangular and is located in the plane $z = 0$ (see Figs. 7 and 8); its chord length is $l = 1.4R_0$, and the semispan is $b = 4R_0 = 2.86l$.

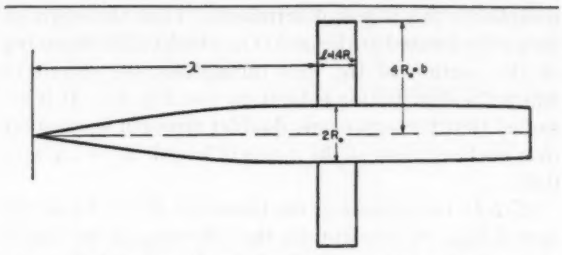

Fig. 7. Wing-body configuration for which the interference effects are calculated by numerical application of the small perturbation theory.

The conditions of the undisturbed flow under consideration are defined as follows:

The angle of attack of the body with respect to the x-axis is $\beta_1 = 8°$.

The Mach Number is $M_\infty = 2$, with the result that $\alpha = \sqrt{M_\infty{}^2 - 1} = 1.732$.

(*C-1-0*) *Calculation of the Perturbation Potential About the Body.*—In order to counteract the potential field related to the velocities induced by the wing, which are normal to the surface of the body, the distribution of singularities along the body axis which ac-

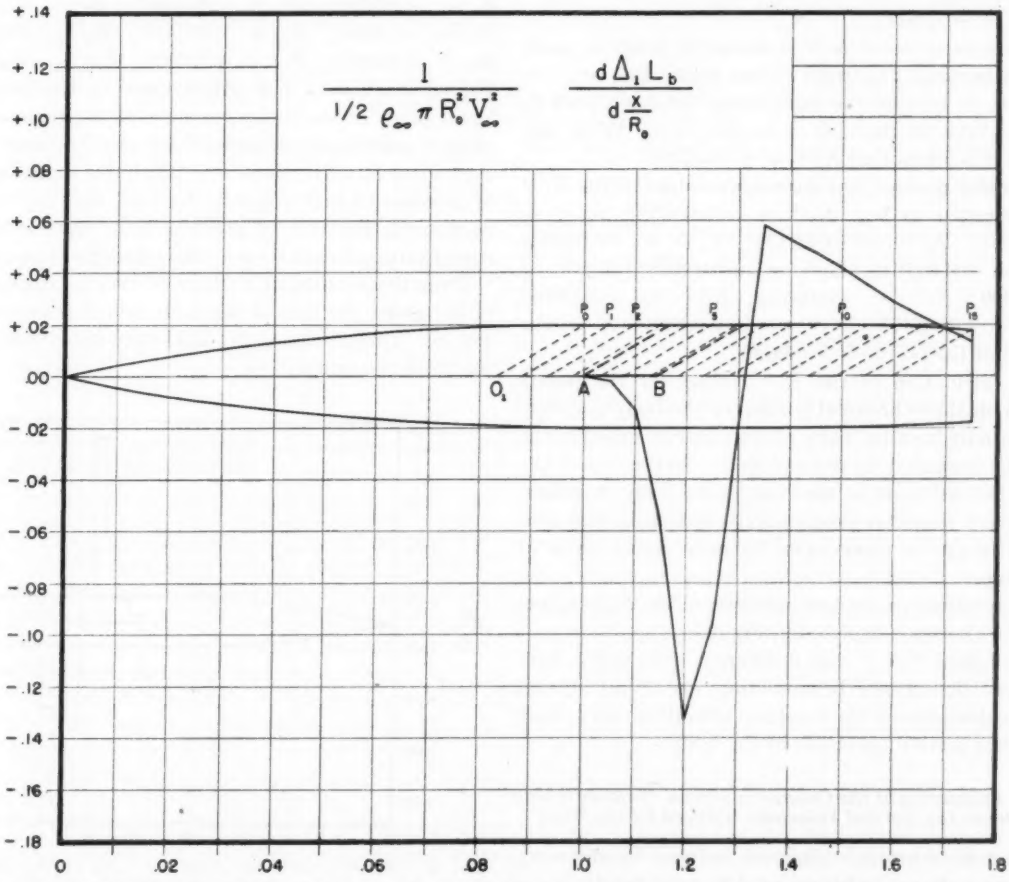

Fig. 8. Distribution along body of increment in lift produced by velocities normal to the body, induced by the wing.

complishes this is now determined. Take the origin of axes to be located at the point O_1, which is the beginning of the portion of the axis throughout the extent of which the distribution is built up (see Fig. 8). It is assumed that the supersonic doublet strength is constant over each segment of the x-axis of length $\Delta^* = \Delta/\lambda = 0.05$.

(C-1-1) Calculation of the Constants $K^{(i)}$.—From the first of Eqs. (8′) one obtains the following, in the case of point P_1 (located on the meridian line that belongs to the plane $\theta = \pi/2$), which possesses the coordinates $\xi^* = 0.2232$, $\zeta^* = 0.10$:

$$\frac{1}{2}(3)K_1^{(1)}\left(\operatorname{arcosh}\frac{2.23}{1.73}+\frac{2.23}{1.73}\sqrt{\left(\frac{2.23}{1.73}\right)^2-1}\right)=$$

$$F_1(2.23) = \frac{-2\beta_2}{\pi}\left[\theta_A - \frac{\sin 2\theta_A}{2}\right]$$

Now we have

$$\sin\theta_A = (\xi^* - \alpha\zeta_0^*)/\alpha\zeta^* = 0.289$$

and, consequently,

$$F_1(2.23) = -0.00146$$

From these values we find that $K_1^{(1)} = -0.000545$.

Analogously, it is found that the next value of $K_1^{(i)}$ is $K_1^{(2)} = -0.00442$.

In determination of $K_1^{(3)}$ it should be borne in mind that neither Eqs. (13) nor (15) are applicable, but it is necessary to employ the expressions involving both θ_A and $\theta_{A'}$ given at the end of Section A-3. With this caution it is found that $K_1^{(3)} = -0.01709$.

In similar manner, the successive values of the $K_1^{(i)}$ are computed to be: $K_1^{(4)} = -0.03652$; $K_1^{(5)} = -0.00631$; $K_1^{(6)} = +0.02124$; $K_1^{(7)} = +0.03636$; $K_1^{(8)} = +0.01701$; $K_1^{(9)} = +0.00868$; $K_1^{(10)} = +0.00399$; $K_1^{(11)} = +0.00112$; $K_1^{(12)} = -0.00068$; $K_1^{(13)} = -0.00177$; $K_1^{(14)} = -0.00238$; $K_1^{(15)}$ (at the end of the body) $= -0.00266$.

The calculation of the $K_1^{(i)}$ values for the points located on the cylindrical portion of the body goes forward rapidly because many of the constants used in the previous steps may be re-employed. In the case of the points located more to the rear on the body, however, the section diameter progressively decreases, and consequently all the terms must be recomputed anew at each step.

The resulting pattern of variation of the $K_1^{(i)}$ values along the x-axis is depicted in Fig. 9.

The values of $K_n^{(i)}$, for n different from unity, have not been determined because they are of no interest in the calculation of the resultant overall action at each diametral section (parallel) of the body.

(C-2) *Evaluation of the Change in Lift on the Body Which Is Due to the Normal Velocities Induced by the Wing*

The field of normal velocities, induced by the wing, produces a change in lift on an element of length, dx, of the body. This increment (or decrement) is given by the relation:

$$\left[\frac{1}{(1/2)\pi R_0^2\rho_\infty V_\infty^2}\right]\left[\frac{d(\Delta_1 L_b)}{d(x/R_0)}\right] = -2\frac{\alpha R}{R_0}\times \int_{\operatorname{arcosh} x/\alpha R}^{0} \dot{f}_1(x-\alpha R\cosh u)\cosh u\,du$$

From this formula we now write:

$$B_n = \left[\frac{1}{(1/2)\pi R_0^2\rho_\infty V_\infty^2}\right]\left[\frac{d(\Delta_1 L_b)}{d(x/R_0)}\right] = 2\alpha\left(\frac{R_n}{R_0}\right)\sum_i K_1^{(i)}\left[\sqrt{\left(\frac{x_n - x_i' - 1}{\alpha R_n}\right)^2 - 1} - \sqrt{\left(\frac{x_n - x_i'}{\alpha R_n}\right)^2 - 1}\right]$$

which applies to the parallel with abscissa x_n and radius R_n. Thus we have:

For the parallel with abscissa $\xi^* = 0.223$:

$$B_1 = 2(1.732)(-0.000545)\sqrt{(2.23/1.73)^2 - 1} = -0.0015$$

For the successive parallels we find: $B_2 = -0.0132$; $B_3 = -0.0550$; $B_4 = -0.1330$; $B_5 = -0.0960$; $B_6 = -0.0193$; $B_7 = +0.0584$; $B_8 = +0.0540$; $B_9 = +0.0480$; $B_{10} = +0.0413$; $B_{11} = +0.0346$; $B_{12} = +0.0282$; $B_{13} = +0.0224$; $B_{14} = +0.01715$; $B_{15} = +0.0126$. The calculations in this case are again easily accomplished because of the reuse of previously calculated constants from step to step; however, after P_6 with abscissa $= 1.3\lambda$ based on the system of coordinates with origin at the nose, the progressively decreasing diameter of cross section requires the recomputation of each term in the equations at each point.

From these values of B_i there evolves the distribution of lift along the axis of the body which is depicted in Fig. 8. The change in lift $\Delta_1 L_b$ may be calculated by means of the summation:

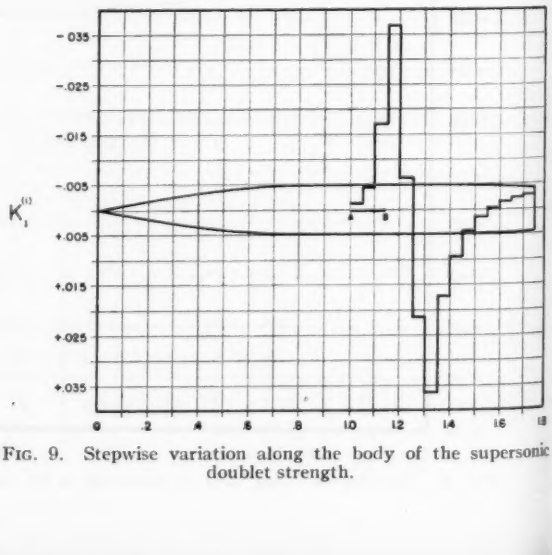

FIG. 9. Stepwise variation along the body of the supersonic doublet strength.

$$\frac{\Delta_1 L_b}{(1/2)\pi R_0^2 \rho_\infty V_\infty^2} = \sum_{i=2}^{15} \frac{B_i + B_{i-1}}{2}\left(\frac{\Delta x}{R_0}\right) + \frac{B_1}{2}\left(\frac{\Delta x}{R_0}\right) = -0.00074$$

If the wing surface, $2bl$, is taken as the reference area, the lift coefficient that corresponds to $\Delta_1 L_b$ turns out to be

$$\Delta_1 C_{Lb} = -0.00074(\pi R_0^2/2bl) = -0.000207$$

(C-3) Computation of the Change in Aerodynamic Moment of the Body Caused by the Normal Velocities Induced by the Wing

The change in aerodynamic moment of the body, taken about the leading edge of the wing, which is due to the normal velocities induced by the wing, is defined as

$$\Delta_1 M_{yb} = -\int_0^{L'} x\,[d(\Delta_1 L_b)/dx]\,dx$$

where the integral is taken over the whole extent, L', of the body axis for which values of $d\,(\Delta_1 L_b)/dx$ different from zero exist. Since the values of $d(\Delta_1 L_b)/dx$ may be assumed to vary linearly between the consecutive parallels of the body, the above indicated integration may be written as

$$\left[\frac{1}{(1/2)\pi R_0^3 \rho_\infty V_\infty^2}\right]\Delta_1 M_{yb} = -\frac{1}{6}\sum_{i=1}^{15}\frac{x_i - x_{i-1}}{R_0} \times (B_i + B_{i-1})\left[\frac{x_i + 2x_{i-1}}{R_0} + \left(\frac{x_i - x_{i-1}}{R_0}\right)\frac{B_i}{(B_i + B_{i-1})}\right]$$

The result of this calculation in the case under consideration is found to be:

$$[1/(1/2)\pi R_0^3 \rho_\infty V_\infty^2]\,\Delta_1 M_{yb} = -0.4268$$

If the reference volume is taken as $2bll$ instead of πR_0^3, then we obtain

$$\left[\frac{1}{(1/2)\rho_\infty 2bl^2 V_\infty^2}\right]\Delta_1 M_{yb} = -0.4268\left(\frac{\pi R_0^2}{2bl^2}\right) = -0.0855$$

(C-4) Determination of the Change in Lift and Moment on the Body Which Is Due to the Longitudinal Component of the Induced Velocities

Since the diametral cross section is constant as far rearward as P_6 (with abscissa = 1.3λ), because $\alpha(R_0 + R_2^*) + l$ reaches back only slightly farther to station 1.313λ, and because the body radius only reduces to $R = 0.998R_0$ at the next calculated point (P_7), it is permissible to use the following simple formula for the increment in lift on the body:

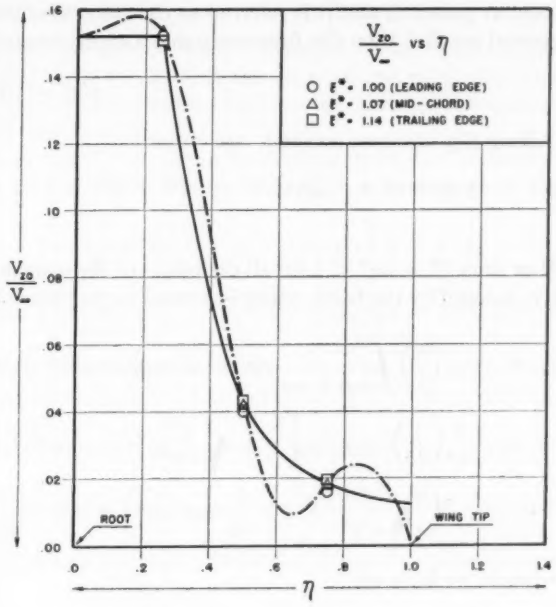

FIG. 10. Body-induced velocities normal to wing.

$$\Delta_2 L_b = \frac{4}{1.73}\left(\frac{\rho_\infty}{2}\right)(V_\infty^2)(0.1396)(2R)(l)$$

so

$$\Delta_2 C_{Lb} = (2.31)(0.1396)(1/4) = 0.0806$$

based on the area $2bl$. The total change in lift on the body due to interference from the wing is, thus,

$$C_{Lb} = -0.0002 + 0.0806 = +0.0804$$

For the case of the moment change due to the longitudinal component of the induced velocity, we use the formula:

$$\Delta_2 M_{yb} = \frac{4(1/2)\rho_\infty V_\infty^2}{\alpha}(\beta_2)(2R)\left(-\frac{l^2}{2} - \frac{\pi\alpha Rl}{4}\right)$$

Thus, the change in moment coefficient, based on the volume $2bl^2$, is:

$$\Delta_2 C_{Myb} = -\frac{4}{\alpha}(\beta_2)\left(\frac{R}{2b}\right)\left[1 + \frac{\pi}{2}(\alpha)\left(\frac{R}{l}\right)\right] = -0.322(1/8)(1 + 1.943) = -0.119$$

When this increment in pitching moment is added to the moment due to the normal component, the total change is found to be:

$$\Delta C_{Myb} = -0.1186 - 0.0855 = -0.289$$

(D) Numerical Application to Show the Interference of Body upon the Wing

(D-0-1) Calculation of the Component of Velocity, Induced by the Body, Which Is Normal to the Plane of the Wing.—In order to determine this velocity component one needs to calculate the function $g(x)$. This function is proportional to the unit intensity of the doublet distribution located along the axis of the body (which is assumed iso-

lated at present), and it is referred to the transverse velocity, $V_\infty \sin \beta_1$. If S denotes the area of an arbitrary general parallel, then this function is given approximately by the formula

$$g(x) = (\beta_1/\pi)(dS/dx)$$

Taking Eq. (43) into account, one obtains

$$g(x - \alpha y \cosh u) = {}^1/_{25}\beta_1\lambda[2\xi^* - 3\xi^{*2} + \xi^{*3} + (-2 + 6\xi^* - 3\xi^{*2})\alpha\eta^* \cosh u + (-3 + 3\xi^*)\alpha^2\eta^{*2}\cosh^2 u - \alpha^3\eta^{*3}\cosh^3 u] \quad (44)$$

Now since $\xi^* - \alpha\eta^* < 1$ for all the points of the wing under consideration, it follows that the component of velocity, induced by the body, which is normal to the plane of the wing is given everywhere by

$$v_{z0} = -v_\infty \left(\frac{\alpha}{\gamma}\right) \int_{\text{arccosh } \xi^*/\alpha\eta^*}^{0} g(x - \alpha y \cosh u) \cosh u \, du$$

$$= -\frac{\alpha}{\eta^*}\left(\frac{1}{25}\right)(v_\infty)(\beta_1)\left[-A_1\sqrt{\frac{\xi^{*2}}{\alpha^2\eta^{*2}} - 1} - \alpha\eta^* A_2\left(\frac{1}{2}\operatorname{arccosh}\frac{\xi^*}{\alpha\eta^*} + \frac{1}{2}\frac{\xi^*}{\alpha\eta^*}\sqrt{\frac{\xi^{*2}}{\alpha^2\eta^{*2}} - 1}\right) - \alpha^2\eta^{*2}A_3 \times \left(\frac{3}{4}\sqrt{\frac{\xi^{*2}}{\alpha^2\eta^{*2}} - 1} + \frac{1}{12}\sinh 3u^*\right) + \alpha^3\eta^{*3}\left(\frac{3}{8}\operatorname{arccosh}\frac{\xi^*}{\alpha\eta^*} + \frac{1}{2}\frac{\xi^*}{\alpha\eta^*}\sqrt{\frac{\xi^{*2}}{\alpha^2\eta^{*2}} - 1} + \frac{1}{32}\sinh 4u^*\right)\right] \quad (45)$$

wherein we have set

$$A_1 = 2\xi^* - 3\xi^{*2} + \xi^{*3}; \qquad A_2 = -2 + 6\xi^*; \qquad A_3 = -3 + 3\xi^* \quad (45')$$

while

$$\sinh 3u^* = \sqrt{(\xi^{*2}/\alpha^2\eta^{*2}) - 1}\,[4(\xi^{*2}/\alpha^2\eta^{*2}) - 1]$$

and

$$\sinh 4u^* = 8(\xi^{*3}/\alpha^3\eta^{*3})\sqrt{(\xi^{*2}/\alpha^2\eta^{*2}) - 1} - 4(\xi^*/\alpha\eta^*)\sqrt{(\xi^{*2}/\alpha^2\eta^{*2}) - 1}$$

For the selected values of β_1 and α in this problem, the following values of v_{z0}/v_∞ are obtained at points on the wing, by use of Eq. (45):

	At the Leading Edge: $\xi^* = 1$			At the Wing Axis: $\xi^* = 1.07$			At the Trailing Edge: $\xi^* = 1.14$		
η^*	0.1	0.2	0.3	0.1	0.2	0.3	0.1	0.2	0.3
$\frac{v_{z0}}{v_\infty}$	0.151	0.0400	0.0164	0.152	0.0417	0.0182	0.150	0.0426	0.0196

These values of v_{z0}/v_∞ are plotted in Fig. 10. Since the differences between the values of v_{z0}/v_∞ at each η^*, for any of the three values of ξ^* considered, are extremely small, a single diagram has been selected as defining the law of variation of the velocity components normal to the plane of the wing. This diagram is shown in solid line on Fig. 10.

(D-0-2) Determination of the Harmonic Components of the Velocity Perturbation Produced by the Body.—Through use of the graph of v_{z0}/v_∞ presented in Fig. 10, the harmonic components of the velocity, perturbed by the body, which is directed normal to the plane of the wing are now computed. The formula of Clairaut de la Vallée Poussin may be written in this case as:

$$G_m = \frac{1}{4}\sum_{i=1}^{7}\left(\frac{v_{z0}}{v_\infty}\right)_i \cos\frac{mi\pi}{8} + \left[\left(\frac{v_{z0}}{v_\infty}\right)_0 + (-1)^m\left(\frac{v_{z0}}{v_\infty}\right)_8\right]\Big/8, \qquad (\text{for } m = 1, 3, 5, 7) \quad (46)$$

where we have let $(v_{z0}/v_\infty)_0$ and $(v_{z0}/v_\infty)_i$ be the values of v_{z0}/v_∞ at the points $\eta = 0$, and $\eta = 0.25\,i$ for $i = 1$ to 8. These coefficients describe a function v_{z0}/v_∞ which is derived from the graph of Fig. 10 by extending it antisymmetrically with respect to the straight line $\eta = 1$ and which is then approximated by a trigonometric polynomial of four cosine terms.

Since we have:

$\eta =$	0	0.25	0.5	0.75	1	1.25	1.5	1.75	2
$\frac{v_{z0}}{v_\infty} =$	0.151	0.151	0.041	0.018	0	−0.018	−0.041	−0.151	−0.151

it follows that $G_1 = +0.1254$, $G_3 = +0.0438$, $G_5 = +0.0027$, and $G_7 = -0.0210$ The curve defined by Eq. (22), with G_m values just derived, is depicted in Fig. 10 by means of a dashed line.

D-1) Calculation of the Potential for the Perturbation About the Wing

In order to counteract the component of velocity, induced by the body, which is normal to the wing, a superimposed velocity field is to be determined. This is accomplished by dividing the chord of the wing into three small intervals of equal magnitude, Δ. In each of these intervals it is assumed that the function $h_m(\xi)$, contained in the expression for the potential of the velocity field, will vary linearly.

(D-1-1) Calculation of the Constants $H_1^{(i)}$.—The constant value of $dh_1/d\xi$ in the first small interval is denoted by $H_1^{(1)}$. Now in this case $\Delta = l/3b = 0.117$; $k = \pi/2$; and therefore $(k/\alpha)\Delta = 0.106$; it follows that:

$$H_1^{(1)}\left[\pi(1.73)J_0(0.106) + \pi\left(\frac{\pi}{2}\right)(0.117)J_1(0.106) + 2\pi\left(\frac{\pi}{2}\right)0.117\sum_{n=1}^{n=\infty} J_{2n+1}(0.106)\right] = -0.125$$

But we have:[9] $J_0(0.106) = 0.997$; $J_1(0.106) = 0.053$; while all of the $J_{2n+1}(0.106)$ are negligible, so that $H_1^{(1)} = -0.0230$.

In an analogous manner, we proceed by letting $H_1^{(2)}$ denote the constant value of $dh_1/d\xi$ in the second small interval, and we find that $H_1^{(2)} = -0.0228$, by making use of the fact that $G_1(\Delta) = G_1(2\Delta)$ in the case under consideration, because G_m is independent of ξ here.

Likewise we find that $H_1^{(3)} = -0.0225$. In the latter two calculations it is also found that the $J_{2n+1}(0.212)$ and $J_{2n+1}(0.317)$ are negligible for $n = 1$ or more.

(D-1-2) Calculation of the Constants $H_3^{(i)}$.—Now in this case $k = 3\pi/2$; $k\Delta/\alpha = 0.317$; and we find that $H_3^{(1)} = -0.0079$.

For the value of $H_3^{(2)}$ it is necessary to evaluate $J_3(0.635)$, which may be accomplished by use of the recurrence formula

$$J_{n-1}(x) + J_{n+1}(x) = (2n/x)J_n(x)$$

Here we have $J_0(0.635) = 0.902$ and $J_1(0.635) = 0.302$, and thus $J_2(0.635) = 0.049$, and then $J_3(0.635) = 0.005$. With these values of J_n we find that $H_3^{(2)} = -0.0073$.

In the case of $H_3^{(3)}$ it is necessary to evaluate $J_3(0.952)$, but the other J_{2n+1} for $n > 1$ are disregarded. It is found that $H_3^{(3)} = -0.0064$.

(D-1-3) Calculation of the Constants $H_5^{(i)}$.—Here $k = 5\pi/2$; $k\Delta/\alpha = 0.529$, and we find that $H_5^{(1)} = -0.00046$; $H_5^{(2)} = -0.00037$; and $H_5^{(3)} = -0.00025$.

(D-1-4) Calculation of the Constants $H_7^{(i)}$.—Here $k = 7\pi/2$; $k\Delta/\alpha = 0.741$, and we find that $H_7^{(1)} = +0.00339$; $H_7^{(2)} = +0.00223$; and $H_7^{(3)} = +0.00085$.

(D-1-5) Approximate Determination of $H_m^{(i)}$ *by Means of Eq. (39).*—It seems to be in order to compare the results just obtained with those that would be computed by means of Eq. (39) in the case of an infinitesimally narrow chord wing.

Since G_m is independent of ξ in this example, Eq. (39) reduces to:

$$h_m(\xi) = -(\sqrt{2}/k\pi)G_m(0)\sin(k\xi/\alpha\sqrt{2})$$

and thus we know that

$$dh_m(\xi)/d\xi = -(1/\pi\alpha)G_m(0)\cos(k\xi/\alpha\sqrt{2})$$

Then if we assume that the values of $H_m^{(i)}$ are those of $dh_m/d\xi$ which obtain at the midpoint of each of the three small intervals previously considered, it is found that:

$H_1^{(1)} = -0.0230$;	$H_1^{(2)} = -0.0229$;	$H_1^{(3)} = -0.0227$
$H_3^{(1)} = -0.0080$;	$H_3^{(2)} = -0.0076$;	$H_3^{(3)} = -0.0068$
$H_5^{(1)} = -0.00048$;	$H_5^{(2)} = -0.00042$;	$H_5^{(3)} = -0.00029$
$H_7^{(1)} = +0.00372$;	$H_7^{(2)} = +0.00272$;	$H_7^{(3)} = +0.00100$

It appears from the above that the agreement between the results obtained by recourse to the approximate formula and those computations previously carried out is fairly good for the smaller values of ξ. In fact, in many cases the approximate solution should be sufficiently accurate for ordinary purposes, with a consequent great saving in time.

(D-2-0) Lift Distribution Along the Chord for the Root Section.—The above-determined values of $H_m^{(i)}$ make it possible to calculate without further ado the chordwise lift distribution for the center profile ($\eta = 0$). Let Δp denote the pressure difference between the lower and upper surface of an arbitrary general profile

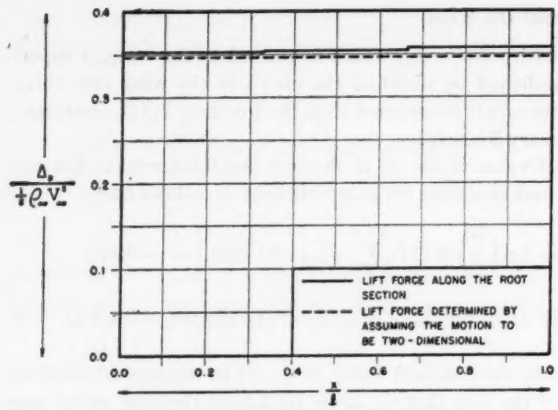

FIG. 11. Increment in local lift coefficient for the root section caused by interference from the body.

or chordwise section. Then

$$\frac{\Delta p}{(1/2)\rho_\infty V_\infty{}^2} = \left[\frac{1}{(1/2)\rho_\infty V_\infty{}^2 b^2}\right]\left(\frac{d^2\Delta L}{d\xi\, d\eta}\right) = -4\pi \sum_m \cos\left(\frac{\pi m}{2}\eta\right) \dot{h}_m(\xi)$$

so that for $\eta = 0$, we arrive at

$$\Delta p/(1/2)\rho_\infty V_\infty{}^2 = -4\pi \sum_m \dot{h}_m(\xi)$$

Consequently, it is found that:

$$\begin{aligned}\Delta p/(1/2)\rho_\infty V_\infty{}^2 &= 0.3507 \text{ (in the first small interval)}\\ &= 0.3546 \text{ (in the second small interval)}\\ &= 0.3551 \text{ (in the third small interval)}\end{aligned}$$

When these data are plotted, the graph of Fig. 11 results. It is worth while to note that the value of $\Delta p/(1/2)\rho_\infty V_\infty{}^2$, calculated by use of the value v_{z0}/v_∞ which exists at the center section (root chord), and as though the motion were two-dimensional, comes out to be:

$$\frac{\Delta p}{(1/2)\rho_\infty V_\infty{}^2} = \left(\frac{4}{\sqrt{M_\infty{}^2 - 1}}\right)\left(\frac{v_{z0}}{v_\infty}\right)_0 = 0.349$$

This close figure is not surprising because the value of v_{z0}/v_∞ is almost constant over a fairly wide range of η (see Fig. 10).

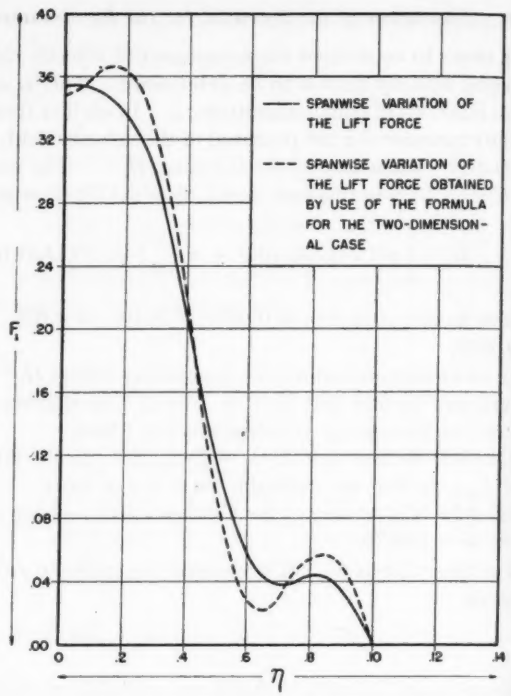
SPANWISE VARIATION OF THE LIFT FORCE
SPANWISE VARIATION OF THE LIFT FORCE OBTAINED BY USE OF THE FORMULA FOR THE TWO-DIMENSIONAL CASE

FIG. 12. Spanwise distribution of the increment in lift produced by interference from the body.

(*D-2-1*) *Spanwise Lift Distribution.*—The spanwise lift distribution is defined by:

$$\left[\frac{1}{(1/2)\rho_\infty V_\infty{}^2(l)(b)}\right]\frac{d(\Delta L)}{d\eta} = -4\pi\,\frac{b}{l}\sum_m \cos\left(\frac{\pi m\eta}{2}\right) h_m\left(\frac{l}{b}\right)$$

Now since $4\pi(b/l) = 35.9$; while $h_1(l/b) = -0.00796$, $h_3(l/b) = -0.00251$, $h_5(l/b) = -0.00013$, and $h_7(l/b) = +0.00076$; and, if we let $F(\eta) = \sum_m h_m(l/b) \cos(\pi m\eta/2)$ and let $F_1(\eta) = -4\pi(b/l)F(\eta)$, then the following table may be constructed:

η =	0	0.1	0.25	0.3	0.4	0.5	0.75
$F(\eta)$ =	−0.00984	−0.00985	−0.00897	−0.00814	−0.00577	−0.00323	−0.00113
$F_1(\eta)$ =	0.354	0.354	0.322	0.292	0.207	0.116	0.0406

These data determine the graph of spanwise lift distribution which is depicted in Fig. 12. It is appropriate to compare this graph with the one that would be obtained if the lift at each profile section along the span were calculated by means of the equation for the two-dimensional case and based on the use of the value of the local angle of attack, v_{z0}/v_∞. The ordinate values of this curve would therefore be given by

$$F_1{}^*(\eta) = (4/\sqrt{M_\infty{}^2 - 1})(v_{z0}/v_\infty) = 2.309\ (v_{z0}/v_\infty)$$

(in the example being investigated). This second curve, which is a proportionally scaled-up representation of v_{z0}/v_∞, is also drawn in on Fig. 12. The difference is, on the whole, not appreciable.

(D-2-2) Computation of the Change in Total Wing Lift.—The total change in lift of the wing is given by Eq. (41) and is now evaluated to be:

$$\frac{\Delta L}{(1/2)\rho_\infty V_\infty{}^2(2bl)} = 8\frac{b}{l}\left[-h_1\left(\frac{l}{b}\right)+\frac{1}{3}h_3\left(\frac{l}{b}\right)-\frac{1}{5}h_5\left(\frac{l}{b}\right)+\frac{1}{7}h_7\left(\frac{l}{b}\right)\right] = +0.166$$

Thus the total change in lift coefficient of the wing-body configuration is:

$$C_L = 0.166 + 0.080 = +0.246$$

This last calculation shows that the increment of lift on the body is about half as large as that on the wing (the latter has included an induced effect in the region occupied by the body). Actually, however, the increase of lift is probably less than that just calculated because: first, the lift of the body produced by the longitudinal velocity component induced by the wing is smaller than the lift on that portion of the wing which is covered by the body; second, the stream impinging upon the wing, considered as a whole or sectionally, has a velocity less than V_∞ as a result of the longitudinal field of flow about the body. This alteration of the flow is not taken into account in the linear theory.

(D-3) Calculation for the Change in Aerodynamic Moment of the Wing, Taken About the Leading Edge

The aerodynamic moment of the wing which is induced on it by the presence of the body is (where the leading edge of the wing is assumed as the axis about which the moments are taken):

$$\Delta M_y = 2\pi\rho_\infty V_\infty{}^2(b^3)\sum_m \int_{-1}^{+1}\cos\left(\frac{\pi m\eta}{2}\right)d\eta\int_0^{l/b}\dot{h}_m(\xi)(\xi)\,d\xi$$

$$= 2\pi\rho_\infty V_\infty{}^2(b^3)\sum_m\left(\frac{-4}{m\pi}\right)(-1)^{(m+1)/2}\left[\left(\frac{l}{b}\right)h_m\left(\frac{l}{b}\right)-\frac{\Delta^2}{2}\left(5H_m{}^{(1)}+3H_m{}^{(2)}+H_m{}^{(3)}\right)\right]$$

and upon substitution of the previously obtained values of $H_m{}^{(i)}$ it is found that $\Delta M_y/(1/2)\rho_\infty V_\infty{}^2(b^3) = -0.0208$; and, if the reference volume is taken as $2bl^2$, we have $\Delta C_{My_w} = -0.0848$. Then the total change in the moment coefficient, taken with respect to the leading edge of the wing, is $\Delta C_{My} = -0.085 - 0.204 = -0.289$.

It may be noted that the pitching moment due to interference of the body upon the wing (-0.0848) is about equal in magnitude to the increment in pitching moment due to the *normal* component of the velocity induced by the wing upon the body (-0.0855), but the increment due to the *longitudinal* component (-0.1186) overshadows the other contributions.

(E) Calculation of the Optimum Angle of Wing Setting

(E-1) Derivation of Formula Giving Optimum Angle of Attack for the Wing

It may be assumed that a small deviation between the plane of the wing and the (x, y)-plane does not alter appreciably the equations given in the foregoing analysis. Thus it may be observed that it is possible to determine the optimum value for the angle of wing setting, i.e., the one that gives the minimum value of the total drag, for a given value of the lift coefficient, C_L, of the wing-body system; however, the results should be considered as merely indicative of the precise optimum.

Let the drag coefficient of the body and that of the wing, both based on the same reference area, be denoted by:

$$C_{Db} = C_{D_0} + C_{Lb}\beta_1, \qquad C_{Dw} = \beta_2 C_{Lw}$$

respectively. The corresponding lift coefficients may be expressed as:

$$C_{Lb} = (\Delta C_{Lb}/\Delta\beta_1)\,\beta_1 + a_1\beta_2$$

and

$$C_{Lw} = (4/\sqrt{M_\infty{}^2-1})\beta_2 + a_2\beta_1$$

For the specific case under consideration we have

$$a_1 = -0.000207/0.1396 = -0.00148$$
$$a_2 = +0.1659/0.1396 = +1.188$$

The coefficient of total lift, therefore, becomes:

$$C_L = A_1\beta_1 + A_2\beta_2$$

where

$$A_1 = (\Delta C_{Lb}/\Delta\beta_1) + a_2$$
$$A_2 = (4/\sqrt{M_\infty{}^2-1}) + a_1$$

and the coefficient of total drag is:

$$C_D = C_{D_0} + A_{11}(\beta_1{}^2) + A_{12}\beta_1(\beta_2) + A_{22}(\beta_2{}^2)$$

where

$$A_{11} = \frac{\Delta C_{Lb}}{\Delta\beta_1}, \qquad A_{12} = a_1 + a_2, \qquad A_{22} = \frac{4}{\sqrt{M_\infty{}^2-1}}$$

We may observe that

$$\beta_1 = (C_L/A_1) - (A_2/A_1)\beta_2$$

and this expression, when inserted into the formula for C_D, produces:

$$C_D = C_{D_0} + A_{11}\left[\frac{C_L}{A_1} - \frac{A_2}{A_1}(\beta_2)\right]^2 + A_{12}\left[\frac{C_L}{A_1} - \frac{A_2}{A_1}(\beta_2)\right]\beta_2 + A_{22}\beta_2^2$$

and thus

$$\frac{dC_D}{d\beta_2} = -2A_{11}\left[\frac{C_L}{A_1} - \frac{A_2}{A_1}(\beta_2)\right]\left(\frac{A_2}{A_1}\right) + A_{12}\left[\frac{C_L}{A_1} - \frac{A_2}{A_1}(\beta_2)\right] - A_{12}\left(\frac{A_2}{A_1}\right)(\beta_2) + A_{22}(\beta_2)$$

and when this is set equal to zero, there is obtained an expression for the optimum β_2 which is:

$$\beta_2 = \frac{C_L}{A_1}\left[\frac{2A_{11}(A_2/A_1) - A_{12}}{2A_{11}(A_2/A_1)^2 - 2A_{12}(A_2/A_1) + 2A_{22}}\right] \quad (47)$$

Then, by examining the terms in $d^2C_D/d\beta_2^2$, it is found that $d^2C_D/d\beta_2^2$ is > 0, because $A_{22} - A_{12}(A_2/A_1)$ is > 0, as may be seen from

$$A_{22} - A_{12}\left(\frac{A_2}{A_1}\right) = \frac{4}{\sqrt{M_\infty^2 - 1}}\left\{\frac{[(\Delta C_{Lb}/\Delta\beta_1) - a_1]}{[(\Delta C_{Lb}/\Delta\beta_1) + a_2]}\right\} - \frac{a_1(a_1 + a_2)}{(\Delta C_{Lb}/\Delta\beta_1) + a_2}$$

Consequently, the value of β_2 given in Eq. (47) corresponds to an actual minimum of C_D.

(E-2) *Optimum Angle of Wing Setting—Numerical Results*

The optimum angle of wing setting is obtained, therefore, as

$$\beta_1 - \beta_2 = \frac{C_L}{A_1}\left\{1 - \left(\frac{A_1 + A_2}{A_1}\right) \times \left[\frac{2A_{11}(A_2/A_1) - A_{12}}{2A_{11}(A_2/A_1)^2 - 2A_{12}(A_2/A_1) + 2A_{22}}\right]\right\}$$

If we assume that the slope of the lift curve[3] for the body is 2 (approximately), where the lift coefficient is based on the maximum cross-sectional area, then in the present case $\Delta C_{Lb}/\Delta\beta_1 = 0.561$; and therefore $\beta_1 - \beta_2 = 0.458C_L$.

For instance, if $C_L = 0.3$, then $\beta_1 - \beta_2 = 0.1375$ $(= 7^\circ\ 53')$ and $\beta_1 = 0.1522$ $(= 8^\circ\ 43')$, and, consequently, $\beta_2 = 0.0147$ $(= 0^\circ\ 50')$.

The optimum value of the angle of wing setting just found is probably somewhat high because of the sources of error already noted. The result just elicited, nevertheless, must be regarded as a clear indication of how the body and the wing must be situated in order to reduce the drag, for a given lift, on a specific wing-body system.

References

[1] von Kármán, Th., and Moore, N. B., *The Resistance of Slender Bodies Moving with Supersonic Velocities with Special Reference to Projectiles*, Trans. of A.S.M.E., Vol. 54, pp. 303–310, 1932.

[2] Ferrari, C., *Campi di Corrente Ipersonora Attorno a Solidi di Rivoluzione*, L'Aerotecnica, Vol. 17, pp. 507–518, 1937.

[3] Tsien, H.-S., *Supersonic Flow Over an Inclined Body of Revolution*, Journal of the Aeronautical Sciences, Vol. 5, No. 12, pp. 480–483, 1938.

[4] Lamb, H., *Hydrodynamics*, 6th Ed., p. 527; Cambridge University Press, London, 1932.

[5] Goursat, E., *Cours d'Analyse Mathématique*, Vol. III, p. 152; Gauthier-Villars, Paris, 1933.

[6] Lamb, H., *Hydrodynamics*, 6th Ed., pp. 57 and 111; Cambridge University Press, London, 1932.

[7] Tonelli, L., *Serie Trigonometriche*, p. 148; Casa Editrice Nicola Zanichelli, Bologna, 1928. Or, Carse, G. A., and Shearer, G., *A Course in Fourier Analysis and Periodogram Analysis*, p. 15; G. Bell and Sons, London, 1915.

[8] Kirkby, S., and Robinson, A., *Wing-Body Interference at Supersonic Speed*. College of Aeronautics Report No. 7, April, 1947, The College of Aeronautics, Cranfield, Bedfordshire.

[9] Jahnke, E., and Emde, F., *Tables of Funktions and Formulae and Curves (Funktionentafeln mit Formeln und Kurven)*, p. 156 ff.; B. G. Teubner, Leipzig, 1933. Reprinted by Dover Publications, New York City, 1943.

Notice to Contributors

Manuscripts submitted for publication *must be* double- or triple-spaced originals. There should be wide margins on both sides of the sheets and triple spacing around formulas to allow for the marking of directions for the printer.

Original drawings (jet black India ink on white paper or tracing cloth) should accompany the manuscript. *(Blueprints are not acceptable.)* Photographs *must be* on glossy white paper.

Only the simplest formulas should be typewritten; all others should be carefully written in pen and ink. The difference between capital and lower-case letters and Greek symbols should be clearly distinguished.

See the Inside Back Cover of this issue for further details.

Problem Types in the Theory of Perfectly Plastic Materials*,†

W. PRAGER‡
Brown University

ABSTRACT

Typical problems of the theory of perfectly plastic materials are discussed for the example given by the structure shown in Fig. 1. A simple graphical representation is developed which facilitates the study of the states of stress and residual stress produced by slowly varying the load.

For monotonically increasing load, three domains of mechanical behavior are defined: elastic deformation, contained plastic deformation, and unrestricted plastic flow. In the domain of contained plastic deformation the instantaneous stresses in the structure depend only on the instantaneous load and can be found from the minimum principle of Haar and von Kármán.

However, if unloading is permitted, the stresses depend on the complete history of loading, and the principle of Haar and von Kármán must be replaced by a minimum principle recently developed by H. J. Greenberg.

Cases in which the precise loading program is known beforehand are not often encountered in engineering. As a rule, only the extremes are known between which the load will vary. Under certain conditions, the structure will then "shake down" to a state of residual stress such that all further variations of the load between the given extremes are supported in a purely elastic manner. This "state of residual stress" is independent of the precise program of loading. Conditions for the existence of such a state of residual stress are discussed, and a minimum principle is conjectured from which this state may be determined.

Finally, structural stability in the plastic range is discussed. It is pointed out that the customary formulation of the stability problem for conservative systems (elastic range) is not adequate for nonconservative systems (plastic range).

ANY METHOD of theoretical or experimental stress analysis is based on a stress-strain law. Hooke's law is generally accepted as an adequate basis for stress analysis in the elastic range. In the plastic range, however, no stress-strain law has found equally general acceptance. The selection of a stress-strain law adequate for the treatment of a specific problem is therefore important. This selection is facilitated by a classification of the problems encountered in the theory of plasticity.

In the following, such a classification of problems is attempted for plastic materials that do not exhibit strain-hardening (perfectly plastic materials). To simplify the mathematical work as much as possible, the various problem types will be discussed for the example given by the system shown in Fig. 1. The two-force members OA, OB, OC join the point O to the fixed points A, B, C. The system is symmetric with respect to the vertical OB, and the load P is acting along this axis of symmetry. The subscripts 1, 2, 3 will be used to refer to the bars OA, OB, OC, respectively, and the forces acting in these bars will be denoted by S_1, S_2, S_3. On account of the symmetry of the system, $S_1 = S_3$.

Consider, first, the mechanical behavior of the system in the elastic range. The elastic strain energy of the system is given by an expression of the form

$$E = kS_1^2 + KS_2^2 \tag{1}$$

where the positive constants k and K depend on the dimensions of the bars. A state of stress in the system (i.e., a set of values S_1, S_2) may be represented by the point with the rectangular coordinates

$$x = S_1\sqrt{k}, \qquad y = S_2\sqrt{K} \tag{2}$$

(see Fig. 2). This point will be called the "force point" and will be designated by F in Fig. 2. According to Eq. (1) the elastic strain energy of the system is then represented by the square of the distance of the force point from the origin.

Equilibrium at O requires that $S_1\sqrt{2} + S_2 = P$ or

$$x\sqrt{2/k} + y\sqrt{1/K} = P \tag{3}$$

For a given value of P, this equation represents a straight line L in the x, y plane. This line will be called the "equilibrium line"; its distance from the origin depends on the intensity of the load P, but its slope is

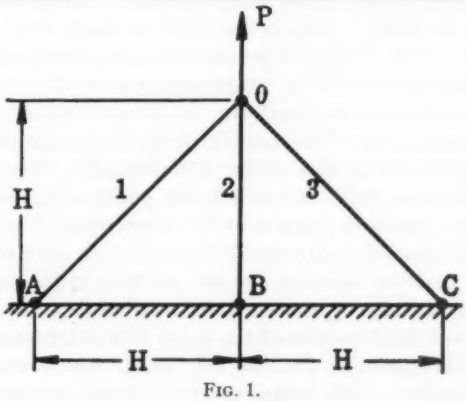

FIG. 1.

Received February 25, 1948.

* This paper was presented at the Symposium on Plasticity held at Brown University on February 9–10, 1948, under the joint sponsorship of the Office of Naval Research and the Bureau of Ships (Contract N7onr-358).

† The author is indebted to F. R. Shanley for valuable suggestions concerning the discussion of structural stability in the plastic range.

‡ Professor of Applied Mechanics.

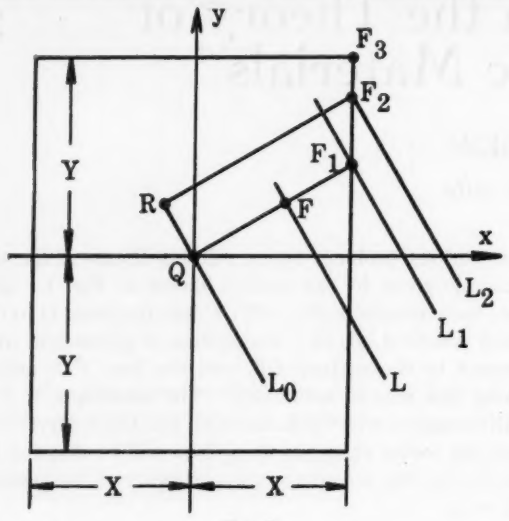

FIG. 2.

independent of P. Any point on this line represents forces S_1 ($= S_3$) and S_2, which are in equilibrium with the given load. According to the principle of minimum strain energy, the state of stress actually produced in the elastic system by the given load corresponds to a smaller value of the strain energy than any other state satisfying the condition of equilibrium. Thus, the actual force point F is the foot of the perpendicular from the origin on the equilibrium line. If the load is increased, the equilibrium line moves away from the origin, maintaining its direction. Accordingly, the force point moves along a straight line through the origin. This line will be called the "line of elastic states."

Consider next the plastic behavior of the system. If the bars are made of a perfectly plastic material with equal yield limits in tension and compression, the absolute values of the forces S_1 ($= S_3$) and S_2 cannot exceed certain yield values. If X and Y denote the corresponding values of x and y, the force point cannot move outside the "yield rectangle" with the sides $x = \pm X$, $y = \pm Y$. As the load is increased starting from zero, the force point moves along the line of elastic states until it reaches a side of the yield rectangle—e.g., the side $x = X$. In Fig. 2 the corresponding force point is denoted by F_1 and the equilibrium line by L_1. If the load is further increased, the bars 1 and 3 yield under constant stress. This means that the force point moves along the side $x = X$ of the yield rectangle. When the equilibrium line has reached the position L_2, for instance, the force point is at the intersection F_2 of this equilibrium line with the line $x = X$. In spite of the fact that the bars OA and OC are now in the plastic state, their elongations remain restricted because the vertical displacement of the point O is determined by the elongation of the bar OB, which is still stressed elastically. Only when the force point reaches the vertex F_3 of the yield rectangle will large plastic elongations become possible.

For monotonically increasing load, three domains of mechanical behavior must therefore be distinguished: *elastic deformation* (Fig. 2, segment QF_1, including end points); *contained plastic deformation* (segment F_1F_3, excluding end points); and *unrestricted plastic flow* (point F_3). In the Theory of Structures only the first two domains are of interest, because large deformations cannot be tolerated. In the study of technological forming processes, on the other hand, only the third domain is of importance, because large deformations are desired here.

Problems of contained plastic deformation have much in common with problems in elasticity, whereas problems of unrestricted plastic flow are closer to problems in fluid dynamics. Accordingly, different theories of plasticity were developed in these two fields of application. The theories of plastic deformation (Haar and von Kármán,[1] Hencky[2]) aim at problems of contained plastic deformation; the theories of plastic flow (Saint Venant,[3] von Mises,[4] Prandtl and Reuss[5]), at problems of unrestricted plastic flow. The stress-strain relations of the former involve the strain itself; those of the latter, only the velocity strain.

As Haar and von Kármán[1] have pointed out, the principle of minimum strain energy of the Theory of Elasticity can easily be modified so as to apply to problems of contained plastic deformation. Indeed, the point F_2 in Fig. 2 is that point on the equilibrium line L_2 which is nearest to the origin without falling outside the yield rectangle. This agrees with the hypothesis of Haar and von Kármán, according to which *the actual state of stress corresponds to a smaller value of the elastic strain energy than any other equilibrium state of stress which satisfies the boundary conditions (prescribed surface stresses) and does not violate the yield condition.*

So far, it has been assumed that the load P increases monotonically. Suppose, now, that the load is decreased after the state of stress represented by the point F_2 in Fig. 2 has been reached. For unloading of a two-force member, the decreases in load and elongation are related by Hooke's law. Accordingly, unloading makes the force point move along a parallel to the line of elastic states. In particular, unloading from the state of stress represented by F_2 in Fig. 2 makes the force point move along F_2R. At the instant when the load is completely removed, the force point reaches the position R on the equilibrium line L_0 through the origin. The point R therefore represents the residual forces after complete unloading from F_2; it will be called the "residual force point."

From the preceding it follows that to each force point on the segment F_1F_3 there corresponds a different residual force point. In other terms, *the residual force point keeps moving along L_0 as long as the permanent elongations of the bars S_1 and S_3 vary but remains station-*

ary whenever these permanent elongations remain unchanged.

If unloading is admitted, the aforementioned modified principle of minimum strain energy is no longer valid. It must be replaced by another minimum principle, the general form of which has recently been established by H. J. Greenberg (in a paper that is to appear in the *Quarterly of Applied Mathematics*). Applied to the example considered here and expressed in the terminology developed above, this principle takes the following form: *As the equilibrium line undergoes a translation in accordance with the variation of the load, the force point describes the shortest path compatible with the conditions that it must remain on the equilibrium line and not leave the yield rectangle.* Whereas the principle of Haar and von Kármán establishes a direct relation between the instantaneous load and the corresponding stresses as they arise during the first loading of the structure, Greenberg's principle establishes a relation between the rate of increase of the load and the corresponding rates of increase of the stresses in the structure. For plastic materials with strain-hardening, similar variational principles have been discussed by Prager[6] and, more recently, by Hodge and Prager.[7]

When unloading has occurred, the state of stress in the structure no longer depends on the instantaneous load alone but also depends on the complete history of loading. Unfortunately, cases in which the precise loading program is given beforehand are not often encountered in engineering. As a rule, only the extremes between which the load will vary are known, but the precise manner of variation is not known. In Fig. 3, let L and L^* be the lines of equilibrium corresponding to the extreme loads. If the structure is first loaded in tension up to the extreme load represented by the line L, then unloaded and loaded in compression up to the extreme load represented by the line L^*, the force point describes the path $QF_1F_2F_3F_4$. As the structure is subjected to further cycles of loading, the force point traces the parallelogram $F_4F_5F_2F_3$. During each of these loading cycles plastic deformations occur while the force point describes the segments F_5F_2 and F_3F_4.

If, on the other hand, the extreme compressive load is represented by the line of equilibrium through F_3 (line $L^{*\prime}$) the force point describes the path $QF_1F_2F_3$ during the first loading and moves along F_3F_2 from F_3 to F_2 and back to F_3 during further loading cycles. No plastic deformations occur during these cycles and the residual force point remains stationary at R. In other terms, the system "shakes down" to a state of residual stress such that all further variations of the load (between the given extremes) are supported in a purely elastic manner. This state of residual stress to which the system will eventually shake down under loads that vary between given extremes is independent of the precise program of loading.

General conditions for the occurrence of "shake down" in trusses have been discussed by Bleich[8] and

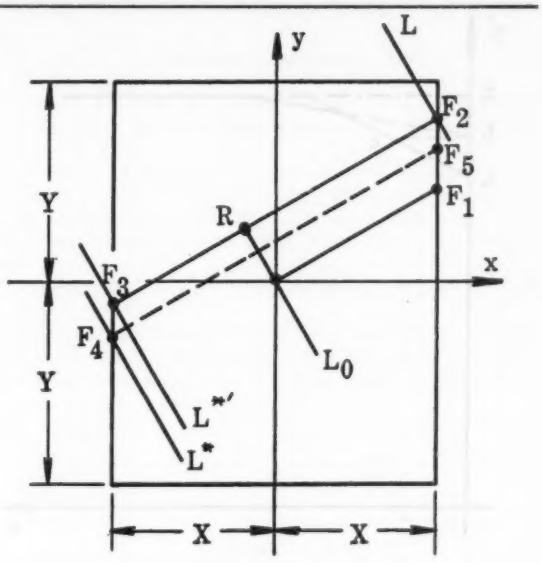

FIG. 3.

Melan,[9] but the corresponding problem for other types of structures does not seem to have received much attention. For the example discussed above, Melan's condition can be formulated as follows: *The system will shake down if there exists at least one parallel to the line of elastic states such that the segment which the extreme lines of equilibrium determine on this parallel lies within the yield rectangle.*

In an attempt at generalizing these results, one might, for instance, study the case of a cylindrical bar subjected to combined torsion and axial tension such that the torque and the axial force vary independently, each between given extreme values. The determination of the shake-down state of residual stress in cases such as this constitutes an as yet unsolved problem of the mathematical theory of plasticity. If shake-down is at all possible for the given extreme loads, *the state of residual stress to which the system shakes down probably corresponds to a smaller value of the elastic strain energy than any other state of residual stress which satisfies the equilibrium conditions in the absence of loads and allows the body to support all further variations of the loads (between the given extremes) in a purely elastic manner.* So far, this tentative theorem has not been proved, however.

Finally, there is the problem of structural stability in the plastic range. The problem of column stability, for instance, is concerned with *the determination of the smallest axial load for which the column can assume a bent, as well as a straight, equilibrium configuration.* The classical treatment of column stability in the plastic range,[10] however, is concerned with a more restricted problem—namely, *the determination of the smallest axial load such that the column can pass from the straight to a bent equilibrium configuration while under the action*

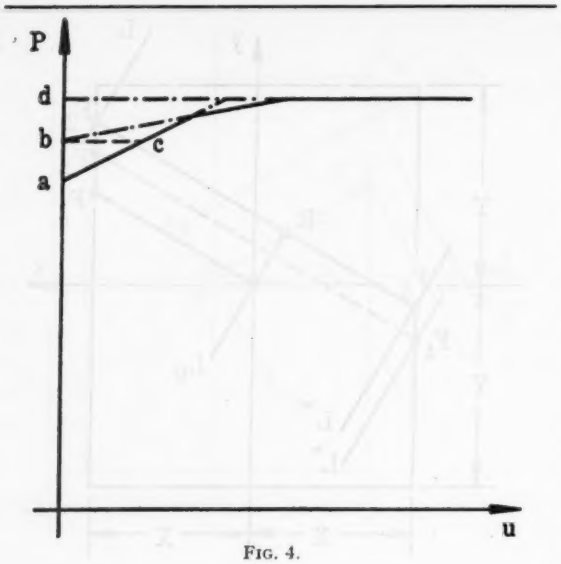

FIG. 4.

of this load. In the elastic range, the difference between these two problems disappears, because the exterior forces necessary to maintain the system in a certain configuration depend only on this configuration and not on the preceding configurations of the system. In the plastic range, however, the history of deformation is of importance, and the two problems formulated above have different solutions.[11]

These remarks can be illustrated on the example of the system shown in Fig. 1. Suppose that the configuration shown in Fig. 1 is assumed by the system under the influence of a *compressive* load P which already produces plastic deformations in the bars OA and OC but not yet in the bar OB. Then let this load P be increased to $P + dP$. If it is assumed that by this increase in load all three bars are further shortened, the forces in the bars OA and OC remain unchanged, since these bars yield in compression under constant loads. The new equilibrium configuration obtained under this assumption is symmetric with respect to the vertical OB. If, on the other hand, it is assumed that the bar OA is lengthened while the bars OB and OC are shortened by the increase in load, the force in OC remains unchanged, while the forces in OB and OC change by amounts proportional to the changes in length which these bars undergo. Further investigation reveals that, once the perfectly plastic bars OA and OC have reached the yield limit, the symmetric system of Fig. 1, subjected to a compressive load P, can absorb an increment dP of the load in either of the two manners just discussed. If the symmetric configuration under the load P is denoted by I and the symmetric and unsymmetric configurations under the load $P + dP$ by II and III, respectively, the system can pass from I to either II or III provided that the load is increased from P to $P + dP$. As a rule, the system can not pass from II to III under the constant load $P + dP$, however. For this to be possible, the load must considerably exceed the smallest load for which both a symmetric and an unsymmetric equilibrium configuration may first occur.

Fig. 4 schematically represents this behavior of the system, as furnished by a linearized theory that neglects all but the first powers of the small displacements from the symmetric configuration I to the unsymmetric configuration III. The ordinate in Fig. 4 represents the load P; the abscissa, the lateral deflection u of the point O. As the load P is increased, starting from zero, the equilibrium configuration remains symmetric (i.e., the deflection u remains zero) as long as all three bars are stressed in the elastic range. When the bars OA and OC reach the yield limit (point a in Fig. 4), lateral deflection becomes possible under increasing load. The linearized theory leads to a *linear* relation between load and lateral deflection. In Fig. 4, this linear relation is represented by the sloping line through the point a. If the occurrence of lateral deflection is prevented by guiding the point O along the vertical OB until the load has reached the value represented by the point b in Fig. 4 and if the system is then allowed to assume an unsymmetric configuration, the relation between load and lateral deflection, as furnished by the linearized theory, is represented by the sloping line through b. The slope of this line is less than that of the line representing the bifurcation of equilibrium from a. Finally, for a certain load represented by the point d, lateral deflection *under constant load* becomes possible.

The linearized theory shows only that various equilibrium configurations are possible but does not indicate which of these will actually be assumed as the system is being loaded. It is to be expected, however, that a more complete theory would show that lateral deflection will begin to develop at a and increase with increasing load following more or less the envelope of the sloping lines in Fig. 4.

The kind of structural instability exhibited by this simple elastic-plastic system differs considerably from that encountered in completely elastic systems. This different behavior is caused by the nonconservative character of elastic-plastic systems. The point c in Fig. 4, for instance, can be reached from a along the sloping line ac. If lateral deflections are not permitted to occur at a and if the system is forced to remain symmetrical until the point b is reached, any lateral deflection will be accompanied by a further rise in load (sloping line through b), so that the point c cannot be reached from b. No general stability theory for nonconservative systems is available as yet, but the behavior of the simple system considered above is probably typical for nonconservative systems in general.

In conclusion, it seems worth while to point out that the preceding discussion applies in a qualitative manner also to the case of strain-hardening materials. Indeed

whereas the bars OA and OC of the simple structure discussed above were assumed to be perfectly plastic, the overall behavior of the structure, as represented by the relation between the load P and the vertical deflection v of the point O, exhibits a sort of strain-hardening insofar as an increase of v requires an increase of P even when the bars OA and OC yield under constant stress.

References

[1] Haar, A., and von Kármán, Th., Goettinger Nachrichten, math.-phys. Kl., pp. 204–218, 1909.

[2] Hencky, H., Zeits. angew. Math. Mech., Vol. 4, pp. 323–334, 1924.

[3] de Saint Venant, B., C. R. Ac. Sci. Paris, Vol. 70, pp. 473–480, 1870.

[4] von Mises, R., Goettinger Nachrichten, math.-phys. Kl., pp. 582–592, 1913.

[5] Prandtl, L., Proc. 1st Internat. Congr. Appl. Mech. Delft, pp. 43–54, 1924; Reuss, A., Zeits. angew. Math. Mech., Vol. 10, pp. 266–274, 1930.

[6] Prager, W., Duke Math. J., Vol. 9, pp. 228–233, 1942.

[7] Hodge, P., and Prager, W., J. Math. Phys. (to appear soon).

[8] Bleich, F., Ossature Metall., Vol. 3, pp. 93–105, 1934.

[9] Melan, E., Sitz.-Berichte Akad. Wiss. Wien, pp. 195–218, 1936.

[10] von Kármán, Th., Forschungsarbeiten a. d. Gebiete d. Ing.-wes. No. 81, 1910.

[11] Shanley, F. R., Journal of the Aeronautical Sciences, Vol. 13, p. 678, 1946; Vol. 14, pp. 261–267, 1947. See also Dr. von Kármán's illuminating discussion of the latter paper (pp. 267–268).

Letter to the Editor

Dear Sir:

The following comments refer to the paper, "Range Performance of Turbojet Airplanes," by Irving L. Ashkenas (JOURNAL OF THE AERONAUTICAL SCIENCES, Vol. 15, No. 2, p. 97, February, 1948).

An important consideration that might well have been included in the paper is that of the relative values of the maximum ranges which would be realized, under the assumed conditions, by cruising at the ceilings that correspond to the flight conditions defined by Eqs. (2), (6), and (10). Had such a comparison been made, a welcome simplification of the practical prediction problem would have been indicated by the trivial differences between the ranges found for the three conditions. While this result may appear contrary to implications of the paper, it is entirely consistent with physical interpretation of the definitive equations.

For convenience of reference, the three conditions of flight are identified as

Case	Condition	Equation
A	$C_D = 1.333\ C_{Dp}$	(2)
B	$C_D = 1.600\ C_{Dp}$	(6)
C	$C_D = 1.500\ C_{Dp}$	(10)

In the paper of reference, it is shown that maximum range at fixed altitude is realized by maintaining the condition of Case A whereas, in the absence of the fixed height stipulation, maximum ranges are obtained in the troposphere and stratosphere by cruising at the ceilings which correspond to Cases B and C, respectively. Let us consider the significance of these three flight conditions.

Fig. 1 illustrates thrust-drag equilibrium for a jet-propelled airplane at the ceiling attainable in the attitude for which D/V—i.e., T_r/V—is minimum. This attitude is characterized by the relationship $C_D = {}^4/_3 C_{Dp}$, the condition identified as Case A. Since constant values of dW/dR (lbs. of fuel consumed per mile flown) are represented by straight lines through the origin—defined by $T = -(V/c)(dW/dR)$—it is evident that maximum range is obtained at this, or any other, fixed altitude by flying at the lift coefficient which corresponds to Case A.

Consider, now, the possibility of obtaining still greater range by cruising at heights above the ceiling for Case A. At the outset, let us assume that the ceiling for Case A is above the tropopause; under this condition, the lines of dW/dR = const. remain unchanged as altitude increases because c is assumed to be constant in the stratosphere. Since an increase of altitude causes the T_a line to be lowered and the points of the T_r vs. V curve to be displaced horizontally, but nonuniformly, toward the right, it is evident that range will be augmented if, with increasing height, the intersection of the T_a line with the T_r curve moves into the region characterized by reduced values of T/V and of dW/dR.

Because the path traversed by the intersection point as altitude increases is not easily visualized in a Cartesian plot of T vs. V, the corresponding logarithmic chart, Fig. 2, is introduced to facilitate analysis. In this chart, all the lines of $dW + dR$ = const. have the slope $+1$. Also, as height increases and density diminishes from σ_1 to σ_2, the T_a line is lowered by the amount $\log(\sigma_2/\sigma_1)$, while the T_r vs. V curve is translated horizontally toward the right—without change of shape—by one-half that distance—i.e., the displacement is $-{}^1/_2 \log(\sigma_2/\sigma_1)$. Therefore, as C_L is increased—to maintain level flight at heights above the ceiling for Case A—the intersection point moves to lower values of T/V (and of dW/dR) until it reaches the point of the T_r vs. V curve characterized by the slope $+{}^1/_2$. This slope corresponds exactly to the flight condition for Case C and *the resulting improvement in range is 2.6 per cent.* To cruise at still higher altitudes and lift coefficients would adversely affect range; for example, by going on to the condition for Case B, the gain would be reduced to 1.9 per cent.

Treatment of the situation in which the ceiling for Case A is well below the tropopause involves an additional complication: In Fig. 2, the lines of dW/dR = const. are displaced upwardly as altitude increases. This results from the variation of c with $\sigma^{0.2}$ in the tropopause. However, an analogous improvement of range is found but, in this instance, the maximum is obtained by cruising at the ceiling for Case B. In the troposphere, Case B yields *7.9 per cent more range than Case A.* (In this region, Case C yields only 7.1 per cent.)

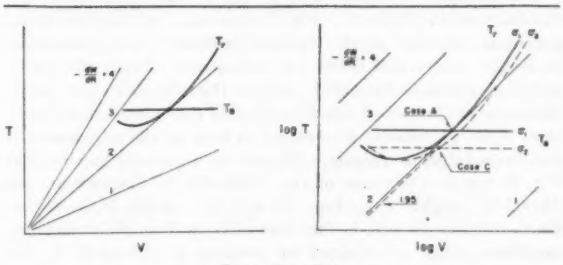

FIGS. 1 and 2.

TABLE 1

Relative Thrust Requirements, Ceiling Densities, and Ranges

Basic Range Equation—

$$\frac{dR}{dW} = -\left[\frac{1}{c}\left(\frac{2}{\rho S W}\right)^{1/2}\right]\left(\frac{C_L^{1/2}}{C_D}\right)$$

Case	A	B	C
Definitive equation	(2)	(6)	(10)
C_D/C_{Dp}	1.333	1.600	1.500
$C_L/(\pi A_e C_{Dp})^{1/2}$	$(0.333)^{1/2}$	$(0.600)^{1/2}$	$(0.500)^{1/2}$
$(C_D/C_L)/(C_{Dp}/\pi A_e)^{1/2}$	2.309	2.066	2.121
$(C_L^{1/2}/C_D)/(\pi A_e/C_{Dp}^3)^{1/4}$	0.5699	0.5501	0.5606
At Fixed Altitude—			
T_c/T_{cA}	1.0	0.8948	0.9186
$(dR/dW)/(dR/dW)_A$	1.0	0.9653	0.9837
When Ceiling with $W = W_2$ Is Below Tropopause—			
σ_{Ac}/σ_c	1.0	1.172	1.129
$(dR/dW)_c/(dR/dW)_{Ac}$	1.0	1.079	1.071
When Ceiling with $W = W_1$ Is Above Tropopause—			
σ_{Ac}'/σ_c'	1.0	1.118	1.089
$(dR/dW)_c'/(dR/dW)_{Ac}'$	1.0	1.019	1.026

(Subscript c indicates ceiling.)

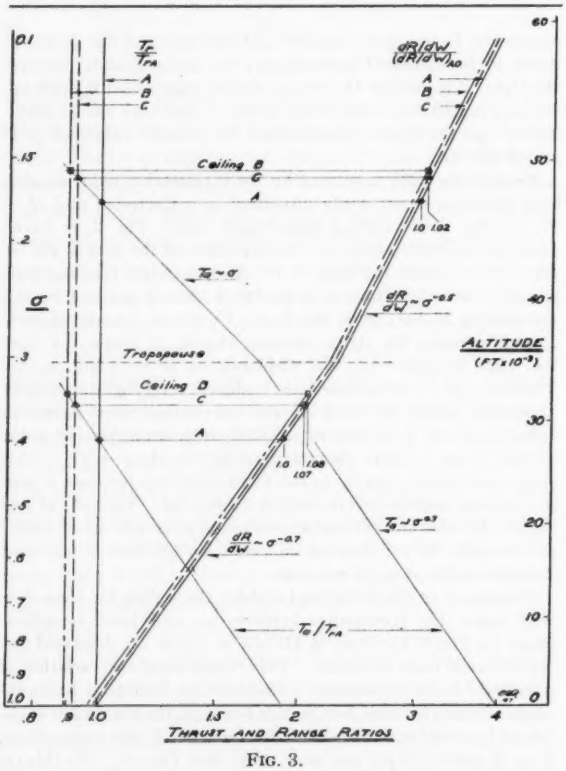

FIG. 3.

The calculations which lead to the results cited above are summarized in Table 1. Fig. 3 presents, in another form, graphical solutions of the typical problems that correspond to heights above and below the tropopause. From this figure and the tabulated data, it is evident that *the maximum ranges attainable at the ceilings which correspond to the three flight conditions differ by constant percentages* so long as the tropopause is not crossed during cruising. [It may be of interest to note that Fig. 3 reveals the cause of the "difficulty in determining the 35,000-ft. weight" from Eqs. (4) and (8)—to which the author refers on page 98. It is that *immediately above the tropopause*, maximum range is obtained by cruising at values of C_L between those for Cases B and C.]

The foregoing comparison shows that, by deviating from the attitude in which T/V is minimum (Case A), improvements in maximum range of 7.9 and 2.6 per cent might be attained in the troposphere and stratosphere, respectively—under the highly simplified conditions assumed. Lest the former figure be thought significant, consideration of the variation of dR/dW with height (see Fig. 3) will indicate the futility of attempting to obtain great turbojet range in the troposphere. At the higher levels, a calculated improvement of 2.6 per cent is certainly not significant when based on simplifying approximations of larger order.

It thus appears that the rigorous analysis of the subject paper actually shows that the accuracy of turbojet range prediction is negligibly (if at all) improved by the consideration of flight conditions which differ from the one that yields maximum range at fixed height. It may be worth noting, specifically, that the equation

$$R_{(\text{mi.})} = \frac{23.8}{c_{35}\, C_{Dp}}\sqrt{\frac{T_{35}\, A_e}{S}}\,\log\left(\frac{W_1}{W_2}\right)$$

which corresponds to cruising at the ceiling for Case A (above the tropopause) differs negligibly from the author's Eq. (11) for Case C. Furthermore, even if such differences were not negligible, recognition of the fixed ratios that, in stratosphere and troposphere, relate the maximum ranges for the three conditions of flight would have the welcome consequence of unifying the range criterion for variable height with that for fixed height. Therefore, as is evident from the basic range equation of Table 1, minimization of the ratio $C_D/C_L^{1/2}$ is the fundamental aerodynamic criterion for the design of long-range turbojet aircraft.

In conclusion, the present writer wishes to commend the author for his clear demonstration of the compatibility of high speed with long range in turbojet aircraft, for pointing out (if not discovering) the constancy of optimum true cruising speed with diminishing weight in the stratosphere, and for calling attention to the remarkable improvement of range which occurs as the cruising altitude is increased.

Before closing, attention should be drawn to a typographic error in the paper: On page 99, the value of $(L/D)_{max.}$ should read $\frac{1}{2}\sqrt{\pi A_e/C_{Dp}}$. It is also noted that the numerical constant of Eq. (11) is based on the density at 35,000 ft. (0.000736) rather than on the value at the tropopause (0.000727); introduction of this correction would make the constant 24.4.

ELLIOTT G. REID
Professor of Aerodynamics
Stanford University
Stanford, California

Harmonic and Transient Motion of a Swept Wing in Supersonic Flow

JOHN W. MILES*

University of California, Los Angeles

SUMMARY

The results of previous papers on the harmonic[1, 3] and transient[2] motion and loading of two-dimensional airfoils in supersonic flow are extended to include the infinite swept airfoil, provided that the component of flow normal to the leading edge remains supersonic. It is shown that the various normal force derivatives are reduced by the cosine of the sweepback angle and that the effective Mach Number corresponds to the component of flow normal to the leading edge. This result is related to the invariance of the magnitude of the circulation under sweepback and Busemann's rule[6] with respect to compressibility effects. The flutter of a swept wing is considered, and it is pointed out that sweepback introduces additional aerodynamic coupling between torsion and bending. The flutter of a supersonic swept wing with subsonic leading edge is discussed, and an approximate treatment is suggested.

NOTATIONS

- b = semichord measured parallel to free-stream velocity
- c = fraction of semichord of flap hinge line aft of mid-chord
- e = fraction of chord of elastic axis aft of line of aerodynamic centers
- h = vertical deflection of wing measured at elastic axis, positive up
- j = $(-1)^{1/2}$, imaginary unit
- k = $(\omega b/U)$, reduced frequency
- s = distance aft of leading edge, measured parallel to free-stream velocity, cf. Eq. (10)
- t = time
- u = hyperbolic radius, cf. Eq. (2)
- w = vertical velocity in plane $z = 0$
- x, y, z = coordinates (wind along x, y to starboard and z positive up)
- z_i = vertical displacement in ith degree of freedom, cf. Eqs. (21)–(23)
- A_{ij} = dimensionless flutter coefficient giving force in ith degree of freedom due to motion in jth degree of freedom, cf. references 1 and 3 (see also end of this section)
- $G(x,s)$ = Green's function giving potential at x due to velocity at s, cf. Eq. (13)
- J_0 = Bessel function, first kind, zero order
- L = lift, positive up
- M = Mach Number; also mid-chord stalling moment
- N = hinge moment, positive in sense to produce down flap
- S = area of disturbed flow intercepted by Mach cone from given point
- U = free-stream velocity
- α = angle of attack, measured as rotation about y axis
- β = $(M^2 - 1)^{1/2}$; also flap deflection relative to airfoil, positive for down flap
- γ = $(\tan\sigma)/\beta$
- ξ, η = source coordinates on (x, y) axes
- κ = $kM(M^2 - 1)^{-1}$
- σ = angle of sweepback of leading edge with respect to y axis
- ϕ = velocity potential
- θ = angle of twist about elastic axis (positive for leading edge up); also Mach coordinate, cf. Eq. (11)
- ω = angular frequency

The flutter derivatives Ars, in the absence of sweep, are defined by[1, 3]

$$\frac{\partial L}{\partial s} = \left(\frac{\pi\rho b^2\omega^2}{\beta}\right) a_s e^{j\omega t} A_{cs}$$

$$\frac{\partial M}{\partial s} = \left(\frac{\pi\rho b^4\omega^2}{\beta}\right) a_s e^{j\omega t} A_{as}$$

$$\frac{\partial N}{\partial s} = \left(\frac{\pi\rho b^4\omega^2}{\beta}\right) a_s e^{j\omega t} A_{bs}$$

where the a_s refer to the following chordwise velocity distributions:

$$s = h: \quad z_h(x, t) = a_h b e^{j\omega t}$$

$$s = \alpha: \quad z_\alpha(x, t) = -a_\alpha b x e^{j\omega t}$$

$$s = \beta: \quad z_\beta(x, t) = -a_\beta b(x - c)e^{j\omega t}, \qquad x > c$$

$$= 0, \qquad x < c$$

INTRODUCTION

THE NONSTEADY MOTION of an unswept two-dimensional airfoil has been considered in three previous papers.[1–3] The purpose of the present note is to extend the results of these papers to a swept wing whose leading and trailing edges are ahead of the Mach waves—i.e., the case of pure supersonic flow.

SOLUTION FOR A POINT SOURCE

The solution to the wave equation for the linearized velocity potential of an oscillating point source moving through an ideal (nonviscous) fluid at a supersonic speed was found in reference 1, but the result, as stated therein, is in error.

Following the analysis of reference 1, the possible solutions for a point source of strength $q(\xi, \eta)d\xi\, d\eta$ located at $\xi, \eta, 0$ are given by

$$d\phi(x, y, z) = -q(\xi, \eta)\frac{d\xi\, d\eta}{u} e^{jk[-M(x-\xi)\mp u]} \qquad (1)$$

$$u = [(x - \xi)^2 - \beta^2(y - \eta)^2 - \beta^2 z^2]^{1/2} \qquad (2)$$

$$\kappa = \frac{Mk}{\beta^2}, \qquad k = \frac{\omega b}{U}, \qquad \beta^2 = M^2 - 1 \qquad (3)$$

Received November 14, 1947.

* Assistant Professor of Engineering, Department of Engineering.

where b is the unit of length and is taken as unity in the intermediate steps of the analysis. Eq. (1) is identical with Eq. (6a) of reference 1, except that both signs must be allowed u in the exponent, inasmuch as both solutions are permissible in the transformed coordinates in which the wave equation is solved.

The vertical component of velocity due to the potential of Eq. (1) vanishes everywhere in the plane $z = 0$, except at the source, where, following (analogously) Puckett's analysis for steady flow,[4] it is given by

$$w(x, 0, 0) = -\lim_{z \to 0} \frac{\partial}{\partial z} \int_a^{x-\beta z} e^{-j\kappa M(x-\xi')}\, d\xi' \times \int_{-\eta_1}^{\eta_1} \left[\frac{q_A \cos \kappa u + q_B \sin \kappa u}{u} \right] d\eta' \quad (4)$$

Eq. (4) represents the integration of the source strength within the region cutout of the area $d\xi\, d\eta$ by the Mach fore-cone subtended from the point $(x, 0, z)$. The source strengths of the two possible solutions given by Eq. (1) are specified by q_A and q_B, and the area intercepted by the Mach cone is bounded by the hyperbola

$$\beta^2(\eta_1^2 + z^2) = (x - \xi')^2 \quad (5)$$

(a is a constant, the exact value of which is immaterial.) Introducing the change of variable

$$\sin \theta = \beta(\eta'^2 + z^2)^{1/2}/(x - \xi') \quad (6)$$

in Eq. (1) and carrying out the differentiation yields

$$w(x, 0, 0) = \lim_{z \to 0} e^{-j\kappa M \beta z} \int_{-\pi/2}^{\pi/2} [q_A \cos (\kappa \beta z \cos \theta) + q_B \sin (\kappa \beta z \cos \theta)] d\theta = \pi q_A \quad (7)$$

Since the velocity potential must vanish with the velocity distribution w, it follows that the desired point source solution is

$$d\phi(x, y, z) = -\frac{1}{\pi} w(\xi, \eta) \frac{d\xi\, d\eta}{u} e^{-j\kappa M(x-\xi)} \cos \kappa u \quad (8)$$

[While Eqs. 16a and 18 of reference 1 give the exponential in u, cos κu was implicitly used in Eq. (11), and all the subsequent results stated therein are correct.]

Solution for a Line Source

The velocity potential at the point $(x, 0, 0)$ on the swept, infinite span airfoil shown in Fig. 1* is given by integrating Eq. (1) over the Mach fore-cone subtended from $(x, 0, 0)$:

$$\phi(x, 0, 0) = -\frac{1}{\pi} \int_S \int w(\xi, \eta) e^{-j\kappa M(x-\xi)} \frac{\cos \kappa u}{u} d\xi\, d\eta \quad (9)$$

where S is bounded by the Mach lines $\eta = \pm [(x - \xi) \div \beta]$ and the leading edge $\xi = \eta \tan \sigma$, if it is assumed that $\tan \sigma < \beta$—i.e., for the case where the component of flow normal to the leading edge remains supersonic. If it is further assumed that the flow is two-dimensional, and the transformations

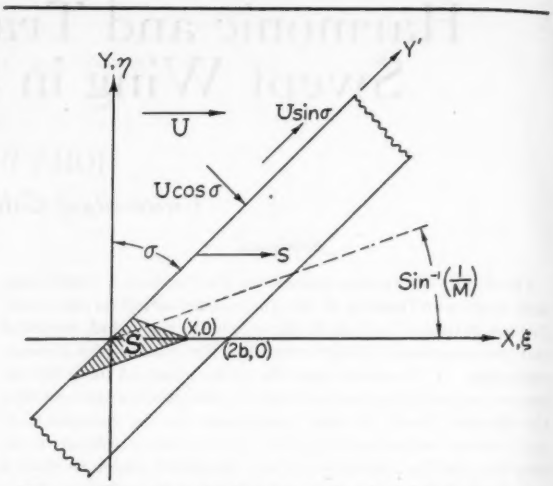

FIG. 1. Plan view of wing swept ahead of Mach waves.

$$s = \xi - \eta \tan \sigma \quad (10)$$

$$\cos \theta = \gamma + (1 - \gamma^2)\beta[\eta/(x - \xi + \eta \tan \sigma)] \quad (11)$$

$$\gamma = \tan \sigma/\beta \quad (12)$$

are introduced, Eq. (9) reduces to

$$\phi(x) = -[1/\beta(1 - \gamma^2)^{1/2}] \int_0^x w(s) G(x, s) ds \quad (13)$$

$$G(x, s) = \frac{e^{-j \frac{\kappa M}{1-\gamma^2}(x-s)}}{\pi} \int_0^{\pi} e^{j \left[\frac{\kappa M \gamma}{(1-\gamma^2)} (x-s) \cos \theta \right]} \times \cos \left[\frac{\kappa(x - s) \sin \theta}{(1 - \gamma^2)^{1/2}} \right] d\theta \quad (14)$$

The integral in Eq. (14) may be evaluated from the result[5]

$$\frac{1}{\pi} \int_0^{\pi} e^{jx \cos \phi} \cos (y \sin \phi) d\phi = J_0[(x^2 + y^2)^{1/2}] \quad (15)$$

to yield

$$G(x, s) = e^{-j \frac{\kappa M}{(1-\gamma^2)} (x-} J_0 \left[\frac{\kappa(x - s)(1 + \beta^2\gamma^2)^{1/2}}{(1 - \gamma^2)} \right] \quad (16)$$

From Eqs. (3) and (12), it is found that

$$\frac{\kappa M}{(1 - \gamma^2)} = \frac{kM^2}{(M^2 - 1 - \tan^2 \sigma)} = \frac{k(M \cos \sigma)^2}{(M \cos \sigma)^2 - 1} \quad (17a)$$

$$\frac{\kappa(1 + \beta^2\gamma^2)^{1/2}}{(1 - \gamma^2)} = \frac{kM \sec \sigma}{(M^2 - 1 - \tan^2 \sigma)} = \frac{k(M \cos \sigma)}{[(M \cos \sigma)^2 - 1]} \quad (17b)$$

* In reference 1 the leading edge was placed at $x = -1$ instead of $x = 0$, but the latter choice is more convenient in the present analysis.

$$\frac{1}{\beta(1-\gamma^2)^{1/2}} = \frac{1}{(M^2-1-\tan^2\sigma)^{1/2}} = \frac{\cos\sigma}{[(M\cos\sigma)^2-1]^{1/2}} \quad (17c)$$

Introducing Eqs. (17) in Eqs. (13) and (16), it is seen that the dependence of the velocity potential on sweepback is specified by

$$\phi(x, k, M, \sigma) = \cos\sigma\phi(x, k, M\cos\sigma, 0) \quad (18)$$

Application of Busemann's Rule

It follows that the nonsteady motion of an infinite airfoil swept ahead of the Mach waves is equivalent to the motion of an airfoil having the same chord ($2b$) and chordwise velocity distribution [$w(s)$] *in the direction of travel* if the forces acting on the latter are reduced by a factor of $\cos\sigma$ and its Mach Number is taken as $M\cos\sigma$, where M is the Mach Number of the actual flow. The various normal force derivatives, whether evaluated for a harmonic time dependence,[1,3] gust loading,[2] or an arbitrary time variation, are given by the same rule if the full velocity U is used in defining these coefficients, except where it enters the Mach Number.

It should be particularly emphasized that the normal (to the leading edge) component of flow is used only in defining the effective Mach Number and not in defining k (since $k = \omega b/U = \omega b\cos\sigma/U\cos\sigma$, the normal component of flow may be used in defining k if the chord is measured normal to the leading edge, and not in the direction of flow, as b is presently defined) or the dynamic pressure. Hence, care must be exercised in applying Busemann's[6] rule that the forces on a swept airfoil are determined only by the component of flow normal to the leading edge. If the chordwise slope of the airfoil is measured normal to the leading edge and no dihedral is present—i.e., if the angle of attack distribution is made up of rotations about the swept axis—this rule may be interpreted literally, but if the angle of attack distribution is made up of rotations about an axis normal to the flow or if geometrical dihedral is present from any other source, the spanwise component of flow interacts with the dihedral angle to produce an additional upwash and contributes to the lift force acting on the airfoil.

That the normal force derivatives with respect to an angle of attack measured as a rotation about the axis should be reduced by $\cos\sigma$, and not $\cos^2\sigma$, is perhaps more easily seen by considering the normal ($U\cos\sigma$) and spanwise ($U\sin\sigma$) components of flow directly. Let it be assumed that the local pressure due to a normal component of flow V and upwash w is given by

$$dF/dS = {}^1/_2\rho V^2 m(w/V) \quad (19)$$

where m will, in general, be an arbitrary function of the geometry. Considering the swept wing, let α be the local angle of attack, measured as a rotation about the y axis. Now, if α is small, it may be regarded as being composed of two components, $\alpha\cos\sigma$ and $-\alpha\sin\sigma$, the former representing a rotation about the swept axis and the latter representing the effective dihedral with respect to the swept axis. The pressure due to the first component is given by Eq. (19), where $V = U\cos\sigma$ and $(w/V) = \alpha\cos\sigma$, while the normal force due to the second component is given by Eq. (19), where $V = U\times\cos\sigma$ and $w = (-\alpha\sin\sigma)(-U\sin\sigma)$; hence, the total pressure is given by

$$\frac{dF}{dS} = \frac{1}{2}\rho(U\cos\sigma)^2 m\left[\alpha\cos\sigma + \frac{(-\alpha\sin\sigma)(-U\sin\sigma)}{(U\cos\sigma)}\right] = \frac{1}{2}\rho U^2(m\cos\sigma)\,\alpha \quad (20)$$

Eq. (20) states that the effect of sweepback is to reduce the local normal force derivative by $\cos\sigma$. Its derivation does not replace the derivation of Eq. (18), inasmuch as it is assumed that m itself is invariant with respect to sweepback, whereas, in actuality, it too must be modified in accordance with Busemann's rule when compressibility is considered.

Eq. (20) may also be interpreted as stating that the magnitude of the circulation about the swept axis is unchanged by sweepback, the $\cos\sigma$ entering from the vector cross product in the Kutta-Joukowsky law ($d\boldsymbol{F}/dS = \rho\boldsymbol{U}\times\bar{\gamma}$ where $\bar{\gamma}$ is the local circulation). While such a postulate (that only the normal component of flow need be considered insofar as compressibility considerations are concerned) might be used to state Eq. (18) directly, particularly in retrospect, this is perhaps asking a little too much of physical intuition. Nevertheless, both rules appear to be generally applicable to problems of both steady and nonsteady flow in the case of purely subsonic or purely supersonic linearized two-dimensional flow and to many cases of three-dimensional flow; in the case of mixed supersonic flow, the rules may be locally applicable, but the variation of m may be complex.

Flutter Considerations

In treating the flutter of a swept wing, it will be generally convenient to describe the structural deformation in terms of bending (h) about a section perpendicular to the swept axis, twisting (θ) about the swept elastic axis, and control surface rotation (β) about a hinge line parallel to the swept axis; the deflections with respect to an axis perpendicular to the free-stream velocity may then be written (neglecting taper effects and assuming all angles to be small, so that they may be treated as vectors)

$$z_h(s, y', t) = \left[\frac{h(y')}{b} + 2e\cos\sigma\,\theta(y')\right] be^{j\omega t} \quad (21)$$

$$z_\alpha(s, y', t) = -\left[\cos\sigma\theta(y') - \sin\sigma\frac{\partial h(y')}{\partial y'}\right]\times b(s-1)e^{j\omega t} \quad (22)$$

$$\left.\begin{aligned} z_\beta(s, y', t) &= -\cos\sigma\beta(y')b(s - 1 - c)e^{j\omega t} \\ &\qquad\qquad s > (1 + c) \\ &= 0 \qquad\qquad s < (1 + c) \end{aligned}\right\} \quad (23)$$

where y' is measured along the swept axis, s is measured in the direction of flow [cf. Eq. (10)], and e, the eccentricity, is the fraction of the chord which the elastic axis lies behind the line of aerodynamic centers.

It then follows the definition of the aerodynamic flutter derivatives, in Eqs. (22) and (23) of reference 1 and Eqs. (4)–(6) of reference 3,* that the forces and moments on a swept supersonic airfoil, based on strip theory, are given by

$$\frac{dL(t)}{dy} = \left[\frac{\pi\rho b^3\omega^2\cos\sigma}{\beta(M\cos\sigma)}\right]e^{j\omega t}\left\{Ach(k, M\cos\sigma)\left[\frac{h(y')}{b} + 2e\cos\sigma\theta(y')\right] + Ac\alpha(k, M\cos\sigma)\left[\cos\sigma\theta(y') - \sin\sigma\frac{\partial h(y')}{\partial y'}\right] + Ac\beta(k, M\cos\sigma)\cos\sigma\beta(y')\right\} \quad (24)$$

$$\frac{dM(t)}{dy} = \left[\frac{\pi\rho b^4\omega^2\cos\sigma}{\beta(M\cos\sigma)}\right]e^{j\omega t}\left\{Aah(k, M\cos\sigma)\left[\frac{h(y')}{b} + 2e\cos\sigma\theta(y')\right] + Aa\alpha(k, M\cos\sigma)\left[\cos\sigma\theta(y') - \sin\sigma\frac{\partial h(y')}{\partial y'}\right] + Aa\beta(k, M\cos\sigma)\cos\sigma\beta(y')\right\} \quad (25)$$

$$\frac{dN(t)}{dy} = \left[\frac{\pi\rho b^4\omega^2\cos\sigma}{\beta(M\cos\sigma)}\right]e^{j\omega t}\left\{Abh(k, M\cos\sigma)\left[\frac{h(y')}{b} + 2e\cos\sigma\theta(y')\right] + Ab\alpha(k, M\cos\sigma)\left[\cos\sigma\theta(y') - \sin\sigma\frac{\partial h(y')}{\partial y'}\right] + Ab\beta(k, M\cos\sigma)\cos\sigma\beta(y')\right\} \quad (26)$$

where (dL/dy) is the lift per unit span, (dM/dy) is the mid-chord stalling moment per unit span, and (dN/dy) is the hinge moment per unit span, y being measured perpendicular to the free air stream. $\beta\,(M\cos\sigma)$ indicates $\beta = (M^2\cos^2\sigma - 1)^{1/2}$.

The results of Eqs. (24)–(26) are also applicable to a purely subsonic swept wing, provided that the appropriate flutter derivatives[9, 10] are used and β (which will be imaginary for $M\cos\sigma < 1$) is replaced by its absolute value.

It is evident from Eqs. (24)–(26) that sweepback introduces an aerodynamic coupling between torsion and bending even when the elastic axis coincides with the line of aerodynamic centers.

* See section on notation for definitions in absence of sweepback.

Subsonic Leading and Trailing Edges

The general result of Eq. (9) is valid for any airfoil in the supersonic régime where a linearized treatment of the flow is allowable; however, in those cases where either the leading or trailing edges of the planform are swept inside the Mach cone—i.e., where the component of velocity normal to these boundaries is subsonic (generally called mixed supersonic flow)—the area S includes disturbed regions off the wing (analogous to the wake region in purely subsonic flow) over which the velocity distribution is not explicitly known, and, in the case of the subsonic trailing edge, the Kutta condition must be satisfied.

While the problem of the two-dimensional oscillating airfoil in mixed supersonic flow appears to be difficult and has not, to the author's knowledge, yet been solved, the solution of particular steady flow problems[7] indicates that the flow should be approximately subsonic over most of the span of an actual wing. Accordingly, the results of Eqs. (24)–(26) could be used for a wing swept behind the Mach cone, with the supersonic derivatives[1, 3, 8] being used over the inboard position of the span and the subsonic derivatives (at $M = 0$,[9] or preferably at $M\cos\sigma$[10]) over the outer portion of the span. The dividing section between the two types of flow is probably best determined by an examination of the pressure distribution over the same wing in steady flow. In following such a procedure, it should be recalled that those supersonic flutter derivatives in the pitching degree of freedom are referred to the mid-chord, whereas the corresponding subsonic derivatives are referred to the quarter chord.

References

[1] Miles, John W., *The Aerodynamic Forces on an Oscillating Airfoil at Supersonic Speeds*, Journal of the Aeronautical Sciences, Vol. 14, No. 6, pp. 351–358, June, 1947.

[2] Miles, John W., *Transient Loading of Airfoils at Supersonic Speeds*, on press.

[3] Miles, John W., *The Aerodynamic Forces on an Oscillating Flap at Supersonic Speeds*, to be published.

(*Continued on page 370*)

Buckling of a Column with Elastic Supports

T. H. LIN* AND K. S. CHING†

Chinese Air Force

ABSTRACT

In this paper, the buckling of a column with equally spaced elastic supports under compressive load is investigated, and an equation is derived for any number of equally spaced elastic supports. It is assumed that the elastic supports give only linear but not rotational restraints on the bar and the bar itself is in long column failure. As the spring constant of the elastic supports increases, waves of buckling increase until there is one half wave between every two adjacent supports and until further increase in the spring constant does not increase the buckling load. This constant is called the maximum critical elastic constant. An equation for calculating this constant is given. Curves of the ratio of buckling load to Euler load vs. spring constant for different modes of buckling are shown so that with a given column on equally spaced elastic supports of known spring constant, the buckling load can be readily calculated.

NOTATIONS

l	=	span between supports
EI	=	flexural rigidity of the column
P	=	end load
P_E	=	Euler's load per span $= \pi^2 EI/l^2$
P_c	=	critical buckling load
K	=	elastic constant of elastic supports
K_c	=	critical elastic constant of elastic supports
Wl	=	total span of the column with elastic supports
V_B	=	energy due to bending
V_K	=	work done by elastic supports
V_P	=	work done by load P
ρ	=	n/W, a parameter
m, n, q	=	constants positive integers

THE GENERAL SOLUTION OF MULTIELASTIC SUPPORTS

CONSIDER A COLUMN BAR with multielastic supports under axial load as shown in Fig. 1. Assuming the buckling curve to be

$$y = \sum_{n=1}^{\infty} A_n \sin (n\pi x/Wl) \tag{1}$$

which satisfies the boundary conditions at $x = 0$ and $x = Wl$. Then

$$V_B = \frac{EI\pi^4}{2W^4l^4}\int_0^{Wl}\left(\sum_{n=1}^{\infty} A_n n^2 \sin\frac{n\pi x}{Wl}\right)^2 dx \tag{2'}$$

$$V_P = \frac{\pi^2 P}{2W^2l^2}\int_0^{Wl}\left(\sum_{n=1}^{\infty} A_n n \cos\frac{n\pi x}{Wl}\right)^2 dx \tag{3'}$$

Using the principle of orthogonality, after integrating,

$$V_B = (\pi^4 EI/4W^3l^3)\sum_{n=1}^{\infty} n^4 A_n^2 \tag{2}$$

$$V_P = (P\pi^2/4Wl)\sum_{n=1}^{\infty} n^2 A_n^2 \tag{3}$$

Let m be a positive integer from 1 to W; then,

$$V_K = {}^1/_2\sum_{m=1}^{W} K[y_{x=ml}]^2$$

or

$$V_K = \frac{K}{2}\sum_{m=1}^{W}\left(\sum_{n=1}^{\infty} A_n \sin\frac{mn\pi}{W}\right)^2 \tag{4}$$

By Rayleigh's principle,

$$V_P = V_K + V_B \tag{5}$$

Substituting the values of V_B, V_P, and V_K from Eqs. (2), (3), and (4) into Eq. (5), we get

$$\frac{P_c\pi^2}{4Wl}\sum_{n=1}^{\infty} n^2 A_n^2 = \frac{EI\pi^4}{4W^3l^3}\sum_{n=1}^{\infty} n^4 A_n^2 + \frac{1}{2}K\sum_{m=1}^{W}\left(\sum_{n=1}^{\infty} A_n \sin\frac{mn\pi}{W}\right)^2 \tag{6}$$

Introducing $S = \pi^2/2WlK$ and solving Eq. (6) for P_c,

$$P_c = \frac{\dfrac{SP_E}{W^2}\displaystyle\sum_{n=1}^{\infty} n^4 A_n^2 + \sum_{m=1}^{W}\left(\sum_{n=1}^{\infty} A_n \sin\frac{mn\pi}{W}\right)^2}{S\displaystyle\sum_{n=1}^{\infty} n^2 A_n^2}$$

According to the theory of minimum energy, the constant A_n should have such values that make P_c a minimum value—that is,

$$\partial P_c/\partial A_q = 0$$

where $q = 1, 2, 3, \ldots, \infty$. The result is

$$\left(\frac{P_E}{W^2}q^2 - P_c\right)Sq^2A_q + \sum_{m=1}^{W}\sin\frac{qm\pi}{W}\times\sum_{n=1}^{\infty} A_n \sin\frac{mn\pi}{W} = 0$$

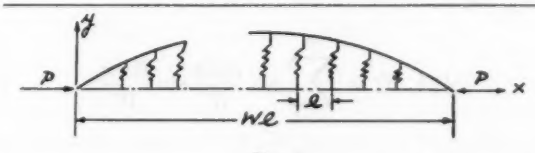

FIG. 1.

Received November 14, 1947.

* S.M., A.F.R.Ae.S. Lieutenant Colonel.

† B.S. Captain.

Define

$$\Psi(A, B) = \sum_{m=1}^{W} \sin \frac{Am\pi}{W} \sin \frac{Bm\pi}{W} \tag{7}$$

and

$$\Phi_\beta = \beta^2 S[(\beta^2 P_E/W^2) - P_c] \tag{8'}$$

Let

$$K = C(P_E/l)$$

where C is a constant. Then,

$$S = (\pi^2/2WC)(1/P_E)$$

Therefore,

$$\Phi_\beta = \frac{\pi^2}{2WC}\beta^2\left(\frac{\beta^2}{W^2} - \frac{P_c}{P_E}\right) \tag{8}$$

As the value of q varies from one to infinity, there is an infinite number of linear equations for determining the value of A_n—i.e.,

$$\Phi_q A_q + \sum_{n=1}^{\infty} \psi(q, n) A_n = 0 \tag{9}$$

where $q = 1, 2, 3, \ldots, \infty$.

In order that the coefficients A_n cannot equal to zero simultaneously, the determinant of the group of linear equations must be zero. Furthermore, since the sine series is used to express the deflection curve, $(2W - 1)$ terms of the sine series would give a result accurate enough for practical use. The error caused by limiting the infinite determinant arbitrarily to the first $(2W - 1)$ terms will be estimated by comparing the results so obtained with exact results as shown in reference 1. The determinant is:

$$\begin{vmatrix}
\phi_1 + \psi(1,1) & \psi(1,2) & \psi(1,3) & \cdots & \psi(1,2W-3) & \psi(1,2W-2) & \psi(1,2W-1) \\
\psi(2,1) & \phi_2 + \psi(2,2) & \psi(2,3) & \cdots & \psi(2,2W-3) & \psi(2,2W-2) & \psi(2,2W-1) \\
\psi(3,1) & \psi(3,2) & \cdots & \cdots & \cdots & \psi(3,2W-2) & \psi(3,2W-1) \\
\cdots & \cdots & \cdots & \phi_W + \psi(W,W) & \cdots & \cdots & \cdots \\
\psi(2W-3,1) & \psi(2W-3,2) & \cdots & \cdots & \cdots & \psi(2W-3,2W-2) & \psi(2W-3,2W-1) \\
\psi(2W-2,1) & \psi(2W-2,2) & \psi(2W-2,3) & \cdots & \psi(2W-2,2W-3) & \phi_{2W-2} + \psi(2W-2,2W-2) & \psi(2W-2,2W-1) \\
\psi(2W-1,1) & \psi(2W-1,2) & \psi(2W-1,3) & \cdots & \psi(2W-1,2W-3) & \psi(2W-1,2W-2) & \phi_{2W-1} + \psi(2W-1,2W-1)
\end{vmatrix} = 0 \tag{10}$$

It is easily seen in the determinant that all of the ψ functions can be classified into four groups:

$$\psi_1 = \psi(A = B \mp W), \qquad \psi_2 = \psi(A = B = W)$$

$$\psi_3 = \psi\left(\frac{A + B}{2W} \mp \text{integer}\right)$$

$$\psi_4 = \psi\left(A \mp B, \frac{A + B}{2} = W\right)$$

Furthermore, it can easily be seen from the determinant that all the ψ functions associated with ϕ functions in the principal diagonal are in the form of ψ_1, and all ψ functions in the secondary diagonals are in the form of ψ_4, with ψ_2 in the center of the determinant.

All of the other elements in the determinant are in the form ψ_3.

By the definition of the function of ψ,

$$\psi(A, B) = \sum_{m=1}^{W} \sin \frac{Am\pi}{W} \sin \frac{Bm\pi}{W}$$

Therefore, by trigonometry,

$$\psi(A, B) = \frac{1}{2}\sum_{m=1}^{W} \cos (A - B)\frac{m\pi}{W} - \frac{1}{2}\sum_{m=1}^{W} \cos (A + B)\frac{m\pi}{W}$$

since

$$\sum_{n=1}^{n} \cos n\theta = -\frac{1}{2} + \frac{1}{2}\frac{\sin (2n + 1)(\theta/2)}{\sin \theta/2}$$

therefore,

$$\psi(A, B) = {}^1/_4(\alpha - \tau)$$

where

$$\alpha = \frac{\sin (2W + 1)[(A - B)\pi/2W]}{\sin [(A - B)\pi/2W]}$$

$$\tau = \frac{\sin (2W + 1)[(A + B)\pi/2W]}{\sin [(A + B)\pi/2W]}$$

For ψ_1,

$$\alpha = 2W + 1, \qquad \tau = 1, \qquad \therefore \psi_1 = W/2$$

For ψ_2,

$$\alpha = 2W + 1, \qquad \tau = 2W + 1, \qquad \therefore \psi_2 = 0$$

For ψ_3,

$$\alpha = (-1)A^{+B}, \qquad \tau = (-1)A^{+B} \qquad \therefore \psi_3 = 0$$

For ψ_4,

$$\alpha = 1, \qquad \tau = 2W + 1, \qquad \therefore \psi_4 = -W/2$$

Therefore the determinant may be simplified by introducing the values of ψ as follows:

$$\begin{vmatrix} \phi_1 + (W/2) & 0 & 0 & \dots & 0 & 0 & -W/2 \\ 0 & \phi_2 + (W/2) & 0 & \dots & 0 & -W/2 & 0 \\ 0 & 0 & \dots & \dots & \dots & 0 & 0 \\ \dots & \dots & \dots & \phi_W & \dots & \dots & \dots \\ 0 & 0 & \dots & \dots & \dots & 0 & 0 \\ 0 & -W/2 & 0 & \dots & 0 & \phi_{2W-2} + (W/2) & 0 \\ -W/2 & 0 & 0 & \dots & 0 & 0 & \phi_{2W-1} + (W/2) \end{vmatrix} = 0 \qquad (11)$$

In order to expand this determinant, we define $\Delta_{1,\,2W-1}$ as the above determinant; then, by eliminating outer rows and columns, we get

$$\Delta_{1,\,2W-1} = \left[\left(\phi_1 + \frac{W}{2}\right)\left(\phi_{2W-1} + \frac{W}{2}\right) - \left(\frac{W}{2}\right)^2\right]\Delta_{2,\,2W-2}$$

where $\Delta_{2,\,2W-2}$ is the determinant with the same construction as in $\Delta_{1,\,2W-1}$ but where the principal diagonal begins with $\phi_2 + (W/2)$ and ends in the form of $\phi_{2W-2} + (W/2)$.

Repeating this process, we get, finally,

$$\Delta_{1,\,2W-1} = \phi_W \prod_{n=1}^{W-1}\left[\left(\phi_n + \frac{W}{2}\right)\left(\phi_{2W-n} + \frac{W}{2}\right) - \left(\frac{W}{2}\right)^2\right] = 0$$

The function $\phi_W = 0$ gives the buckling load with each of the span of the whole bar as a Euler's column. That means there are no lateral movements of any elastic supports. The part

$$\prod_{n=1}^{W-1}\left[\left(\phi_n + \frac{W}{2}\right)\left(\phi_{2W-n} + \frac{W}{2}\right) - \left(\frac{W}{2}\right)^2\right] = 0$$

gives the buckling loads for various deflections of the elastic supports.

The above equation may be written in the form

$$\prod_{n=1}^{W-1}[\phi_n\phi_{2W-n} + (W/2)(\phi_n + \phi_{2W-n})] = 0 \qquad (12)$$

where the function ϕ is defined by Eq. (8).

Eq. (12) is the final result of this buckling problem; the number of complete buckling waves is $n/2$, and, consequently, the wave length is $2Wl/n$.

Value of Maximum Critical Elastic Constants

If the value of $C_{max.}$ is the maximum critical value of the elastic constant the bar will buckle in the form that has maximum number of waves. Therefore, $C_{max.}$ may be obtained by putting $P_c = P_E$ and $n = W - 1$ in Eq. (12). We get:

$$C_{max.} = \left(\frac{\pi^2}{2}\right)\left(\frac{4W^6 - 9W^4 + 6W^2 - 1}{5W^6 + W^4}\right) \qquad (13)$$

and the value of $C_{max.}$ when W approaches infinity is

$$\lim_{W \to \infty} C_{max.} = 2\pi^2/5 = 3.95$$

The exact value is "4," as discussed in reference (1); the error is nearly 1 per cent.

Comparison of β and C

The β in Timoshenko's book equals $1/C$ in the present paper, so the following table is a comparison.

W	2	3	4	5	6	7	9	11
β	.500	.333	.293	.276	.268	.263	.258	.255
$\frac{1}{C}$	.504	.337	.296	.279	.271	.266	.261	.259

and the result $C = 2X[1 + \cos(\pi/W)]$ by Ebner's formula gives the value of $1/\beta$ as tabulated in Timoshenko's book.[1]

The values for $C_{max.}$ up to 20 elastic supports have been calculated with Eq. (13) and plotted in Fig. 2.

Numerical Calculations

Take an element out of Eq. (12) and let $\rho = n/W$. Then, after manipulation,

$$C = [\rho(2-\rho)\pi]^2 \frac{[\rho^2 - (P_c/P_E)][(2-\rho)^2 - (P_c/P_E)]}{[\rho^2 + (2-\rho)^2](P_c/P_E) - [\rho^4 + (2-\rho)^4]} \tag{14}$$

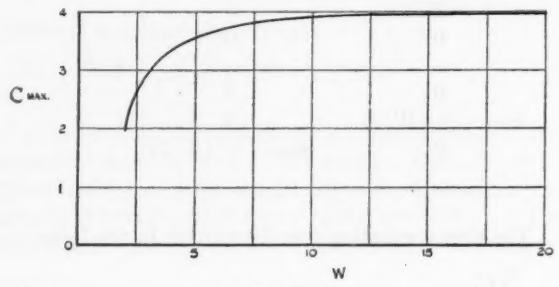

Fig. 2.

The difficulty is to find what is the value of ρ for obtaining the minimum value of P_c/P_E. Evidently an envelope is desirable for this purpose, but it is difficult to obtain such an equation. Therefore, a set of curves for ρ varying from 0.1 up to 0.9, which covers all the range of ρ since the range of n is from 1 to $W - 1$, has been computed and is shown in Fig. 3. This figure will help the stress analyst to find the value of ρ for a particular value of W, and with a few trials it is easy to get the correct answer by using Eq. (14).

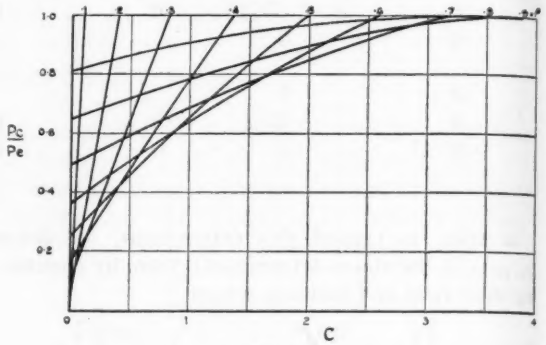

Fig. 3.

Example

Given Data:

$I = 0.004$ in.^{4}
$l = 21$ in.
$E = 10 \times 10^6$ lbs. per sq. in.
$K = 75$ lb. per in.
$W = 6$
$A = 0.04$ sq.in.

$$P_E = \frac{\pi^2 \times 10^7 \times 0.004}{21 \times 21} = 900 \text{ lbs.}$$

$$\frac{P_E}{l} = \frac{900}{21} = 42.7 \text{ lbs. per in.}, \qquad \therefore C = \frac{75}{42.7} = 1.75$$

The values of ρ in this case are: $\rho = 5/6 = 0.83$, $\rho = 4/6 = 0.67$, $\rho = 3/6 = 0.5$, $\rho = 2/6 = 0.33$, and $\rho = 1/6 = 0.17$.

From Fig. (4) we see that the minimum value of ρ is about 0.6. Therefore, use $\rho = 0.67$. Substituting into Eq. (12) or Eq. (14) or estimating from Fig. 4.

$$P_c/P_E = 0.80$$

Therefore, $P_c = 0.80 \times 900 = 720$ lbs.

The corresponding stress

$$S = 720/0.04 = 18{,}000 \text{ lbs. per sq.in.}$$

The number of complete buckling waves is $4/2 = 2$. The wave length $= (2)(6)(21)/4 = 63$ in.

References

[1] Timoshenko, *Theory of Elastic Stability.*
[2] Aitkin, A. C., *Determinants and Matrices.*

Machmeters for High-Speed Flight Research

HERBERT SCHAEFER*

Kollsman Instrument Division of Square D Company

SUMMARY

The Machmeter, an instrument designed to indicate the Mach Number at which an aircraft is flying, is being used as a test instrument as well as a flight instrument. The objective of this paper is to give a résumé of the theory and design of various types of Machmeters now in use.

After an explanation of the Mach Number and a brief survey of transonic and supersonic flow conditions, the aerodynamics of the Machmeter is presented. For the supersonic speed, a simplified exact equation is given for the stagnation pressure as a function of the flight Mach Number and the free-stream pressure. Graphs are presented showing the relations of pressure and temperature at the stagnation point vs. the flight Mach Number.

After a short description of the design of a subsonic Machmeter, a more detailed description of the newly developed transonic Machmeter follows, mentioning a number of design details. Then the Mach Number Limit Switch is briefly discussed, followed by a description of the Maximum Allowable Airspeed or Mach Airspeed Indicator, the aerodynamic theory of which is also presented.

The location of the pressure vents is discussed, and a new type of supersonic static pressure probe is suggested.

The possibility of a Machmeter operated by temperature parameters is mentioned, but it is considered not feasible because of the difficulties in obtaining the proper temperature values in flight.

With the experience already gained in developing Machmeters, it seems certain that, in order to keep step with the pace of the increase in flying speeds, Machmeters with increased ranges of Mach Number and altitude can be designed and built.

(I) INTRODUCTION

THE INCREASE in flying speed during the last decade has brought into practical aerodynamics as a new parameter, the Mach Number, the ratio of true air speed to the speed of sound. The dependence of aerodynamic phenomena on the Mach Number has been known to aeronautical engineers for a long time, but for the flying speeds attained until recently, this dependence on the Mach Number was negligible, and so, except in the domain of ballistics, the Mach Number was chiefly of theoretical interest. However, as flying speeds reached such magnitudes that in certain regions around an aircraft local air speeds were attained which approached or even exceeded the local speed of sound, it became imperative to know the Mach Number at which the aircraft was flying in order to determine the safe operational speed limits. For this purpose the Machmeter, an instrument designed to indicate the Mach Number at which an aircraft is flying, was developed. For operational use in high-speed aircraft, a sister instrument of the Machmeter, the Maximum Allowable Airspeed Indicator or Mach Airspeed Indicator, was also developed. The theory and design of various types of Machmeters is the topic of this paper.

Presented at the Instruments Session, Sixteenth Annual Meeting, I.A.S., New York, January 26–29, 1948.

* Project Engineer.

(II) CONCEPT OF THE MACH NUMBER

The Mach Number is defined as the ratio of the flow velocity of a fluid to the velocity of sound in that fluid. It was named in honor of the Austrian physicist Ernst Mach, who worked on basic research in high-speed aerodynamics and ballistics as early as the last century. In the case of an aircraft, it is the so-called "Free-Stream Mach Number" or "Flight Mach Number" that is of chief interest; its definition is, the ratio of the true air-speed V of the aircraft with respect to the undisturbed air ahead to the speed of sound in the same air c:

$$M = V/c \tag{1}$$

The term true air speed is self-explanatory. The speed of sound in air is equal to the velocity of propagation of small pressure disturbances through the air.

Thermodynamic changes occurring during the propagation of such small pressure disturbances can be considered as being adiabatic, since all the changes of the parameters involved are small and no heat exchange with the surrounding air occurs. Assuming, furthermore, that the air is a perfect gas, which follows the general thermodynamic equation of state $p/\rho = RT$, the speed of sound is given by the equation

$$c = \sqrt{dp/d\rho} = \sqrt{kp/\rho} = \sqrt{kRT} \tag{2}$$

In these equations the symbols represent the following thermodynamic parameters: p, the barometric pressure; ρ, the mass density; T, the absolute temperature; R, the gas constant; and $k = c_p/c_v$, the ratio of the specific heats at constant pressure and constant volume, the numerical value of which is usually taken for air to be $k = 1.400$.

Since in the atmosphere, pressure, density, and temperature are all variables, the speed of sound is a variable also. As the temperature diminishes with altitude, the speed of sound also diminishes, since it varies as the square of the absolute temperature, as indicated by Eq. (2). Under standard conditions, the magnitude of the velocity of sound is 761.06 m.p.h. at sea level and is 662.23 m.p.h. at the tropopause—i.e., an altitude of 35,332 ft. This value remains approximately constant up to 100,000 ft. In the upper atmosphere the temperature and, consequently, the speed of sound

will increase and decrease several times with increase in altitude, as recent research has shown.[1]

From the dependence of the sonic speed on altitude, it is evident that two aircraft flying at a certain true air speed at two different altitudes will fly at different Mach Numbers. If an aircraft is diving with constant true air speed, the flight Mach Number will continuously decrease because the speed of sound is increasing. This fact has probably saved the life of many a pilot who was diving, with his aircraft out of control, because it was flying faster than its critical Mach Number; during the dive the flight Mach Number became subcritical, and so the pilot could regain control of his aircraft.

The physical significance of the Mach Number becomes evident if Eq. (1) is squared:

$$M^2 = V^2/c^2 = V^2/kRT$$

for then, the numerator represents a direct measure of the controlled or directed kinetic energy of the flow. The denominator represents the random translatory and rotary kinetic energy of the molecules, because it contains the absolute temperature which measures that energy. The square of the Mach Number represents, therefore, the ratio of the directed kinetic energy to the random molecular energy.[2] Another manner of defining the square of the Mach Number is that it represents the ratio of the mass forces to the elastic forces.[3] It is interesting to note that in aerodynamic equations the Mach Number rarely occurs in the first power but is almost always squared.

(III) Flow Phenomena in Transonic and Supersonic Flow

A little digression into the fundamentals of high-speed aerodynamics will show at once the great importance of the Machmeter as a tool for high-speed flight research. This is particularly true for transonic speeds, in which the flow around the aircraft is a mixture of subsonic and supersonic flow. Since both these types of flow follow different physical laws, a particularly difficult flow pattern results. It is chiefly for the research in this transonic region that a transonic Machmeter with a range of flight Mach Numbers 0.5 to 1.5 was developed.

If an airflow takes place at extremely slow speed—that is, at a low Mach Number with subsonic flow velocity—the air can be assumed to be incompressible. Up to a Mach Number of 0.15—i.e., an air speed of only 15 per cent of the speed of sound—the errors introduced by the assumption of incompressibility are of a magnitude of about 1 per cent. Since an incompressible fluid has no elasticity, the influence of the Mach Number, which represents the ratio of the mass forces to the elastic forces, is negligible. The important parameter for such flows is the Reynolds Number, the ratio of the inertia forces to the viscous forces. If the speed of flow is increased and, therefore, the Mach Number is also increased, the effect of compressibility becomes increasingly greater. When the flow velocity is increased still more, the Mach Number finally becomes greater than unity—that is, the flow velocity is now greater than the velocity of sound and is therefore supersonic. Flow phenomena that occur in this domain are entirely different from those in subsonic flow. The most important of these are the following:

Pressure disturbances cannot be propagated into every part of the fluid but are restricted to certain domains within the fluid which lie downstream from the point of disturbance.

Flow through convergent stream tubes is decelerated, while flow through divergent stream tubes is accelerated; this is exactly the opposite of the behavior of subsonic flows.

Furthermore, discontinuities with an increase in entropy, or so-called shocks, can occur in supersonic flow; these are impossible in subsonic flow.

The reasons for this entirely different behavior of supersonic flow is, mathematically expressed, that the differential equations of motion for supersonic flow are hyperbolic, while those for subsonic flow are elliptic.[4]

It is particularly the phenomenon of the occurrence of shocks that causes the most difficulties in high-speed flight. A shock is actually nothing but a special detached interior boundary layer in a fluid, which represents a discontinuity sheet through which the pressure, density, temperature, and entropy increase suddenly while the flow velocity drops.[5] Such shock discontinuity sheets are extremely thin. Taylor and Maccoll, for instance, give the thickness of a shock wave through which the velocity drop is approximately $^1/_{10}$ of the speed of sound as less than 0.0033 mm. = 0.00013 in.[6] Such shock waves will occur as soon as the local sonic speed is reached somewhere near the aircraft. Usually they will appear first on the upper surface of the wing and then, as the speed is increased, on the lower surface as well. The reason for their occurrence lies in the fact that pressure disturbances from the trailing edge of the airfoil cannot pass through the region of supersonic flow, because the speed of their propagation is only that of the speed of sound. The pressure disturbances, therefore, accumulate at the boundary between the subsonic and the supersonic flow and form a shock wave. Such shock waves have the tendency to distort the entire flow pattern around an aircraft and simultaneously disturb the pressure distribution around the wings. The creation of a region of high pressure behind the shock will cause adverse pressure gradients within the boundary layer, because a propagation of pressure through the subsonic part of the boundary layer from the downstream to the upstream side of the shock is possible. This phenomenon usually causes boundary separation. The occurrence of shock waves on the lifting surfaces causes, in gen-

eral: decrease in lift; increase in drag; pronounced changes in aerodynamic stability; loss of effectiveness of the control surfaces, which in extreme cases may even reverse their intended effects; structural damages to the control surfaces and other parts of the aircraft because of violent oscillations due to shock stall; and severe buffeting.[7,8]

The Mach Number of the undisturbed flow, or flight Mach Number, at which the maximum local Mach Number becomes unity in some region around the aircraft, is called the lower critical Mach Number. The disturbing phenomena listed above will not occur immediately at this particular Mach Number, but at one somewhat higher than the critical flight Mach Number, although still below unity.[8] However, this critical Mach Number is not valid for all flight conditions; the aircraft will have several critical Mach Numbers: one for straight and level flight, one for diving, and so on. The lower critical Mach Number is an important parameter for the pilot of a high-speed aircraft, because it warns him that he entered the transonic range with its impending dangers.

At a certain flight Mach Number the flow around an aircraft becomes entirely supersonic, except for the boundary layer and small regions near the nose of the aircraft and the leading edges of the airfoils. This flight Mach Number is called the upper critical Mach Number. This parameter is also important to the pilot, because it indicates the end of the transonic range and marks the beginning of completely supersonic flow around the aircraft.[8]

The lower critical Mach Number of an aircraft and many of the detrimental compressibility phenomena can be ascertained with the subsonic Machmeter, which has a maximum range up to Mach Number 1.0. This instrument has already been in use for many years. It is now up to the newly developed transonic Machmeter, the range of which is extended beyond Mach Number 1.0, to assist the test pilot in forcing his way beyond the transonic flight region into the domain of completely supersonic flow, which until today has been the realm of meteors, jet-propelled missiles, and rockets.

Machmeters are not exclusively flight research instruments; they are also used operationally. Furthermore, they have proved their usefulness for aerodynamic research in wind tunnels.

(IV) Aerodynamics of the Machmeter

There are several possibilities for obtaining the free-stream or flight Mach Number by measuring various aerodynamic parameters in flight. One method makes use of the stagnation pressure p_3 at the head of a pitot tube and the static atmospheric pressure p_1. These two parameters may be used either as differential pressure $\Delta p = p_3 - p_1$, as in the case of the conventional air-speed indicator, or as a pressure ratio p_3/p_1. Another possibility is to use the stagnation temperature T_3 and the free-stream temperature T_1.

In the following section the aerodynamic relations between these parameters and the flight Mach Number will be developed. Since the subsonic and the supersonic flow conditions are different, both cases are treated separately.

(A) *Subsonic Air Speed*

In the mathematical treatment of this problem the following simplifying assumptions can be made:

(a) The air is considered to be a continuous medium.
(b) The air is considered to be an ideal gas obeying the general thermodynamic equation of state.
(c) Being an ideal gas, as assumed under (b), its viscosity is zero.
(d) The airflow is considered one-dimensional; this assumption is justifiable, because only a small stream tube is being considered, which is leading directly to the small orifice at the head of the pitot tube.
(e) The coordinate system of reference is fixed in the aircraft, which is traveling with constant velocity through the undisturbed air; this defines the resulting flow as a steady flow, and all time derivatives vanish.
(f) The motion is considered irrotational.
(g) No outside forces, such as gravity, are influencing the flow.
(h) The flow occurs without any exchange of heat with the surroundings—i.e., it is adiabatic.
(i) The entropy of the air remains constant—i.e., the flow is isentropic.

With the above assumptions the general equation of energy in the following form can be used as the starting point of the derivation.[9]

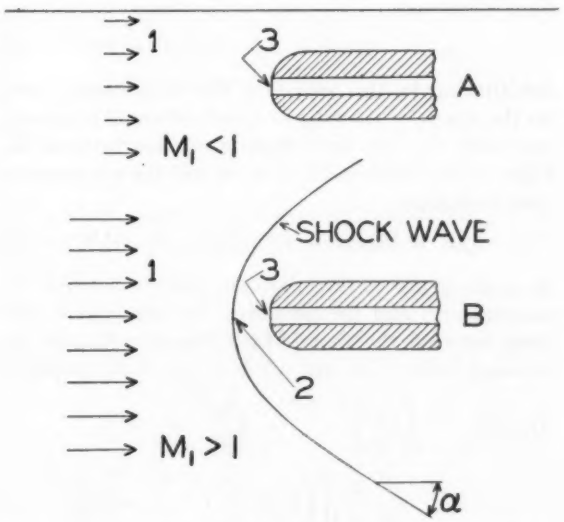

Fig. 1. Schematic diagram of a pitot tube at A, subsonic, and B supersonic speed.

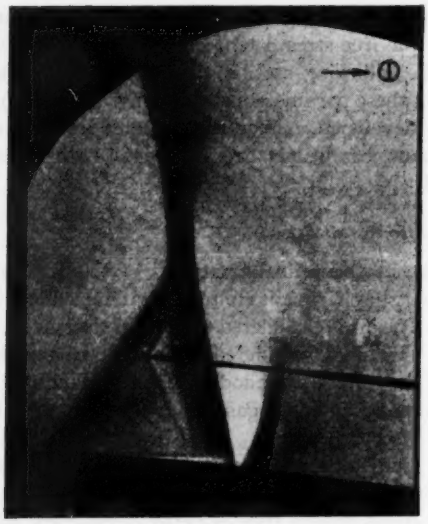

FIG. 2. Bow wave ahead of a pitot tube within a λ-shock in a wind tunnel at $M = 1.225$. (Fig. 4 of reference 10.)

$$u(du) + di = 0 \tag{3}$$

In this equation u represents the velocity in the flight direction of the aircraft and i the heat content or enthalpy of the air. By designating the free-stream conditions with the suffix 1 and the conditions at the stagnation point of the pitot tube with 3 (see Fig. 1) and integrating between stations 1 and 3, Eq. (3) becomes, with $u_3 = 0$,

$$u_1^2 = 2(i_3 - i_1) \tag{4}$$

Introducing the relation between the enthalpy i and the speed of sound c

$$i = [k/(k-1)]\,(p/\rho) = c^2/(k-1) \tag{5}$$

Eq. (4) becomes

$$u_1^2 = [2/(k-1)]c_1^2[(c_3/c_1)^2 - 1] \tag{6}$$

Substituting in this equation the temperature ratio for the square of the ratio of speeds of sound in accordance with Eq. (2), the following relation between the flight Mach Number $M_1 = u_1/c_1$ and the temperature ratio is obtained.

$$M_1 = \left\{[2/(k-1)]\,[(T_3/T_1) - 1]\right\}^{1/2} \tag{7}$$

By making use of the adiabatic relation between the temperatures and the pressures, the subsequent relations between the flight Mach Number M_1 and the pressure ratios p_3/p_1 and $\Delta p/p_1 = (p_3 - p_1)/p_1$ follow.

$$M_1 = \left\{\frac{2}{k-1}\left[\left(\frac{p_3}{p_1}\right)^{(k-1)/k} - 1\right]\right\}^{1/2} = \left\{\frac{2}{k-1}\left[\left(1 + \frac{\Delta p}{p_1}\right)^{(k-1)/k} - 1\right]\right\}^{1/2} \tag{8}$$

The dependence of the temperature ratio and the pressure ratio on the flight Mach Number is then

$$T_3/T_1 = 1 + [(k-1)/2]\,M_1^2 \tag{9}$$

$$p_3/p_1 = \left\{1 + [(k-1)/2]\,M_1^2\right\}^{k/(k-1)} \tag{10}$$

(B) *Supersonic Air Speed*

In the supersonic case the equations developed for the subsonic case are not applicable but must be somewhat modified.

Since the nose angle of a pitot tube will always be above the critical angle because of the finite diameter of the pitot orifice, a bow wave will always precede the pitot tube when it travels with supersonic speed through the air. (See Fig. 1.) This bow wave is a curved detached shock wave that at some distance behind the pitot tube blends into the Mach cone. Fig. 2 is an interesting schlieren photograph of a so-called λ-shock in a wind-tunnel test. It clearly shows the pitot tube projecting into the λ-shock, and the bow wave ahead of the nose of the tube. This photograph was taken at a Mach Number of 1.225 (Fig. 4 of reference 10).

The problem now is to find first the flow conditions through the shock wave and then the slowing up of the air stream to zero velocity at the stagnation point at the nose of the pitot tube.

The only part of the bow wave that is of interest here is the center region through which the stream tube passes, which leads to the pitot orifice. This part of the shock wave will be curved, but the radius of curvature for this small area of the bow wave will be extremely large, at least for moderately high Mach Numbers, so that it is permissible to assume here the radius of curvature to be infinite. Since this small area in the center of the bow wave will be perpendicular to the stream tube, the problem can be treated as if a plane shock wave were ahead of the pitot opening.

From the general theory of plane compression shocks, it follows directly that the flow in the straight stream tube between the bow wave and the pitot orifice will be subsonic over its entire length (Prandtl's relation $u_1 u_2 = c_*^2$, in which 2 designates the state behind the shock wave and c_*, the critical speed of sound). Furthermore, no deflection of the velocity vector will occur because of the flow through the shock wave, so that the assumptions (d) (one-dimensional flow) and (f) (irrotational flow), which were made for the subsonic case, are still valid. These last assertions are valid, however, only for the small stream tube in the center of the shock wave.

While the air cannot be considered an ideal gas with no viscosity in the bow wave proper, this assumption can be retained for the air before and behind the bow wave. The same holds true with regard to the adiabatic flow before and behind the bow wave.

The assumptions (a) (the air being a continuous medium), (e) (coordinate system moving with the air-

TABLE 1
Constants of Eqs. (15) and (16) for Various Values of $k = c_p/c_v$

k	A	B	D	F
1.4	166.9216	7	5/2	1.2876
1.3	1628.218	26/3	10/3	1.2177
1.2	285311.7	12	5	1.1466
1.1	2.852826×10^{13}	22	10	1.0741

plane and steady flow condition), and (g) (no gravity), can also be retained.

Condition (i), (constant entropy) cannot hold true through the shock wave. Also, the entropy will not be constant behind the curved shock wave, but will vary from point to point. However, the flow ahead of the bow wave and in the small stream tube behind the center part of the bow wave can be considered as being isentropic, but with different values of entropy.

The temperature ratio between the stagnation temperature T_3 and the free-stream temperature T_1 for supersonic flow is identical with that for subsonic flow as given in Eq. (9). This follows immediately from the integration of the energy equation, Eq. (3).

$$(1/2)u_1^2 + i_1 = (1/2)u_2^2 + i_2 = i_3 \qquad (11)$$

In this equation suffixes 1 and 2 denote arbitrary states along a stream line, and the suffix 3 denotes the state of rest. The energy equation holds true whether states 1 and 2 are on the same side of a shock or on opposite sides. The enthalpy of the state of rest, i_3 is, therefore, the same in both cases. Since for an ideal gas the enthalpy is $i = c_pT$, and c_p is a constant, it follows that the stagnation temperature T_3 is independent of any shock condition.[4]

The pressure ratio through the plane shock can be determined by applying to the flow the laws of conservation of mass, of conservation of momentum, and of conservation of energy. Designating the conditions behind the shock with the suffix 2, the pressure ratio through the shock becomes

$$\frac{p_2}{p_1} = \left(\frac{2k}{k+1}\right) M_1^2 - \left(\frac{k-1}{k+1}\right) \qquad (12)$$

This relation was first given by Prandtl. The second law of thermodynamics—which states that the entropy of a closed system can only remain constant, or increase, but cannot decrease—limits this equation to pressure increases through the shock—i.e., only compression shocks are possible.

After passing through the shock wave, the air is slowed down to zero velocity at the stagnation point at the orifice of the pitot tube, thereby being compressed adiabatically. The equations derived for the subsonic case can be applied to this compression, except that the conditions of state 2 behind the shock wave have to be substituted for the free-stream conditions of state 1. The adiabatic compression behind the shock wave is then

$$p_3/p_2 = \{1 + [(k-1)/2]\ (M_2^2)\}^{k/(k-1)} \qquad (13)$$

in which M_2 represents the Mach Number behind the shock wave, which is smaller than 1.0.

Combining the two pressure ratios, Eqs. (12) and (13), Lord Rayleigh, in 1910, obtained the following equation for the ratio of the stagnation pressure to the static pressure:[11]

$$\frac{p_3}{p_1} = \left[\left(\frac{2k}{k+1}\right) M_1^2 - \left(\frac{k-1}{k+1}\right)\right] \times \left\{\frac{(k+1)^2}{4k} + \frac{k^2-1}{4k}\left[\frac{1}{\left(\frac{2k}{k+1}\right) M_1^2 - \frac{k-1}{k+1}}\right]\right\}^{k/(k-1)} \qquad (14)$$

To extract the flight Mach Number M_1 in a simple exact form from this somewhat cumbersome equation seems a hopeless task. However, the equation can be simplified somewhat by introducing the magnitude of the ratio of the specific heats k. Then it can be written in the form

$$p_3/p_1 = AM_1^2/[B - (1/M_1^2)]^D \qquad (15)$$

With increasing Mach Number this equation tends to the limiting equation

$$(p_3/p_1)_{M_1 \to \infty} = FM_1^2 \qquad (16)$$

The constants A, B, D, and F, which are dependent on k, are listed in Table 1. For air, with $k = 1.400$, Eqs. (15) and (16) read

$$p_3/p_1 = 166.9216\ M_1^2/[7 - (1/M_1^2)]^{3.5} \qquad (17)$$

and

$$(p_3/p_1)_{M_1 \to \infty} = 1.2876\ M_1^2 \qquad (18)$$

For a Mach Number of 4.0 in air, the difference between the two equations is approximately 2 per cent. (See Table 2.)

TABLE 2
Pressure Ratio: Stagnation Pressure to Static Pressure p_3/p_1 for Various Values of $k = c_p/c_v$ and Different Flight Mach Numbers M_1; and the Differences Between the Values p_3/p_1 in Percentages Obtained by Using the Limiting Eq. (16) and the Exact Eq. (15).

	$k = 1.4$		$k = 1.3$		$k = 1.2$		$k = 1.1$	
M_1	p_3/p_1	Diff. %	p_3/p_1	Diff. %	p_3/p_1	Diff. %	p_3/p_1	Diff. %
1.0	1.893	−32.0	1.832	−33.5	1.772	−35.3	1.710	−37.2
1.5	3.413	−15.1	3.265	−16.1	3.116	−17.2	2.964	−18.5
2.0	5.640	−8.7	5.370	−9.3	5.096	−10.0	4.817	−10.8
3.0	12.06	−3.9	11.44	−4.2	10.81	−4.5	10.17	−4.9
4.0	21.07	−2.2	19.96	−2.4	18.83	−2.6	17.68	−2.8
5.0	32.65	−1.4	30.92	−1.5	29.15	−1.7	27.35	−1.8
6.0	46.82	−1.0	44.31	−1.1	41.76	−1.2	39.16	−1.3

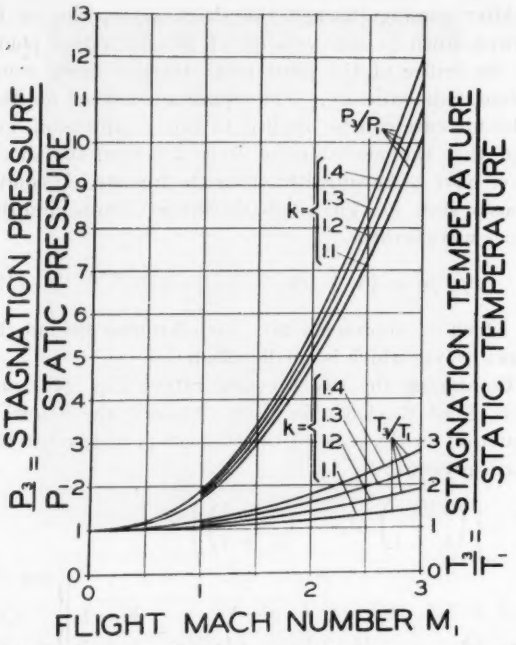

FIG. 3. Diagram of ratios: stagnation pressure to static pressure p_3/p_1 and stagnation temperature to static temperature T_3/T_1 vs. flight Mach Number M_1 for various values of $k = c_p/c_v$.

Zahm derived an expression somewhat similar to Eq. (15), which, however, is not quite so simple as the above.[12]

For high Mach Numbers these equations are not valid anymore, because appreciable heat exchange will occur, and condition (h) (adiabatic flow), under which the above equations were derived, no longer holds true. They are also not valid for very high altitudes, for there the air can be considered no more as a continuous medium, because of the long molecular paths due to the low density.

The curves for the temperature ratio T_3/T_1 and the pressure ratio p_3/p_1 versus the free stream, or flight Mach Number, are shown in Fig. 3. Since, in the near future, there may be some interest in Machmeters for wind tunnels that are operated with a different gas than air, families of curves for different values of the ratio of the specific heats k have been plotted. These curves show that a standard Machmeter, calibrated for air, can be recalibrated without too much difficulty for some other gas. For instance, the N.A.C.A. has investigated the possibility of using Freon-12 for aerodynamic testing. This gas has a value of $k = 1.125$, its density is approximately four times that of air, and its velocity of sound is less than one-half that of air.[12]

Although the equations of the pressure ratio for the subsonic and the supersonic cases are different, the pressure ratio curves are continuous at Mach Number $M_1 = 1.0$, since the first derivatives of both equations, which indicate the slopes of the curves, are identical at this point. However, the second derivatives, of which the radii of curvature are functions, are different for both equations at that particular point.

Fig. 4 shows the actual calibration curves of Machmeters operated by the differential pressure $\Delta p = p_3 - p_1$ for $k = 1.40$. A family of curves of Δp versus flight Mach Number M_1 for altitudes h from 0 to 100,000 ft. has been plotted. The barometric pressures for the various altitudes have been taken to be the pressures of the U.S. Standard Atmosphere.[14] It is at once apparent that such a Machmeter must have an altitude correction or, expressed more precisely, a barometric pressure correction. The mechanism of a Machmeter consists, therefore, of a lever arrangement actuated by a diaphragm that responds to the differential pressure; with changes in altitude, this lever arrangement is modified by a second diaphragm that responds to barometric pressure changes.

(V) The Subsonic Machmeter

The subsonic Machmeter had already been developed during the war for the Army. It has been used extensively, both in test work and in flight operations. It is calibrated in accordance with Eq. (8) for a range of flight Mach Numbers 0.3 to 1.0 and a range of altitudes from 0 to 50,000 ft. (see Fig. 4) with an accuracy of ± 0.01 Mach Number over the entire range of calibration. The temperature range of operation is from $-55°$ to $+70°$C. with an accuracy of ± 0.02 at these

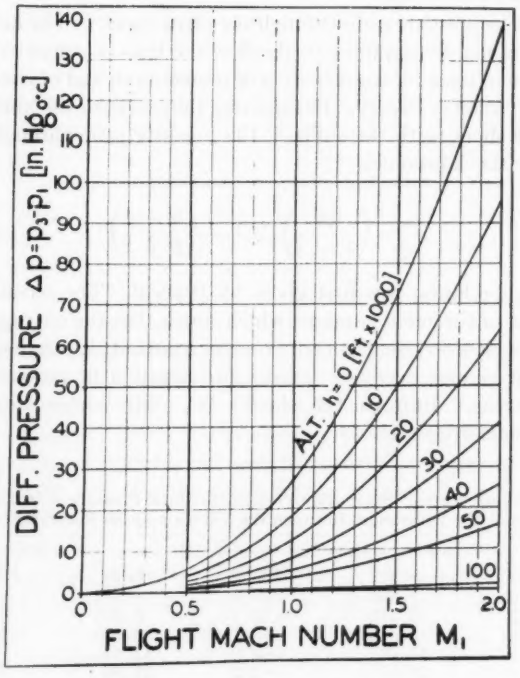

FIG. 4. Diagram of differential pressure $\Delta p = p_3 - p_1$ vs. flight Mach Number M_1 for various altitudes h and $k = 1.40$.

extreme temperatures. More accurate calibration is possible but requires a great deal more calibration time than the standard instrument.

The differential pressures operating this instrument range from 0.221 to 26.718 in. Hg (0°C.), the first value corresponding to $M_1 = 0.3$ at $h = 50{,}000$ ft., while the last value corresponds to $M_1 = 1.0$ at sea level.

A schematic diagram of the operation of the subsonic Machmeter is shown in Fig. 5. The stagnation pressure or pitot pressure p_2 is led into the open diaphragm, while the static barometric pressure p_1 is led into the inside of the airtight case of the instrument. The resulting movement of the open diaphragm, which is a function of the differential pressure Δp, by means of a lever arm rotates the first rocking shaft, which in turn rotates the sector rocking shaft through a pair of levers. From this sector rocking shaft the movement is transmitted to the handstaff by means of a sector and pinion. The altitude correction is accomplished with an evacuated altitude diaphragm, which responds to the static pressure p_1. With increase in altitude—i.e., decrease in static pressure—this diaphragm expands and pushes the first rocking shaft to the left. This movement causes a shortening of the effective lever arm of the sector rocking shaft lever, thereby changing the amount of rotation caused by the open diaphragm.

The temperature compensation of this instrument is accomplished with a bimetallic bracket mounted on the altitude diaphragm, as is shown in the diagram. This bracket preloads the diaphragm by means of two push pins, which engage the center piece, thereby changing the expansion of the diaphragm in such a manner as to offset the temperature error of the instrument.

The actual instrument is not so simple as this schematic diagram may indicate. The open diaphragm is actually restrained by a leaf spring; screws restrain the deflection of this spring so that with increase of

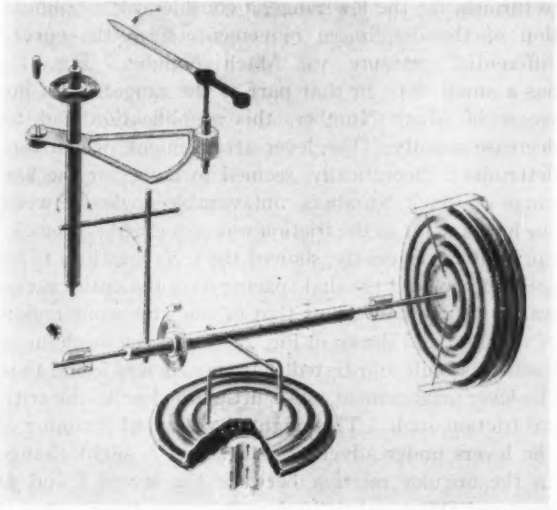

FIG. 5. Schematic diagram of the subsonic Machmeter.

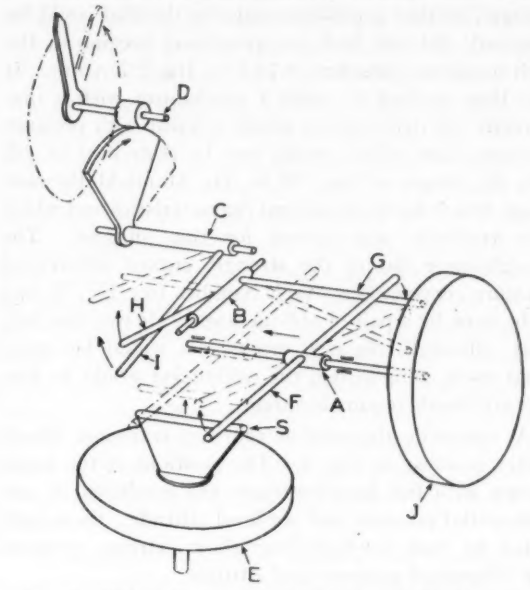

FIG. 6. Schematic diagram of the transonic Machmeter.

Mach Number the pointer movement is uniform. The altitude diaphragm must be made with extreme accuracy so as to meet a certain expansion characteristic with change of barometric pressure. Furthermore, the two levers connecting the two rocking shafts are not perpendicular to their respective shafts, as shown in the schematic diagram, but one of them is in an oblique position. In spite of a number of adjustments, which are also not shown in the diagram, the calibration of this instrument is rather delicate and tedious, since any adjustment made on one part of the mechanism has immediate effect on the other part.

(VI) The Transonic Machmeter

The transonic Machmeter, which is rather a recent development for the present high-speed research, is calibrated in accordance with Eqs. (8) and (17) for the subsonic and supersonic speeds, respectively. Its range is for flight Mach Numbers 0.5 to 1.5 and for altitudes from 0 to 50,000 ft. The first instruments had an accuracy of ±0.01 Mach Number for the range of 0.65 to 1.35; the two extremes of the range were within ±0.015. It is expected that future instruments will have the accuracy of ±0.01 throughout. The temperature range of operation is the same as that of the subsonic Machmeter.

The differential pressures operating the instrument are from 0.640 to 72.208 in. Hg (0°C.), the first value corresponding to $M_1 = 0.5$ at $h = 50{,}000$ ft., while the last value corresponds to $M_1 = 1.5$ at sea level.

The first intention was to use, for this transonic Machmeter, a modified mechanism of the subsonic instrument. Preliminary tests with restraining of the dia-

phragm, so that a uniform scale on the dial could be obtained, did not look too promising because of the high maximum pressure of 72.2 in. Hg (2.7 Atm.). It was then decided to build a mechanism with a diaphragm, the deflection of which is linear with pressure increase, and which would not be restrained at all. The diaphragm of the 100 in. Hg Manifold Pressure Gage, which has good general characteristics and which was available, was chosen for this purpose. The straightening out of the strongly curved differential pressure curve versus Mach Number (see Fig. 4) was to be done by a pair of oblique levers. It was also felt, that, although this new mechanism would be somewhat more complicated, the calibration would be simpler and would require less time.

A schematic diagram of the first transonic Machmeter is shown in Fig. 6. The positions of the levers shown with full lines represent the condition of zero differential pressure and sea-level altitude; those indicated by dash-dot-dash lines show extreme positions for differential pressure and altitude.

The operation of the instrument is as follows:

As in the case of the subsonic Machmeter, the stagnation or pitot pressure p_3 is led into the open diaphragm E, while the static pressure p_1 is led into the inside of the airtight instrument case. The movement of the open diaphragm is transmitted by means of the lever F, which is mounted on rocking shaft A, to rocking shaft B. The rotation of this rocking shaft is essentially proportional to the differential pressure. Then a pair of oblique levers I and H transmits the rotation of rocking shaft B to rocking shaft C; the obliqueness of the levers is so computed that the rotation of rocking shaft C is approximately proportional to the Mach Number. The pointer of the instrument is rotated by means of a sector on rocking shaft C and a pinion on the handstaff D.

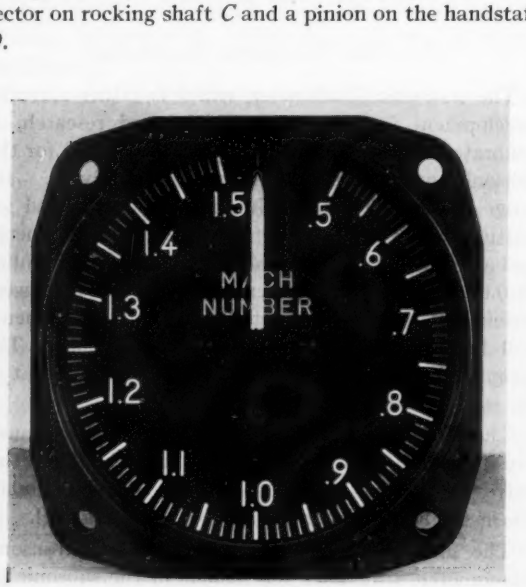

FIG. 7. Front view of the transonic Machmeter.

The altitude correction is attained in the following manner:

Each calibration curve of the family of curves in Fig. 4 is spaced from the abscissa in the ratio of the barometric pressure at any altitude to the sea-level pressure, p_h/p_{SL}. This means that, for instance, if an aircraft is flying at a Mach Number of 1.2 at an altitude of 50,000 ft., the deflection of the air-speed diaphragm will correspond to a differential pressure of only (3.437/29.921)42.114 = 4.838 in. Hg; without an altitude correction the pointer would, therefore, indicate a Mach Number of about 0.46. In order to read the correct Mach Number of 1.2, the rotation of rocking shaft B has to be speeded up in the proper ratio. By moving rocking shaft A closer to rocking shaft B, the effective length of the lever arm G is shortened. For a certain rotation of rocking shaft A, the rotation of rocking shaft B is now increased. This axial displacement of rocking shaft A is accomplished by the altitude diaphragm J, which expands with decrease of static pressure.

The actual instrument is not so simple as the schematic diagram. A set of four cells is used for the open diaphragm, which has a straight-line movement with increase in pressure. The total deflection of the diaphragm for the full range of 1.5 Mach Numbers is 0.260 in., while the deflection for the lowest calibration point of Mach Number 0.5 is only 0.0023 in. This small movement deflects the pointer approximately 140° from the zero point of the mechanism to the graduation 0.5. On the finished instrument, however, the pointer is restrained by a stop at the zero graduation, which is only about 25° away from the 0.5 graduation. Fig. 7 shows the dial arrangement of the first transonic Machmeter.

The specification called for a dial with nearly uniform spacing of the graduations. This meant that the oblique lever arrangement of levers I and H would have to furnish, for the low range, a considerable amplification of the diaphragm movement, since the curve, differential pressure vs. Mach Number (Fig. 4), has a small slope in that part of the range; with increase of Mach Number, this amplification had to decrease rapidly. The lever arrangement, which was determined theoretically, seemed to have, for the low range of Mach Numbers, unfavorable angles between the levers as far as the friction was concerned. A mock-up, built subsequently, showed the lever relations to be satisfactory, and the dial spacing over the entire range was as nearly uniform as that of the supersonic region of the final dial shown in Fig. 7. When the mechanism itself was built and tested, however, it was found that the lever arrangement was a little too close to the critical friction angle. This might have caused jamming of the levers under adverse conditions. A slight change in the angular relation between the levers I and H removed this potentially dangerous condition; but it also somewhat spoiled the appearance of the dial in

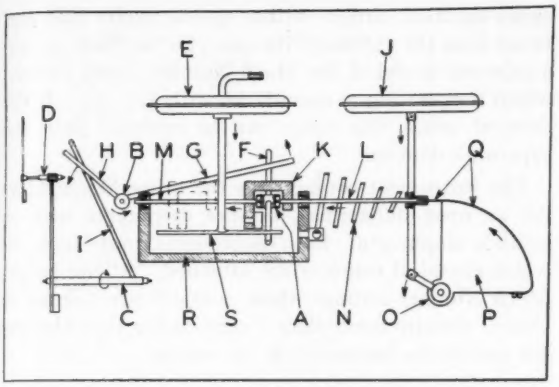

FIG. 8. Schematic diagram of the altitude compensation of the transonic Machmeter.

regard to uniformity at the beginning of the scale, as can be seen in the photograph.

An interesting feature of the instrument is the mechanism for the altitude correction. It is shown schematically in Fig. 8.

Rocking shaft *A*, with its lever *F* and counterweight, is jewel-mounted in a balanced magnesium frame *K*. The frame is supported by two highly polished and hardened slide rods *L* and *M* of 0.031-in. diameter. The ends of these rods, which are clamped into the frame *K*, have 0.012-in. diameter pivots carrying the rocking shaft *A*. The rods slide in jewel bearings. In spite of the considerable complication, rocking shaft *A* is mounted in separate bearings of small size in order to reduce the friction of the mechanism to a minimum. The axial movement of this assembly is accomplished by a conical hairspring *N*, which is mounted on a collet clamped on the right end of the slide rod *L*. This conical hairspring has a dual purpose. First, it is installed in such a manner that it will always try to pull the rocking shaft assembly to the left. The altitude diaphragm controls the amount of axial displacement the spring can effect. Second, the hairspring turns the sliding rods while an axial displacement takes place. This rotation, which is approximately 35° for an axial displacement of slightly more than 1 in., reduces the friction in the comparatively large jewels in which the sliding rods are mounted.

The altitude diaphragm *J*, which affects the altitude compensation, consists of two evacuated cells. Its expansion for an altitude change from sea level to 50,000 ft. is 0.320 in. This movement is transmitted through a crank mechanism to rocking shaft *O* on which a sector *P* with a groove at its periphery is mounted. Connection between this part of the mechanism and the rocking shaft *A* is made by an extremely thin beryllium copper ribbon *Q*, which is attached on one end to the hub of the conical hairspring *N* and at the other end to the sector *P* after it is guided through its groove. The expansion of the altitude diaphragm is matched to the crank mechanism motion in such a manner that the resulting movement displaces rocking shaft *A* in the proper amount so as to change the effective lever arm of lever *G* for the required altitude compensation.

Fig. 9 shows a photograph of the delicate assembly of rocking shafts *A* and *B* on a special mounting plate *R*. The position of the various components corresponds approximately to a Mach Number of 1.5 at an altitude of 10,000 ft. The magnesium frame *K*, the rocking shaft *A* with its lever *F* and counterweight, the sliding rods *L* and *M*, and the conical hairspring *N* can easily be recognized. The beryllium copper ribbon *Q*, one end of which is attached to the collet of the hairspring while the other is free, can also be noted. The little brass collet *W* near the jewel bearing of the slide rod *M* has been installed only in order to hold the assembly in this position while being photographed. If it were removed, rocking shaft *A* would be pulled by the hairspring all the way to the left beyond the 50,000-ft. position.

The engagement between levers *F* and *G* is clear on this photograph. Lever *H* shows a slight bend near the rocking shaft *B*. This bend represents the slight change in the lever arrangement between levers *H* and *I*, which improved the friction conditions considerably.

It is important that the slide rod *S*, from which the lever *F* picks up the diaphragm movement, is perfectly parallel to the rocking shaft *A*. For this reason, the slide rod *S* is mounted on a separate frame *T*. The pivots about which this frame turns are inserted in the same mounting plate *R*, in which the pivots and jewels for rocking shafts *A* and *B* are mounted. The frame rocks only over a small angle, so that the lateral displacement of slide rod *S* is small and can be compensated by the calibration of the instrument. The frame is carefully balanced by the counterweight *U*. The locations of the pivots are indicated by the letters *V*. The differential pressure diaphragm *E* engages the slide rod *S* by means of another rod that is resting on it.

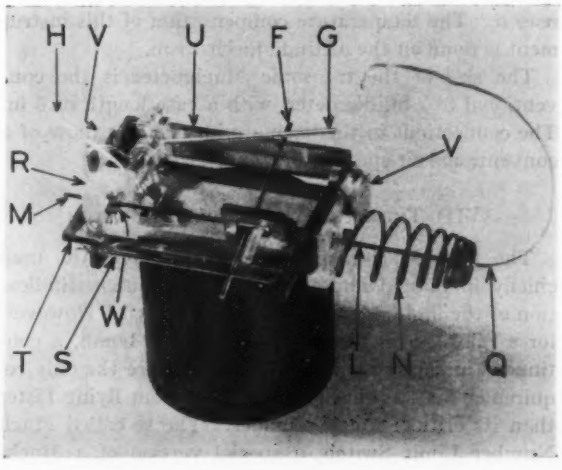

FIG. 9. Slide mechanism of the transonic Machmeter.

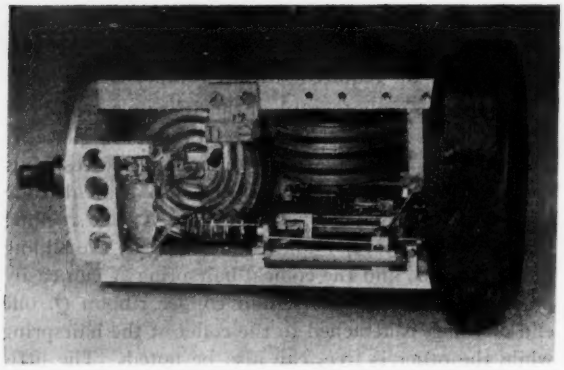

FIG. 10. Side view of the transonic Machmeter with the instrument case partially cut away.

The whole slide mechanism, consisting of rocking shafts A and B and frame T, as seen in Fig. 9, is placed into the mechanism; the proper line-up with the rest of the instrument is secured by two locating pins. This slide mechanism can be seen in place in Fig. 10, which shows a side view of the instrument with most of the case cut away.

The mechanism frame consists of a front plate, a back plate, and three long posts connecting them. On two of the posts the two sets of diaphragms are mounted, while the third carries the slide mechanism. The sector rocking shaft O of the altitude mechanism is mounted in jewels in a special bracket, which can be seen on the left side of the photograph. The odd-shaped part covering most of the sector rocking shaft is the counterweight for the sector and the lever arm. The rocking shaft C is mounted between the front plate and a post, which is inserted into one of the larger posts. The oblique lever arm I of this rocking shaft can be seen in engagement with the lever arm H of rocking shaft B on the right side of the mechanism.

Both diaphragms are weight compensated, so that errors due to acceleration are negligible. Of course, all movable parts are carefully balanced for the same reason. The temperature compensation of this instrument is done on the altitude mechanism.

The size of the transonic Machmeter is the conventional $3^1/_8$-in. diameter, with a case length of 6 in. The connections in the back are identical to those of a conventional air-speed indicator.

(VII) The Mach Number Limit Switch

The two Machmeters described above are used chiefly in piloted aircraft where a continuous indication of the flight Mach Number is required. However, for a pilotless missile, such as the buzz bomb, a continuous indication is not necessary. Here the only requirement is to prevent the missile from flying faster than its critical Mach Number. The so-called Mach Number Limit Switch, a special version of a Machmeter, performs this task. This instrument opens and closes electrical circuits within specific limits that can be set from the outside of its case. So far, there is only a subsonic model of the Mach Number Limit Switch, which is operating in accordance with Eq. (8). If the demand arises, this range can be extended into the supersonic domain.

The instrument contains, as the other Machmeters do, an open differential pressure diaphragm and an altitude diaphragm. Both diaphragms rotate levers to which electrical contacts are attached. At the proper Mach Number settings, these contacts are opened or closed, thereby controlling a servomotor that changes the rate of the fuel supply to the engine.

(VIII) The Mach Airspeed Indicator

A paper on Machmeters would not be complete without a short discussion of its sister instrument, the Maximum Allowable Airspeed or Mach Airspeed Indicator. This instrument, which was developed for operational use, was used extensively during the war on fast fighter aircraft and is now being increasingly adopted in fast-flying commercial transport aircraft.

The Mach Airspeed Indicator is a combination instrument consisting of two entirely different mechanisms, the pointers of which indicate on the same dial. One of these instruments is a conventional air-speed indicator with approximately one revolution of the pointer for the full range. The mechanism of the other instrument, which operates a warning pointer, is actually an altimeter that is calibrated in maximum allowable air speed for a certain Mach Number.

Before installation in a particular aircraft, this Mach mechanism, as it is usually called, is set by means of a screw driver to the highest flight Mach Number at which this type of aircraft can safely be flown. This Mach Number appears in a small window of the dial. The indicated air speed corresponding to the safe Mach Number is then indicated by a warning pointer, which is somewhat wider than the air-speed pointer; the warning pointer is painted either red or in red and yellow stripes. As the aircraft ascends, the warning pointer indicates lower and lower air speeds, because the indicated air speed for a given Mach Number diminishes with altitude, since the value of the speed of sound decreases with increase in altitude.

The mathematical relation between the indicated air speed V_i and the altitude h for a given flight Mach Number M_1 for subsonic speeds follows from the subsequent considerations:

The differential pressure $\Delta p = p_3 - p_1$ for any indicated air speed is a constant, regardless of altitude.

$$\Delta p_h = \Delta p_{SL} \text{ for } V_i = \text{const.} \tag{19}$$

The subscripts designate any altitude and sea level. By substituting Eq. (10) with the appropriate suffixes, Eq. (19) reads, with p_h and p_{SL} as the static

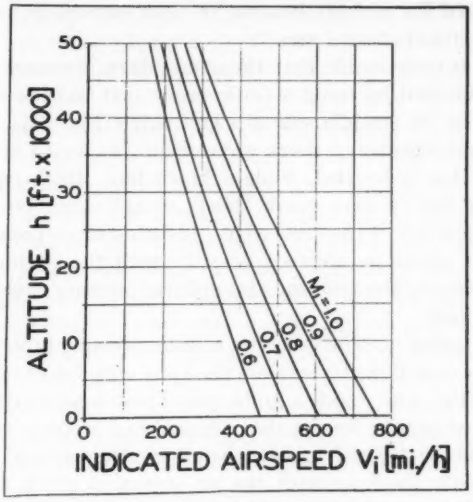

FIG. 11. Diagram of altitude h vs. indicated air speed V_i for various flight Mach Numbers M_1 and $k = 1.40$.

pressures and M_h and M_{SL} as the free-stream Mach Numbers at any altitude and at sea level,

$$p_h \left\{\left[1 + \left(\frac{k-1}{2}\right) M_h^2\right]^{k/(k-1)} - 1\right\} = p_{SL}\left\{\left[1 + \left(\frac{k-1}{2}\right) M_{SL}^2\right]^{k/(k-1)} - 1\right\} \quad (20)$$

Under standard sea-level conditions, the true air speed equals the indicated air speed, so that

$$V_{SL} = V_i \quad (21)$$

Substituting the Mach Number at sea level

$$M_{SL} = (V/c)_{SL} = V_i/c_{SL} \quad (22)$$

in Eq. (20) and solving for the indicated air speed, the following relation is obtained:

$$V_i = \left\{\left(\frac{2}{k-1}\right) c_{SL}^2 \left\{\left[1 + \frac{p_h}{p_{SL}} \times \left[\left(1 + \frac{k-1}{2} M_1^2\right)^{k/(k-1)} - 1\right]\right]^{(k-1)/k} - 1\right\}\right\}^{1/2} \quad (23)$$

This value represents the Maximum Allowable Indicated Airspeed for any one flight Mach Number as a function of the static pressure p_h at any altitude Fig. 11 is a graph showing the relation between indicated air speed V_i and altitude h for various flight Mach Numbers M_1.

The calibration of the air-speed mechanism is in accordance with the well-known relation developed more than a hundred years ago by de Saint-Venant and Wantzel in 1839.

$$= \left\{\frac{2k}{k-1}\frac{p_{SL}}{\rho_{SL}}\left[\left(1 + \frac{\Delta p}{p_{SL}}\right)^{(k-1)/k} - 1\right]\right\}^{1/2} \quad (24)$$

This equation is obtained by setting the right-hand side of Eq. (20) equal to the differential pressure Δp and introducing the indicated air speed V_i by means of Eqs. (22) and (2).

Fig. 12 shows a schematic view of both mechanisms of the Mach Airspeed Indicator. The stagnation or pitot pressure p_2 is led into the open diaphragm, while the static pressure is led into the airtight instrument case. The expansion of the open diaphragm is, therefore, a function of the pressure differential $\Delta p = p_2 - p_1$.

The air-speed mechanism is operated by the open diaphragm A, which rotates the rocking shaft B by means of a crank mechanism. Rocking shaft B in turn, by means of a sector and pinion, rotates the handstaff C, which carries the air-speed pointer D.

The Mach mechanism is operated by a closed evacuated diaphragm E, the expansion of which is a function of the static pressure, which rotates rocking shaft F by means of a sliding lever. The rotation is transmitted from there to rocking shaft G through a pair of right angle levers and then, by means of a sector and pinion, to the handstaff H, which carries the warning pointer I. The change in calibration for the various flight Mach Numbers is accomplished through rotating the shaft J, which carries a cam and which is connected to the subdial K by gears. Rotation of the cam will effect an axial displacement of rocking shaft F, thereby changing the effective length of the lever arm on rocking shaft G.

As an additional feature, the instrument has an adjustable stop L, which may limit the movement of the warning pointer. This feature is of importance at low

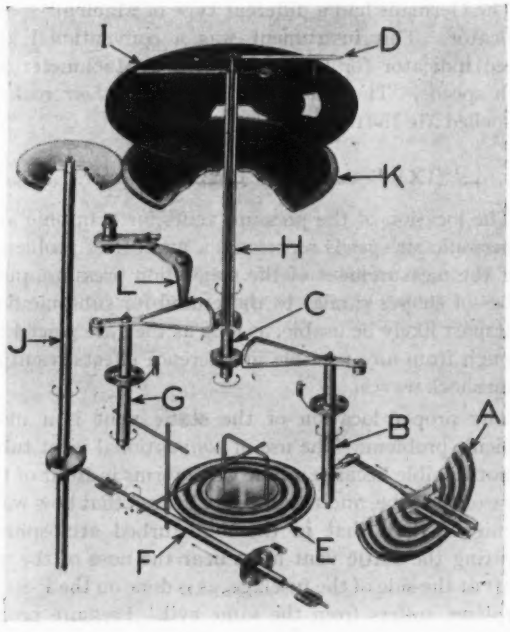

FIG. 12. Schematic diagram of the Mach Airspeed Indicator.

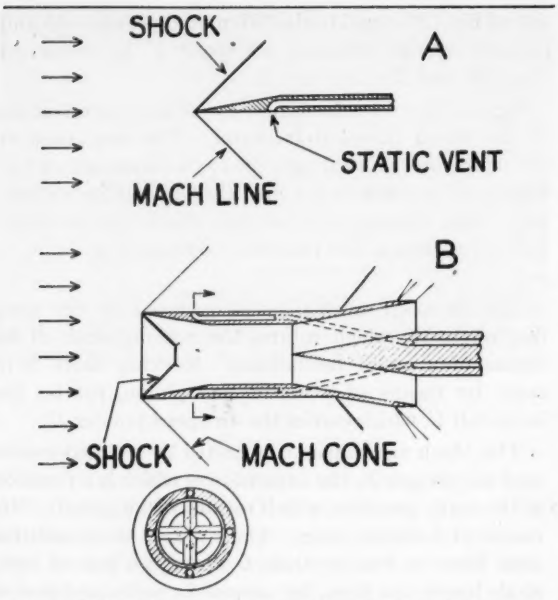

FIG. 13. Schematic diagram of two supersonic static pressure probes.

altitudes, where the placard speed of the aircraft may be lower than the maximum allowable air speed with respect to compressibility dangers.

The Mach Airspeed Indicator is used by the pilot in the same manner as the conventional air-speed indicator. Simultaneously, in addition to the air-speed indication, he can see from the angle formed between the two pointers how near to the dangerous air speed his flying speed is; as long as the two pointers do not cross, he is flying safely.

The Germans had a different type of Mach air-speed indicator. This instrument was a conventional air-speed indicator for low speeds and a Machmeter for high speeds. They probably used it in their rocket-propelled Me 163 fighters.

(IX) Location of Pressure Vents

The location of the pressure vents for transonic and supersonic air speeds represents a number of problems. For the measurement of the stagnation pressure, pitot tubes of shapes similar to those used for subsonic flow will most likely be usable, as long as they are placed far enough from any possible interference effects resulting from shock waves.

The proper location of the static vent is a more difficult problem. The use of conventional pitot tubes is not feasible because a bow wave forms in front of the nose of the tube, and the pressure behind that bow wave is higher than that in the undisturbed atmosphere; locating the static vent holes near the nose of the aircraft at the side of the fuselage, as is done on the P-80 jet airplane, suffers from the same evil. Pressure probes of the type used for wind-tunnel tests may not readily be used for aircraft because of their extremely small diameter of about 1 mm.[10]

It is conceivable that the atmospheric pressure can be obtained by using a static probe that has the vent hole on the straight side of a knife edge (Fig. 13a). In this arrangement a shock wave would be created at the side that is beveled, while a Mach line, which represents only a very weak shock, would occur on the straight side of the knife edge. If such a static pressure sonde could be aligned perfectly with the oncoming air stream, the ambient atmospheric pressure could be obtained.

It seems feasible to design a static pressure probe for supersonic flows by bending the knife edge into a cylinder (Fig. 13b); such a probe would look somewhat like a Venturi tube, except that a number of pressure vents would be located evenly spaced on the outside. If properly lined up with the air stream, a shock wave would form, which would be drawn into the tube opening; on the outside, only a Mach cone would result, the disturbance of which is negligible, so that the ambient atmospheric pressure could be measured. The rim angle would have to be extremely small and the inside diameter of the probe, comparatively large. The static probe could be kept in line with the air stream by servomotors; the differential pressure between the four static vents, which would exist when the probe was not in proper alignment, could control the servomotors.

The location of the static pressure vents somewhere on the fuselage is another possibility for static pressure determination. Locations on the surface of aerodynamic bodies, where the surface pressure is identical with the atmospheric pressure, also exist in supersonic flows. For instance, wind-tunnel measurements of the pressure distribution over the A-4 rocket (V-2) show that for free-stream Mach Numbers from 1.56 to 3.24 there is such a location about 10 m. aft of the nose. Calibration tests up to a Mach Number of 2.0 on actual A-4 rockets in White Sands, N.M., show excellent agreement between the measured values of atmospheric pressure during the rocket ascent and values obtained from balloon sondes at about the same time. Only in the range near Mach Number 1.0 are the values taken by the A-4 rocket somewhat higher than those of the balloon sonde.[15] Such locations where the surface pressure is identical with the atmospheric pressure can probably also be found on aircraft flying at supersonic speeds.

(X) Machmeter Based on Temperature Measurement

The use of temperature as the parameter to operate a Machmeter is possible in principle. The mechanism could be made similar to that of the pressure-operated instrument. The diaphragms would now be connected to temperature bulbs, which would be installed outside the aircraft: one, for measuring the stagnation tem-

perature and the other, for measuring the free-stream temperature. Liquid in the temperature bulbs and the connecting capillaries would be the medium of operation.

From the point of view of instrument design, such a scheme seems perfectly feasible. However, the one difficulty lies in the measuring of the proper values of the stagnation temperature T_3 and the atmospheric temperature T_1 at transonic and supersonic speeds, or at least measuring values that can be corrected in a simple manner. The measurement of these temperatures, however, represents a difficult task because of radiation and convection effects. These are functions of the altitude and the Mach Number, the latter being the parameter to be obtained from the instrument. In a report by Wood,[16] a graph showing equilibrium surface temperatures as a function of free-stream Mach Number for various altitudes indicates that the corrections that would have to be applied to the actually measured temperature values would be extensive. These considerations seem to rule out such Machmeters.

(XI) Conclusions

Machmeters will acquire more and more importance for the steadily increasing flying speeds. Greater range in Mach Number, as well as in altitude, will be needed in the near future. Of these two problems, the increase in altitude range represents the greater difficulty. One glance at Fig. 4 or Table 3 shows the small differential pressures available at 100,000 ft., for example, as compared with those at sea level.

It is likely, that for high-speed aircraft the conventional air-speed indicator will be superseded by the Machmeter. Perhaps a combination instrument, showing indicated air speed for the low-speed range and Mach Number for the high-speed range, might eventually be the best solution for a flight speed instrument.

The location of the static vent is one problem in connection with Machmeters which still seems to require considerable experimental research, particularly at high Mach Numbers.

From the experience gained in developing several Machmeters, it seems certain that, as demands for greater ranges in Mach Number and altitude occur, new Machmeters can be developed to keep step with those requirements.

Table 3

Differential Pressure $\Delta p = p_2 - p_1$ (In. Hg 0°C.) for Various Mach Numbers M_1 and Altitudes h (Ft.)

M_1	h = 0	50,000	100,000	150,000
	p_1 = 29.9212	3.4370	0.3225	0.0444
0.5	5.572	0.640	0.0601	0.0083
1.0	26.718	3.069	0.2880	0.0396
1.5	72.208	8.294	0.7783	0.1071
2.0	138.847	15.949	1.4965	0.2060
2.5	225.191	25.867	2.4272	0.3342
3.0	330.957	38.017	3.5672	0.4911
3.5	456.059	52.387	4.9155	0.6767
4.0	600.461	68.974	6.4720	0.8910

k = 1.400.

References

[1] Warfield, C. N., *Tentative Tables for the Properties of the Upper Atmosphere*, N.A.C.A. T.N. No. 1200.

[2] Bailey, N. P., *The Thermodynamics of Air at High Velocities*, Journal of the Aeronautical Sciences, Vol. 11, No. 3, pp. 227 ff., July, 1944.

[3] Stack, J., *Compressible Flows in Aeronautics*, Journal of the Aeronautical Sciences, Vol. 12, No. 2, pp. 127 ff., April, 1945.

[4] Sauer, R., *Theoretische Einfuehrung in die Gasdynamik;* Julius Springer, Berlin, 1943 (reprinted by J. W. Edwards, Ann Arbor, Mich.).

[5] Friedrichs, K. O., *Fluid Dynamics* (Mimeographed Notes), Brown University, 1941.

[6] Taylor, G. I., and Maccoll, J. W., *The Mechanics of Compressible Fluids, Durand's Aerodynamic Theory, Vol. III, Div. H.;* Julius Springer, Berlin, 1934.

[7] Stack, J., *Some Problems in Compressible Flows for Airplanes*, mimeographed preprint of paper presented before the Society of Automotive Engineers and the Institute of the Aeronautical Sciences, New York, March 20, 1947.

[8] Liepmann, H. W., and Puckett, A. E., *Introduction to the Aerodynamics of Compressible Fluids;* John Wiley & Sons, Inc., New York, 1947.

[9] Applied Mathematics Group, New York University, *Supersonic Flow and Shock Waves*, AMP Report 38.2R.

[10] Ackeret, J., Feldmann, F., and Rott, N., *Investigations of Compression Shocks and Boundary Layers in Gases Moving at High Speed* (Mitteilungen aus dem Institut fuer Aerodynamik an der E.T.H. in Zürich, No. 10), January, 1947; N.A.C.A. T.M. No. 1113.

[11] Rayleigh, Lord, *Aerial Plane Waves of Finite Amplitude*, Proc. Roy. Soc. of London, Series A, Vol. 84, pp. 247 ff., 1910.

[12] Zahm, A. F., *Pressure of Air on Coming to Rest from Various Speeds*, N.A.C.A. T.R. No. 247.

[13] Huber, P. W., *Use of Freon-12 as a Fluid for Aerodynamic Testing*, N.A.C.A. T.N. No. 1024.

[14] Brombacher, W. G., *Altitude-Pressure Tables Based on the United States Standard Atmosphere*, N.A.C.A. Report No. 538.

[15] Best, N. R., *Pressure Measurements from V-2 Rockets*, mimeographed preprint of paper presented before the Institute of the Aeronautical Sciences and the American Meteorological Society Joint Meeting, New York, January 30, 1947.

[16] Wood, G. P., *Calculation of Surface Temperatures in Steady Supersonic Flight*, N.A.C.A., T.N. No. 1114.

An Improved Schlieren Apparatus*

FRANK W. BARRY† AND GILBERT M. EDELMAN†
Massachusetts Institute of Technology

SUMMARY

This paper describes an improved schlieren apparatus that forms two separate images of the test section simultaneously. One image indicates vertical density gradients; the other, horizontal density gradients. The determination of transient density fields is more accurate with this modified schlieren system than with the ordinary schlieren system taking two successive pictures. At present, this apparatus is being used to study the interaction between shock waves and boundary layers.

DISCUSSION

THE SCHLIEREN APPARATUS is an optical instrument that is used in the study of supersonic flow phenomena. With this instrument photographs are taken in which the pattern and intensity of the light and dark areas are a measure of the density gradients in the field of view.

In the usual construction of the schlieren equipment, a single straight knife edge is used, and the resulting picture shows density gradients normal to that knife edge. If density gradients in another direction are desired, the knife edge must be rotated and another picture taken.

The time required to make such an adjustment, and hence the time lag between successive pictures, is not significant when the flow is steady. However, when the flow is not steady and schlieren pictures corresponding to two different knife edge orientations are desired, such pictures should be taken simultaneously to obtain comparable pictures.

A device has been developed at the Gas Turbine Laboratory of the Massachusetts Institute of Technology for this purpose. Two pictures are taken simultaneously on a single negative. One of these

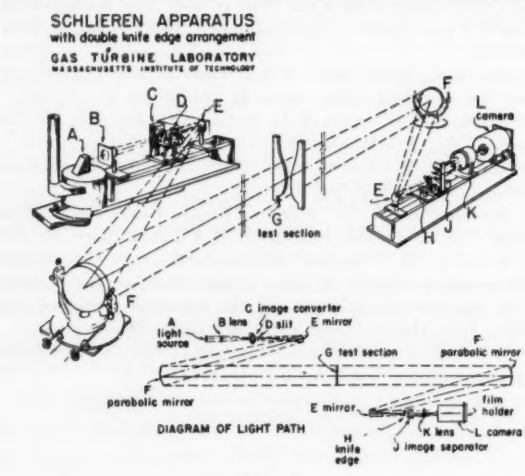

FIG. 1.

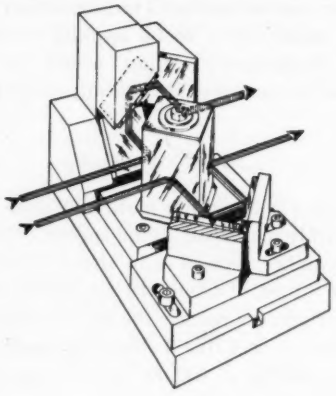

SCHLIEREN LIGHT-SOURCE CONVERTER

FIG. 2.

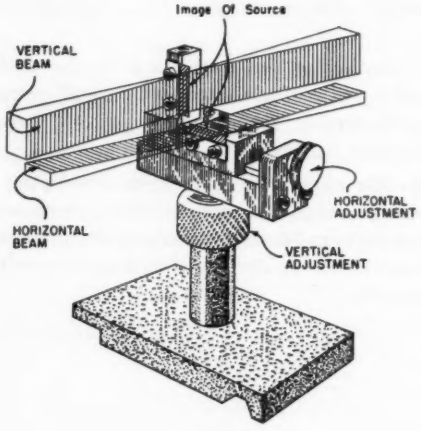

SLIT FOR SCHLIEREN APPARATUS
GAS TURBINE LABORATORY
MASSACHUSETTS INSTITUTE OF TECHNOLOGY

FIG. 3

Received March 12, 1948.

* This work was carried out as part of the Guided Missiles Program at the Massachusetts Institute of Technology and was sponsored by the Navy Department, Bureau of Ordnance.

† Research Assistant, Gas Turbine Laboratory.

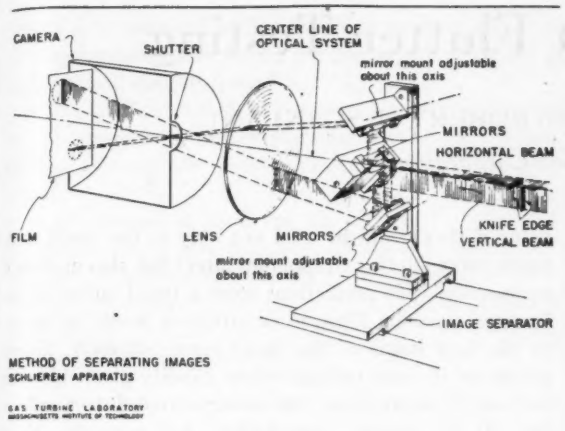

FIG. 4.

FIG. 5.

pictures shows density gradients in a vertical direction; the other shows density gradients in a horizontal direction. In this device the light from a single line source is split by optical means into a horizontal and a vertical beam. Each of these beams passes one of two mutually perpendicular knife edges in the schlieren system and produces the two separate images on the viewing screen or film. Each beam is independent and the effect is such as would be produced by two separate schlieren systems.

Fig. 1 is an illustration of the complete schlieren apparatus with the double knife-edge arrangement. The light source unit is shown on the left and the camera unit on the right. Light from source *A* passes through lens *B* to the light source converter, *C*.

Fig. 2 illustrates the optics of the light source converter, *C*. The flat, converging light beam is split into two parts by an aluminized glass block. One of the two resulting beams emerges without change in either orientation or direction. The other beam emerges without change in direction, but in passing through the mirror system it is rotated through 90°.

Referring to Fig. 1, the slits *D* are placed at the point where the two beams from *C* focus as an L-shaped image of the sources. The light that passes through the slits *D* is reflected by the plane mirror *E* to the parabolic mirror *F*, from which it emerges as a parallel beam composed of the light from both of the beams that emerged from *C*. This parallel beam passes through the test section *G* to a second parabolic mirror and a second plane mirror and forms a second L-shaped image of the sources at the knife edges *H*. The knife edges *H* are similar in construction to the slits *D*, which are detailed in Fig. 3.

From *H*, the two distinct beams pass to the image separator shown in Fig. 4. The image separator increases the distance between the beams and permits the formation of two separate images of the test section *G* on the film by the lens *K*.

Fig. 5 is presented as an example of the photographs which have been taken with this apparatus at an exposure of about 5 microsec. The upper picture shows density gradients normal to the flow, such as exist in the boundary layers, and the lower picture shows density gradients parallel to the flow direction. The flow direction is upwards.

A Note on Flight Flutter Testing

ROBERT ROSENBAUM* AND ROBERT H. SCANLAN†

Republic Aviation Corporation

SUMMARY

An attempt has been made to correlate theoretically calculated decay effects of wing oscillations at subcritical flutter speeds with results obtained during actual flight flutter testing at these speeds. The theory discussed has been found to give reasonably good agreement with the limited number of test data obtained in flight from a single airplane. Conclusions of a general nature are as yet unwarranted, but at least a new point of view is presented which applies to interpretation of both test and theoretical results.

INTRODUCTION

FLUTTER ANALYSTS have been excessively hampered in the progress of their work by a serious lack of practical confirmation of their calculated results. On the other hand, results of flight flutter testing have not been very well supported by theory; flight testing for flutter in aircraft must necessarily occur *below* critical flutter velocities where usual theory does not hold. Flight testing for a condition of flutter is a difficult and possibly dangerous procedure. The typical flight flutter testing that has been done has been aimed merely at predicting the actual flutter speed of the aircraft in question. The procedure is usually to measure and plot some parameter, such as the rate of decay of flutter-type oscillations versus true air speed; this plot is the usual flutter trend or g-V curve. As the rate of decay lessens, it is assumed that a truly harmonic or flutter condition is approached; extrapolation of the trend curve is then used to indicate approximately the velocity at which flutter will occur. Knowledge of the actual flutter speed is, of course, the primary engineering goal of the usual test, but this test has two shortcomings: first, the actual flutter speed may be approached rather abruptly and, hence, not safely; and second, even if approximated by extrapolation of test results, the critical speed represents only a single "test" item to be compared against a single calculated item. Usually insufficient attention is given to a comparison of subcritical oscillatory test items with theory. The trend curve is thus, in a sense, used incorrectly in that the most engineering attention is concentrated not on the test points that *comprise* the curve but on the extrapolated flutter point that is *off* the curve. When, during tests, damped subcritical oscillations of flutter type occur, it would be of extreme practical value if they could be used not only in the usual test trend curve (to be extrapolated later) but also in direct comparison with predictions from a trend curve given by some theory. Thus, more attention would be given to the best items of the trend curve—namely, those points *on* it—and perhaps more validity given also to its least accurate item—the extrapolated flutter velocity. It is entirely conceivable, for example, that extremely small rates of decay can occur in subcritical flutter oscillations which nevertheless occur at velocities far below the critical flutter velocity. The question is: What should be considered a small rate of decay? A single test oscillation showing an apparently small rate of decay at a given air speed might, in itself, be alarming unless placed in its proper position in a trend curve. But hesitancy to complete the trend curve by flying to test velocities beyond this point can be readily understood unless some theory exists to point out the noncritical nature of such a condition.

The aim of this note is to present a simple modification of standard flutter theory, which suggests a possible means of prediction of preflutter decay rates over a considerable range (hence, also a safe range) of air speeds. This theory is supported by some test results that are in reasonably good agreement with it. The ultimate validity of this theory rests on support by many more such test results.

THEORY[1]

The typical flutter stability determinant, evaluated for a given flutter parameter $1/k$ and set equal to zero, results in a polynomial, the complex roots of which have a form like the following:

$$Z = X + iY = (1 + ig)\left(\frac{\omega_\alpha}{\omega}\right)^2$$

where g is the damping coefficient required for flutter at the frequency ω and ω_α is (as taken in this case) the "torsional" natural frequency of the system considered. Thus,

$$X = (\omega_\alpha/\omega)^2$$

and the critical flutter velocity is given by

$$v = b_r\omega_\alpha(1/k)/\sqrt{X}$$

or

$$v(\text{m.p.h.}) = \omega_\alpha(\text{c.p.m.})\left(\frac{b_r}{14}\right)\frac{(1/k)}{\sqrt{X}}$$

Received May 6, 1947. Revised and received February 16, 1948.

* Now, Chief, Dynamics Section, Airframe and Equipment Engineering Division, Civil Aeronautics Administration.

† Now, Associate Professor of Aeronautical Engineering, Rensselaer Polytechnic Institute.

where b_r is some reference semichord (in feet) and $1/k$ is the dimensionless flutter parameter $v/b_r\omega$. Also, g is calculated directly from $g = Y/X$.

Using a given set of $1/k$ values, g is plotted versus v/ω_α to present the flutter characteristics of the airplane in question in the particular flutter mode investigated.

It is assumed in obtaining the above g-V curve that motion of the system is neither damped nor diverging, but simple harmonic. For study of this system *below* the critical flutter speed, the motion must be assumed as damped. In this case the motion will be harmonic $e^{i\omega t}$, modified by a typical damping factor $e^{-\lambda t}$,

$$e^{i\omega t}(e^{-\lambda t}) = e^{i(\omega_1 + i\lambda)t}$$

This is equivalent to assigning a complex value to the flutter frequency:

$$\omega = \omega_1 + i\lambda$$

This is a legitimate procedure provided that the determinant elements themselves are accounted for under this assumption. In the flutter stability determinant each element is a combination of aerodynamic and mechanical terms. For the mechanical terms there is no error involved in assuming ω complex. For the "noncirculatory" aerodynamic terms[2] there is no error in assuming ω complex. However, in the "circulatory" aerodynamic terms there is a function

$$C(k) = F(1/k) + iG(1/k)$$

which is developed expressly on the assumption that the airfoil motion is harmonic (ω is real). For such terms the assumption of a damped oscillatory motion is in error. However, the basic fact that the airfoil *oscillates* (even though damped) assures that the harmonic hypothesis upon which $C(k)$ is calculated is approximated fairly well.

It might be noted that the approximation inherent in the aerodynamic effect of damped oscillations can actually be evaluated.[3-5] However, to retain simplicity the authors have not taken this effect into account. Thus, there results a typical flutter analysis in which the structural damping required for the existence of a flutter condition below the critical flutter speed are used with little or no modification.

In the usual solution of the flutter polynomial the two unknowns chosen are g and ω. The choice of g as one of the unknowns is arbitrary; instead, any one of several physical parameters (e.g., frequency ratio, aileron balance) could be taken as unknown. If now $\omega = \omega_1 + i\lambda$ is allowed to be complex (i.e., the motion is assumed damped), the frequency ω_1 and the rate of decay λ may be chosen as the unknowns. Then the actual value g_a of damping coefficient must be substituted for g. The value of g_a is determined from ground vibration test. The same roots Z of the characteristic flutter stability polynomial will then have the form shown previously with the new values for g and ω:

FIG. 1

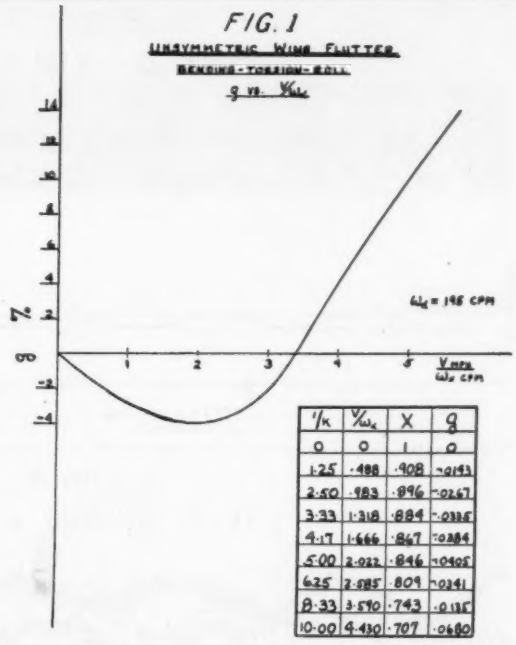

1/k	V/ωα	X	g
0	0	1	0
1·25	·488	·908	-0193
2·50	·983	·896	-0267
3·33	1·318	·884	-0335
4·17	1·666	·867	-0384
5·00	2·022	·846	-0405
6·25	2·585	·809	-0341
8·33	3·570	·743	-0135
10·00	4·430	·707	·0680

$$Z = X + iY = (1 + ig)\left(\frac{\omega_\alpha}{\omega}\right)^2 = (1 + ig_a)\left(\frac{\omega_\alpha}{\omega_1 + i\lambda}\right)^2$$

From this relation

$$\omega_1 + i\lambda = \omega\sqrt{(1 + ig_a/(1 + ig)}$$

$$\cong \omega[(1 + {}^1/_2 ig_a)/(1 + {}^1/_2 ig)]$$

$$\cong \frac{\omega\left[\left(1 + \frac{g_a g}{4}\right) + \frac{i}{2}(g_a - g)\right]}{1 + (g^2/4)}$$

$$\cong \omega[1 + (i/2)\,(g_a - g)]$$

since usually g_a and g are less than 0.1. Thus,

$$\omega_1 = \omega = \omega_\alpha/\sqrt{X}$$

and

FIG. 2

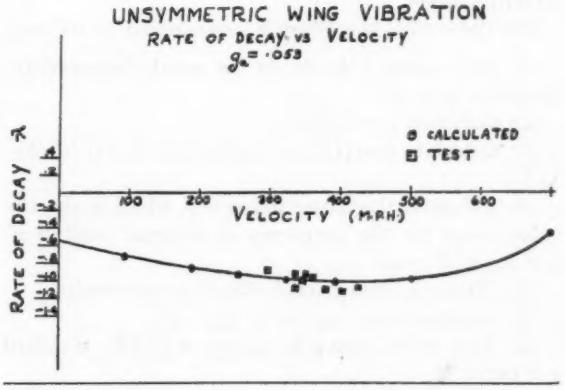

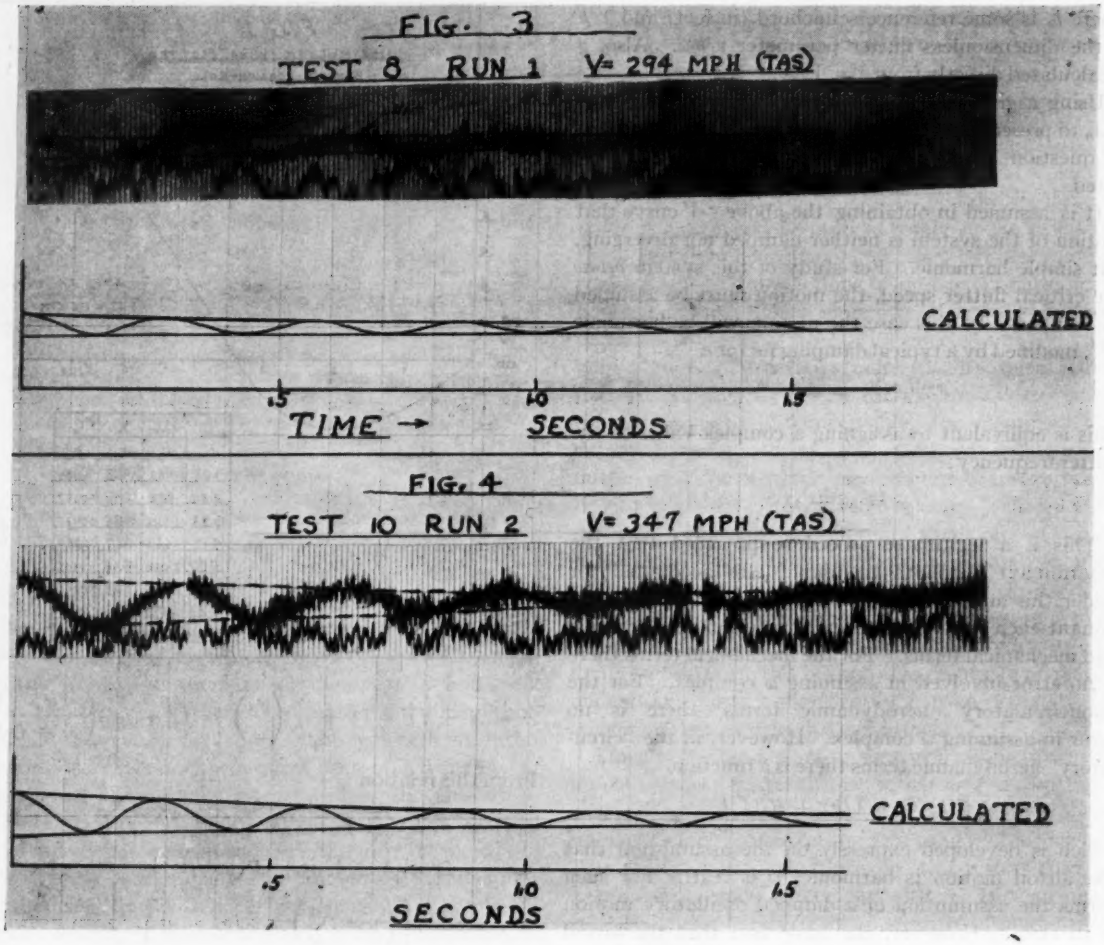

$$\lambda = \frac{\omega}{2}(g_a - g) = \frac{\omega_\alpha}{2\sqrt{X}}(g_a - g)$$

With these approximations there can be predicted the oscillatory frequency ω_1 which should follow a mechanical disturbance of the airfoil at any speed up to the critical flutter speed and the decay exponent λ which is proportional to the logarithmic decrement of the damped oscillatory wave to be expected below the critical flutter speed.

The theoretical procedure is summarized as follows:

(1) For a given $1/k$, obtain the usual characteristic roots $Z = X + iY$.

(2) Calculate $g = Y/X$.

(3) Calculate v(m.p.h.) = ω_α(c.p.m.) $(b_r/14)$ $[(1/k)/\sqrt{X}]$.

(4) Calculate the flutter frequency, which is also the value taken for the frequency of damped oscillation: $\omega = \omega_\alpha/\sqrt{X} = \omega_1$.

(5) Obtain g_a from ground vibration test results.

(6) Calculate $\lambda = (\omega_\alpha/2\sqrt{X})\,(g_a - g)$.

(7) Plot g vs. v(m.p.h.)/ω_α(c.p.m.), the standard g-V curve.

(8) Plot λ vs. v (m.p.h.).

(9) Plot $\pm e^{-\lambda t}$ as the envelope of a sinusoidal wave of frequency ω_1.

Then predicted decay characteristics of the motion of aircraft and wing below its critical flutter velocity can be compared with test results over a range of velocities.

The type of flutter analysis used by the authors in the subsequent example is that outlined in reference 1—namely, a Rayleigh-type analysis based on uncoupled wing vibration modes.

Test

The test procedure is as follows:

(1) Obtain records of the oscillatory characteristics of a given aircraft wing after passage of a forcing impulse at a given true air speed $(v)_{test}$.

(2) Obtain the true oscillatory frequency ω from test records.

(3) Determine $(\lambda)_{test}$ from the logarithmic decrement of the test oscillations, as follows:

$$(\lambda)_{test} = (\omega/2\pi)\,\log_e\,(A_i/A_{i+1})$$

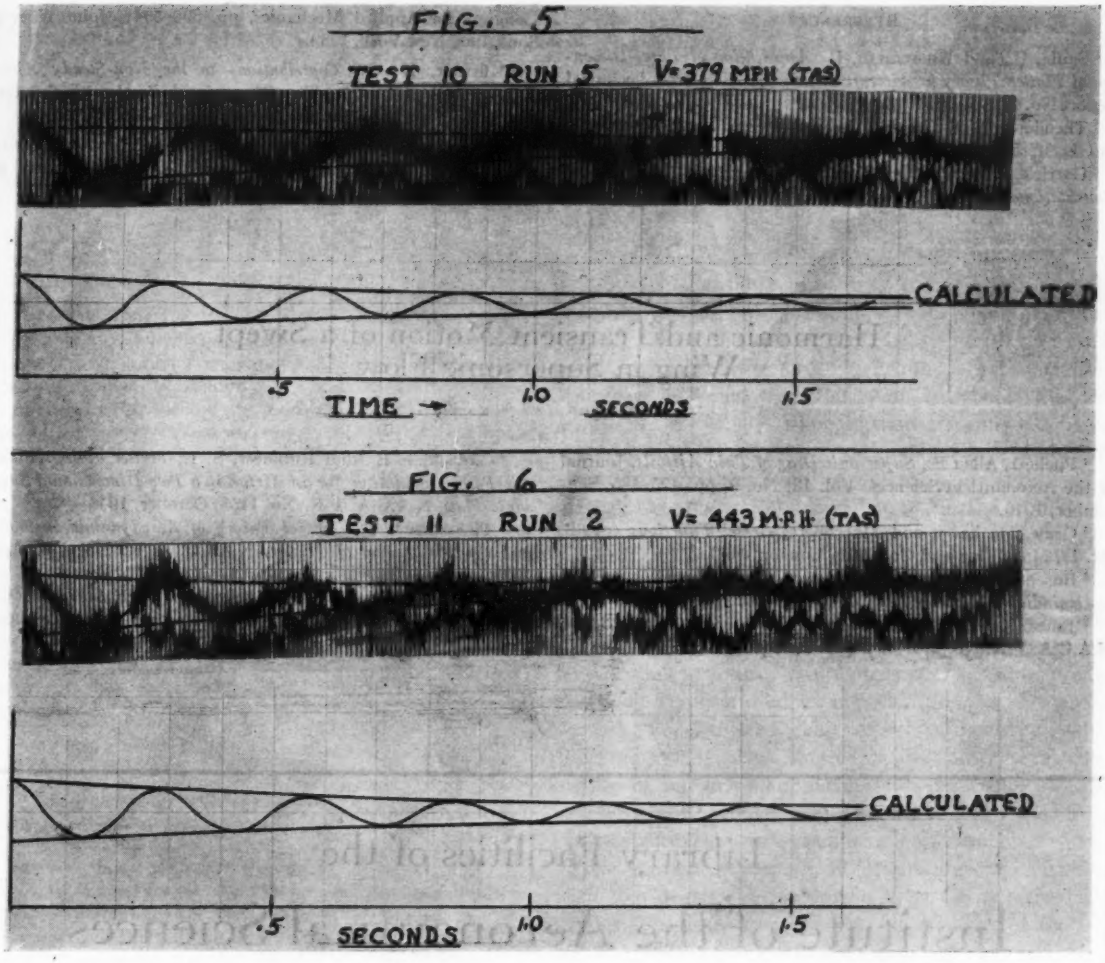

where A_i is the maximum amplitude of the ith wave.

(Test measurements should be made after the forcing impulse has ceased. In the results given in this paper a series of λ values for successive waves of each oscillation were calculated and numerically averaged to obtain a "test value" of λ.)

(4) Plot $(\lambda)_{test}$ versus $(v)_{test}$.

Figs. 1–6 show the results of a series of tests made on a large four-engined aircraft of conventional design at the Republic Aviation Corporation. The flutter mode considered was unsymmetric, involving bending and torsion of the wings and roll of the entire aircraft. During level flight at various speeds the ailerons were abruptly deflected and released, causing unsymmetric oscillations of the wings. The test results were obtained on a recording oscillograph using electromagnetic accelerometer pickups located near the trailing edge of the wing in each outboard nacelle. The decay characteristics of the waves shown in Figs. 3–6 were obtained only for that portion of the motion which was free of the original forcing impulse of the ailerons. The aileron rotation records (not shown) were found to damp out much more rapidly than those of the wing itself. Hence, theoretical prediction of the motion made on the basis of wing bending and torsion and airplane roll (without aileron degree of freedom) was considered adequate for comparison with test.

The above outlined procedure for measuring decrements in flight is not claimed to be new. It has been used in various related manners both in this country and in Germany. It is possible that an oversimplified picture has been drawn without sufficient warning. It is realized that the modes of decay of an aircraft are complicated, even on the ground. They are, of course, dependent on the type of excitation or impulse given the aircraft. Experience indicates that for the case of a multiengined aircraft the unsymmetric flutter mode is usually the most critical one. Thus, in the particular example investigated, the excitation of the unsymmetric critical mode by a throw of the ailerons was feasible. Whether the scheme presented here can be generally used to predict flutter trends remains to be shown by other experimental results of considerable variety.

REFERENCES

[1] Smilg, B., and Wasserman, L., *Application of Three-Dimensional Flutter Theory to Aircraft Structures*, Air Corps Technical Report No. 4798, July, 1942.

[2] Theodorsen, T., *General Theory of Aerodynamic Instability and the Mechanism of Flutter*, N.A.C.A. T.R. No. 496, 1940.

[3] Garrick, I. E., *On Some Fourier Transforms in the Theory of Non-Stationary Flows*, Proceedings of the Fifth International Congress for Applied Mechanics, pp. 590–594; John Wiley & Sons, Inc., New York, 1939.

[4] Küssner, H. G., *Contributions to the Non-Steady Airfoil Theory—Part III. The Two-Dimensional Problem of the Arbitrarily Moving Wing*, Luftfahrtforschung, pp. 355–361, 1940.

[5] Jones, W. P., *Aerodynamic Forces on Wings in Non-Uniform Motion*, British Aeronautics Research Council, August 28, 1945.

Harmonic and Transient Motion of a Swept Wing in Supersonic Flow

(*Continued from page 346*)

[4] Puckett, Allen E., *Supersonic Drag of Thin Airfoils*, Journal of the Aeronautical Sciences, Vol. 13, No. 9, pp. 475–485, September, 1946.

[5] Gray, Mathews, and Macrobert, *Bessel Functions* (p. 62, Ex. 1), Macmillan and Co., Ltd., London, 1931.

[6] Busemann, A., *Aerodynamisches Auftrieb bei Uberschallgeschwindigkeit*, Proc. Volta Congress, 1935.

[7] Jones, Robert T., *Thin Oblique Airfoils at Supersonic Speed*, N.A.C.A. T.N. No. 1107, September, 1946.

[8] Garrick, I. E., and Rubinow, S. I., *Flutter and Oscillating Air-Force Calculations for an Airfoil in a Two-Dimensional Supersonic Flow*, N.A.C.A. T.N. No. 1158, October, 1946.

[9] Theodorsen, T., *General Theory of Aerodynamic Instability and the Mechanism of Flutter*, N.A.C.A. T.R. No. 496, April, 1935.

[10] Possio, Camillo, *L'Azione Aerodinamica Sul Profilo Oscillante in un Fluido Compressibile a Velocita Iposonora*, L'Aerotecnica, Vol. XVIII, Fasc. 4, pp. 441–458, April, 1938.

Library Facilities of the

Institute of the Aeronautical Sciences

To serve Institute members and others in the aeronautical industry, the Institute of the Aeronautical Sciences offers the facilities of:

The W. A. M. Burden Library
2 East 64th Street
New York 21, N.Y.

The facilities of this library are available for reference study at the Institute.

The Paul Kollsman Lending Library
2 East 64th Street
New York 21, N.Y.

This library loans books without charge to members and others in the United States over eighteen years of age. Full information will be sent on request.

The Pacific Aeronautical Library
6715 Hollywood Boulevard
Los Angeles 28, Calif.

This is a service and reference library for West Coast members and organizations. Full information as to its facilities will be sent on request.

Stability of an Oscillating Airfoil in Supersonic Airflow*

M. V. BARTON†
The University of Texas

SUMMARY

The conditions for the determination of the stability of a two-dimensional airfoil oscillating harmonically with two degrees of freedom in a supersonic flow are developed. The stability is expressed in terms of the position of the axis of rotation of the airfoil, the reduced frequency, the Mach Number, the ratio of the amplitudes of the torsional and flexural modes, and the phase angle between the modes and evaluations are made for Mach Numbers ranging from 1.2 to 2.0 and for reduced frequencies from 0.1 to 2.0. The range of reduced frequencies and Mach Numbers for instability of a two degree of freedom system are indicated. It is shown that instability for single degree of freedom torsional motion does not occur at a Mach Number greater than 1.58. The effects of the pivot position on the stability for various phase angles and amplitude ratios of the two modes of motion of the airfoil are discussed.

Tables of aerodynamic parameters for an oscillating airfoil in a supersonic flow are given as a supplement to previously published values.

NOTATION

V	= free-stream velocity (ft. per sec.)
M	= Mach Number
θ	= Mach angle = $\sin^{-1}(1/M)$
ρ	= density of air (slugs per cu.ft.)
α	= angular displacement of airfoil about pivot (rad.)
α_0	= amplitude of α
y	= transverse displacement of pivot (ft.)
y_0	= amplitude of y
c	= chord of airfoil (ft.)
μ	= distance in fraction of chord aft from leading edge to pivot
Ω	= circular frequency of oscillation of airfoil (rad. per sec.)
k	= reduced frequency = $\Omega c/V\cos^2\theta$
$y_0/\alpha_0 c$	= amplitude ratio
ϕ	= phase angle
P_0	= lift force per unit span (lbs. per ft.)
M_0	= aerodynamic moment per unit span about pivot (lbs. ft. per ft.)
$\overline{P}_\alpha$, $M_\alpha{}^*$, M_1, etc.	= aerodynamic parameters

INTRODUCTION

THE DETERMINATION of the air forces on an oscillating airfoil in a supersonic flow is important because of the problem of flutter and aerodynamic instability of high-speed aircraft and supersonic missiles. Several investigators including Possio,[1] Borbely,[2] Miles,[3] and Temple and Jahn[4] determined the air forces on an oscillating airfoil in a two-dimensional supersonic flow by means of a linearized theory. This theory and the method of solution of the equations are fully discussed in the references cited and will not be considered here. Other investigators such as Garrick and Rubinow,[5, 9] Keller, Komm, and Johnson;[6] and Barton and Poindexter,[7] as well as some of those referred to formerly, have made numerical evaluations of the parameters involved. Some of these investigators, along with others, have applied the air-force calculations to the problem of flutter at supersonic speed in which the effect of the structural parameters such as elastic axis position, structural damping, stiffness, and inertia have been considered. This report is concerned with the stability of a two degree of freedom system consisting of an airfoil oscillating torsionally and transversely simultaneously and does not consider the effect of the structural parameters on the motion.

The motion of an airfoil oscillating harmonically with two degrees of freedom can be characterized by the amplitude ratio of the two components of motion and the phase angles between them. In an actual flutter situation the amplitude ratio and phase angle depend on the structural characteristics of the wing as well as the aerodynamic forces. This report does not consider the determination of the amplitude ratios and the amplitude ratios as such; it is only concerned with the stability of the system for specified values of these quantities. Since flutter cannot occur unless the motion is such that the air is supplying energy to the system, then, if the values of reduced frequency and Mach Number for this condition can be determined for specified motions of the airfoil, the limits of the aerodynamic parameters in which flutter occurs can be established. In other words, the regions of the aerodynamic parameters in which flutter can occur can be established in terms of the motion of the airfoil.

The results obtained in this investigation are primarily useful for a better understanding of the phenomenon of supersonic flutter without the introduction of the complications of structural effects. It should be emphasized that the results and methods do not replace the usual type of flutter investigation in which the structural parameters are included, although the results may act as a guide in selecting the range of values

Received December 17, 1947.

* This investigation was undertaken as a part of the research program at the Defense Research Laboratory, under Contract NOrd-9195 with the Bureau of Ordnance of the Navy Department. The author wishes to express his appreciation to the Bureau of Ordnance for support of this work.

† Professor of Aeronautical Engineering, Research Engineer, Defense Research Laboratory.

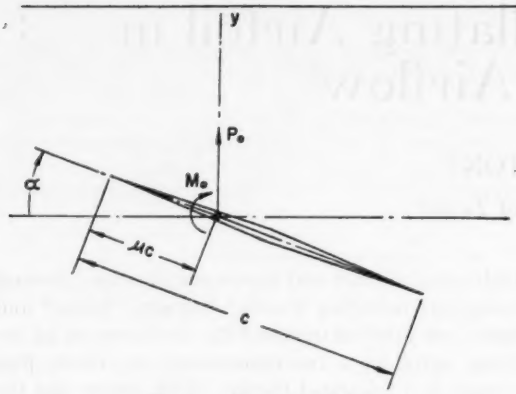

FIG. 1. Forces on airfoil.

of Mach Numbers and reduced frequencies to be considered.

The stability is investigated for Mach Numbers from 1.2 to 2.0 and for reduced frequencies of 0.1 to 2.0.

AERODYNAMIC FORCES

The aerodynamic parameters used here have been evaluated by using the Borbely equations for the air forces on an oscillating airfoil in a supersonic flow. The assumptions and limitations of the theory have been thoroughly discussed in the references cited and will not be considered here except to repeat that the flow is assumed two-dimensional, an infinitely thin airfoil is used, boundary layer and friction effects are neglected, the airfoil performs small oscillations, and the results are not valid for Mach Numbers near unity.

Consider an airfoil as shown in Fig. 1 oscillating harmonically in rotation about a pivot a distance μc behind the leading edge, while simultaneously the pivot is moving harmonically transversely to the undisturbed fluid flow direction. The aerodynamic lift and moment at the pivot per unit length of span are given by

$$\left.\begin{aligned} P_0 &= \rho\Omega^2 c^3\left[(\bar{P}_\alpha + iP_\alpha^*)\alpha + (\bar{P}_y + iP_y^*)\frac{y}{c}\right] \\ M_0 &= \rho\Omega^2 c^4\left[(\bar{M}_\alpha + iM_\alpha^*)\alpha + (\bar{M}_y + iM_y^*)\frac{y}{c}\right] \end{aligned}\right\} \quad (1)$$

The values of the aerodynamic parameters, $\bar{P}_\alpha$, and so on, depend on the pivot position, the Mach Number, and the reduced frequency.

Since the airfoil is assumed to oscillate harmonically, the angular rotation and transverse displacement can be taken as

$$\left.\begin{aligned} \alpha &= \alpha_0 e^{i\Omega t} \\ y &= y_0 e^{i(\Omega t+\phi)} \end{aligned}\right\} \quad (2)$$

STABILITY CRITERION

The work done by the lift and moment per cycle of oscillation is

$$W = \int_0^{2\pi/\Omega} P_0\, dy + \int_0^{2\pi/\Omega} M_0\, d\alpha \quad (3)$$

where $P_0\, dy$ and $M_0\, d\alpha$ are scalar products.

Substituting the values of Eqs. (1) and (2) into (3) gives

$$W = 2\pi\rho\Omega^2 c^4\alpha_0^2\left\{M_\alpha^* + \frac{y_0}{\alpha_0 c}[(\bar{M}_y - \bar{P}_\alpha)\sin\phi + (M_y^* + P_\alpha^*)\cos\phi] + \left(\frac{y_0}{\alpha_0 c}\right)^2 P_y^*\right\} \quad (4)$$

It is apparent that positive work is done and the system is unstable when

$$M_\alpha^* + \frac{y_0}{\alpha_0 c}[(\bar{M}_y - \bar{P}_\alpha)\sin\phi + (M_y^* + P_\alpha^*)\cos\phi] + \left(\frac{y_0}{\alpha_0 c}\right)^2 P_y^* > 0 \quad (5)$$

The system is neutrally stable when the same quantity is zero and it is stable when this quantity is less than zero.

For a single degree of freedom torsional motion, we let $y_0 = 0$ so that only rotation about the pivot is allowed and the condition for torsional instability becomes $M_\alpha^* > 0$.

For the case of single degree of freedom motion in flexure such that $\alpha_0 = 0$, the condition for instability is $P_y^* > 0$. This mode of motion was found stable for all the values of Mach Number and reduced frequency investigated.

It is sometimes convenient to be able to delineate the stable and unstable regions in terms of the Mach Number, reduced frequency, and pivot position, as well as the amplitude ratio and phase angle. This is accomplished by substituting the aerodynamic parameters in terms of μ into the condition for neutral stability. The substitutions to be made are:

$$\left.\begin{aligned} M_\alpha^* &= M_1 + \mu M_2 + \mu^2 P_1 \\ \bar{M}_\alpha &= M_3 + \mu M_4 + \mu^2 P_2 \\ M_y^* &= M_5 + \mu P_1 \\ \bar{M}_y &= M_6 + \mu P_2 \\ P_\alpha^* &= P_3 + \mu P_1 \\ \bar{P}_\alpha &= P_4 + \mu P_2 \\ P_y^* &= P_1 \\ \bar{P}_y &= P_2 \end{aligned}\right\} \quad (6)$$

so that the condition for neutral stability becomes

$$\mu^2 P_1 + \mu\left(M_2 + 2\frac{y_0}{\alpha_0 c}P_1\cos\phi\right) + \left\{M_1 + \frac{y_0}{\alpha_0 c}[(M_6 - P_4)\sin\phi + (M_5 + P_3)\cos\phi] + \left(\frac{y_0}{\alpha_0 c}\right)^2 P_1\right\} = 0 \quad (7)$$

The values for the M's and P's for various reduced frequencies and Mach Numbers are given in Tables 1 through 5. These values are included here as a supple-

TABLE 1

Mach Number 1.2

$\frac{c\Omega}{V}$	k	P_2	P_1	P_4	P_3	M_4	M_4	M_1	M_2	M_3	M_4
0.03056	0.1	−3.4197	−98.506	3,224.95	−62.624	−1,611.4	3,227.4	41.723	−13.41	2.279	49.209
0.06111	0.2	−3.3992	−48.998	802.92	−31.046	−400.34	805.18	20.649	−6.633	2.263	24.414
0.09167	0.3	−3.3664	−32.385	354.43	−20.405	−176.11	356.66	13.534	−4.342	2.236	16.065
0.12222	0.4	−3.3205	−23.997	197.46	−15.003	−97.647	199.66	9.9091	−3.169	2.200	11.832
0.15278	0.5	−3.2626	−18.905	124.86	−11.696	−61.357	127.01	7.6837	−2.45	2.153	9.2476
0.18333	0.6	−3.1927	−15.464	85.442	−9.4409	−41.675	87.540	6.1589	−1.951	2.098	7.4901
0.21389	0.7	−3.1119	−12.969	61.716	−7.7895	−29.833	63.748	5.0382	−1.581	2.0335	6.2090
0.24444	0.8	−3.0211	−11.071	46.351	−6.5171	−22.176	48.311	4.1714	−1.289	1.9614	5.2279
0.27500	0.9	−2.9214	−9.5723	35.847	−5.5007	−16.954	37.731	3.4764	−1.050	1.8822	4.4503
0.30556	1.0	−2.8131	−8.3576	28.369	−4.6668	−13.247	30.166	2.9047	−0.8491	1.7968	3.8147
0.33611	1.1	−2.6978	−7.3529	22.869	−3.9676	−10.530	24.575	2.4238	−0.6745	1.7061	3.2937
0.36667	1.2	−2.5769	−6.5084	18.716	−3.3718	−8.4905	20.327	2.0141	−0.5189	1.6110	2.8527
0.39722	1.3	−2.4511	−5.7902	15.515	−2.8589	−6.9278	17.027	1.6604	−0.3802	1.5125	2.4787
0.42778	1.4	−2.3216	−5.1739	13.004	−2.4121	−5.7115	14.416	1.3544	−0.2527	1.4119	2.1591
0.45833	1.5	−2.1896	−4.6411	11.006	−2.0210	−4.7530	12.315	1.0844	−0.1360	1.3093	1.8851
0.48889	1.6	−2.0564	−4.1786	9.3969	−1.6770	−3.9893	10.604	0.84878	−0.0271	1.2066	1.6497
0.51944	1.7	−1.9229	−3.7761	8.0877	−1.3731	−3.3760	9.1921	0.64191	0.0745	1.1043	1.4475
0.50000	1.8	−1.7904	−3.4246	7.0134	−1.105	−2.8806	8.0168	0.46016	0.1698	1.0034	1.2743
0.58056	1.9	−1.6598	−3.1176	6.1252	−0.8668	−2.4781	7.0300	0.300813	0.2596	0.90468	1.1264
0.61111	2.0	−1.5320	−2.8497	5.3868	−0.6573	−2.1499	6.1957	0.161441	0.3437	0.80898	1.0009

TABLE 2

Mach Number 1.4

$\frac{c\Omega}{V}$	k	P_2	P_1	P_4	P_3	M_3	M_4	M_1	M_2	M_3	M_4
0.04898	0.1	−1.061	−41.622	850.12	−0.841	−424.90	850.83	0.557	19.957	0.70717	20.796
0.09796	0.2	−1.055	−20.730	211.98	−0.380	−105.81	212.69	0.2454	9.959	0.70236	10.339
0.14694	0.3	−1.0453	−13.734	93.818	−0.208	−46.729	94.512	0.128	6.620	0.69446	6.8276
0.19592	0.4	−1.0316	−10.210	52.463	−0.1086	−26.054	53.147	0.0582	4.9444	0.68378	5.0530
0.24490	0.5	−1.0142	−8.0766	33.325	−0.0392	−16.487	33.994	0.0082	3.9352	0.66964	3.9744
0.29388	0.6	−0.99323	−6.6398	22.933	0.016	−11.294	23.586	−0.0314	3.2600	0.65298	3.2445
0.34286	0.7	−0.96896	−5.6019	16.674	0.0610	−8.1677	17.308	−0.0649	2.7758	0.63363	2.7146
0.39184	0.8	−0.94161	−4.8144	12.616	0.1002	−6.1426	13.228	−0.0941	2.4111	0.61187	2.3108
0.44082	0.9	−0.91135	−4.1947	9.8394	0.135	−4.7586	10.427	−0.1202	2.1271	0.58791	1.9919
0.48980	1.0	−0.87855	−3.6936	7.8578	0.167	−3.7727	8.4197	−0.1439	1.900	0.56194	1.7330
0.53878	1.1	−0.84344	−3.2798	6.3969	0.195	−3.0473	6.9311	−0.1653	1.714	0.53422	1.5188
0.58776	1.2	−0.80642	−2.9324	5.2904	0.2217	−2.4994	5.7954	−0.1849	1.560	0.50505	1.3388
0.63673	1.3	−0.76767	−2.6368	4.4337	0.2454	−2.0771	4.9085	−0.2027	1.431	0.47466	1.1857
0.68571	1.4	−0.72761	−2.3825	3.7587	0.2670	−1.7455	4.2022	−0.21880	1.321	0.44337	1.0545
0.73469	1.5	−0.68654	−2.1624	3.2186	0.2864	−1.4814	3.6301	−0.23335	1.228	0.41140	0.94136
0.78367	1.6	−0.64479	−1.9706	2.7803	0.30432	−1.2687	3.1594	−0.24631	1.148	0.37909	0.84340
0.83265	1.7	−0.60277	−1.8025	2.4209	0.32012	−1.0954	2.7677	−0.25778	1.079	0.34666	0.75843
0.88163	1.8	−0.56066	−1.6550	2.1235	0.33435	−0.95318	2.4378	−0.26795	1.0191	0.31441	0.68474
0.93061	1.9	−0.51881	−1.5250	1.8751	0.34674	−0.83548	2.1575	−0.27656	0.96755	0.28256	0.62081
0.97959	2.0	−0.47756	−1.4104	1.6661	0.35752	−0.73751	1.9175	−0.28387	0.92301	0.25141	0.56549

TABLE 3

Mach Number 1.6

$\frac{c\Omega}{V}$	k	P_2	P_1	P_4	P_3	M_3	M_4	M_1	M_2	M_3	M_4
0.06044	0.1	−0.52316	−26.469	438.13	4.5848	−219.01	438.48	−3.0569	17.813	0.34865	13.228
0.12088	0.2	−0.52031	−13.196	109.34	2.3060	−54.608	109.69	−1.5401	8.8904	0.34636	6.5849
0.18131	0.3	−0.51562	−8.7541	48.455	1.5527	−24.164	48.798	−1.0388	5.9104	0.34258	4.3578
0.24175	0.4	−0.50905	−6.5211	27.147	1.1802	−13.511	27.485	−0.79170	4.4153	0.33735	3.2351
0.30219	0.5	−0.50071	−5.1708	17.286	0.96040	−8.5807	17.616	−0.64633	3.5149	0.33072	2.5544
0.36263	0.6	−0.49067	−4.2652	11.930	0.81671	−5.9040	12.253	−0.55149	2.9121	0.32273	2.0955
0.42306	0.7	−0.47904	−3.6117	8.7027	0.71613	−4.2913	9.0163	−0.48567	2.4793	0.31345	1.7632
0.48350	0.8	−0.46587	−3.1171	6.6097	0.64249	−3.2462	6.9127	−0.43751	2.1534	0.30297	1.5109
0.54394	0.9	−0.45131	−2.7286	5.1764	0.58694	−2.5309	5.4678	−0.40149	1.8990	0.29140	1.3121
0.60438	1.0	−0.43546	−2.4152	4.1527	0.54339	−2.0207	4.4316	−0.37344	1.6945	0.27887	1.1511
0.66481	1.1	−0.41847	−2.1565	3.3970	0.50910	−1.6444	3.6623	−0.35129	1.5272	0.26542	1.0181
0.72525	1.2	−0.40042	−1.9397	2.8237	0.48114	−1.3596	3.0748	−0.33347	1.3875	0.25121	0.90638
0.78569	1.3	−0.38156	−1.7552	2.3791	0.45821	−1.1392	2.6156	−0.31887	1.2696	0.23638	0.81136
0.84613	1.4	−0.36197	−1.5966	2.0279	0.43896	−0.96552	2.2489	−0.30666	1.1687	0.22104	0.72978
0.90656	1.5	−0.34180	−1.4590	1.7459	0.42271	−0.82656	1.9512	−0.29635	1.0820	0.20530	0.65924
0.96700	1.6	−0.32122	−1.3388	1.5164	0.40873	−0.71392	1.7057	−0.28750	1.0067	0.18932	0.59793
1.02744	1.7	−0.30037	−1.2333	1.3276	0.39653	−0.62164	1.5007	−0.27973	0.94099	0.17318	0.54446
1.08788	1.8	−0.27939	−1.1403	1.1705	0.38574	−0.54532	1.3276	−0.27283	0.88349	0.15706	0.49775
1.14831	1.9	−0.25845	−1.0580	1.0388	0.37610	−0.48162	1.1799	−0.26657	0.83296	0.14104	0.45687
1.20875	2.0	−0.23766	−0.98504	0.92742	0.36734	−0.42812	1.0527	−0.26084	0.78846	0.12525	0.42113

TABLE 4

Mach Number 1.8

$\frac{c\Omega}{V}$	k	P_2	P_1	P_4	P_3	M_3	M_4	M_1	M_2	M_3	M_4
0.6914	0.1	−0.29773	−19.314	279.47	5.353	−139.71	279.66	−3.5693	15.907	0.19841	9.6530
0.13827	0.2	−0.29615	−9.6345	69.778	2.6829	−34.860	69.975	−1.7897	7.493	0.19714	4.8099
0.20741	0.3	−0.29346	−6.3986	30.949	1.7952	−15.446	31.144	−1.199	4.9835	0.19502	3.1881
0.27654	0.4	−0.28983	−4.7735	17.359	1.3534	−8.6511	17.551	−0.9043	3.7256	0.19211	2.3722
0.34568	0.5	−0.28515	−3.7931	11.069	1.090	−5.5066	11.258	−0.7292	2.9681	0.18834	1.8784
0.41481	0.6	−0.27946	−3.1351	7.6537	0.9151	−3.7991	7.8375	−0.6131	2.4613	0.18385	1.5462
0.48395	0.7	−0.27290	−2.6619	5.5947	0.7915	−2.7701	5.7732	−0.5312	2.0981	0.17860	1.3066
0.55309	0.8	−0.26546	−2.3043	4.2591	0.6943	−2.1028	4.4317	−0.4704	1.8243	0.17268	1.1248
0.62222	0.9	−0.25721	−2.0241	3.3441	0.6287	−1.6459	3.5103	−0.42351	1.6106	0.16614	0.98205
0.69136	1.0	−0.24826	−1.7983	2.6904	0.5725	−1.3197	2.8494	−0.38648	1.4392	0.15902	0.86667
0.76049	1.1	−0.23858	−1.6122	2.2073	0.5269	−1.0789	2.3587	−0.35654	1.298	0.15140	0.77147
0.82963	1.2	−0.22840	−1.4564	1.8405	0.4896	−0.89624	1.9839	−0.33198	1.181	0.14333	0.69160
0.89877	1.3	−0.21759	−1.3238	1.5557	0.45799	−0.75465	1.6906	−0.31124	1.082	0.13485	0.62366
0.96790	1.4	−0.20644	−1.2100	1.3304	0.43142	−0.64283	1.4566	−0.29379	0.9969	0.12609	0.56536
1.03704	1.5	−0.19486	−1.1111	1.1492	0.40839	−0.55311	1.2663	−0.27870	0.9232	0.11705	0.51485
1.10617	1.6	−0.18303	−1.0247	1.0015	0.38841	−0.48016	1.1094	−0.26559	0.85927	0.10784	0.47086
1.17531	1.7	−0.17102	−0.94873	0.87971	0.37088	−0.42016	0.97823	−0.25410	0.80322	0.09851	0.43235
1.24444	1.8	−0.15889	−0.88157	0.77814	0.35534	−0.37030	0.86731	−0.24387	0.75391	0.08917	0.39858
1.31358	1.9	−0.14675	−0.82198	0.69267	0.34144	−0.32853	0.77252	−0.23473	0.71031	0.07984	0.36887
1.38272	2.0	−0.13463	−0.76896	0.62015	0.32894	−0.29324	0.69076	−0.22645	0.67166	0.07061	0.34272

TABLE 5
Mach Number 2.0

$\frac{c\Omega}{V}$	k	P_3	P_2	P_4	P_5	M_3	M_4	M_2	M_5	M_6	M_1
0.07500	0.1	−0.19210	−15.386	205.22	5.1330	−102.59	205.35	−3.4226	12.824	0.12802	7.6905
0.15000	0.2	−0.19109	−7.6788	51.256	2.5705	−25.612	51.383	−1.7143	6.4050	0.12720	3.8345
0.22500	0.3	−0.18939	−5.1033	22.745	1.7169	−11.357	22.871	−1.1455	4.2615	0.12585	2.5445
0.30000	0.4	−0.18706	−3.8111	12.766	1.2914	−6.3675	12.891	−0.86202	3.1875	0.12398	1.8961
0.37500	0.5	−0.18408	−3.0322	8.1486	1.0369	−4.0587	8.2702	−0.69277	2.5414	0.12159	1.5045
0.45000	0.6	−0.18047	−2.5103	5.6402	0.86786	−2.8048	5.7590	−0.58023	2.1093	0.11873	1.2414
0.52500	0.7	−0.17629	−2.1353	4.1281	0.74769	−2.0489	4.2434	−0.50040	1.7996	0.11540	1.0519
0.60000	0.8	−0.17154	−1.8523	3.1470	0.65792	−1.5587	3.2587	−0.44085	1.5664	0.11161	0.90847
0.67500	0.9	−0.16625	−1.6308	2.4748	0.58856	−1.2228	2.5821	−0.39473	1.3845	0.10742	0.79595
0.75000	1.0	−0.16050	−1.4525	1.9943	0.53326	−0.98294	2.0971	−0.35808	1.2384	0.10285	0.70516
0.82500	1.1	−0.15431	−1.3057	1.6390	0.48830	−0.80570	1.7369	−0.32835	1.1187	0.097953	0.63037
0.90000	1.2	−0.14773	−1.1829	1.3694	0.45106	−0.67124	1.4621	−0.30370	1.0188	0.092769	0.56767
0.97570	1.3	−0.14079	−1.0785	1.1597	0.41971	−0.56682	1.2470	−0.28297	0.93404	0.087307	0.51437
1.05000	1.4	−0.13360	−0.98886	0.99370	0.39300	−0.48428	1.0754	−0.26533	0.86158	0.08166	0.46861
1.12500	1.5	−0.12615	−0.91104	0.86012	0.36993	−0.41792	0.93594	−0.25010	0.79887	0.075818	0.42894
1.20000	1.6	−0.11848	−0.84294	0.75109	0.34985	−0.36388	0.82093	−0.23683	0.74420	0.069848	0.39435
1.27500	1.7	−0.11069	−0.78300	0.66102	0.33217	−0.31933	0.72482	−0.22514	0.69619	0.063797	0.36402
1.35000	1.8	−0.10281	−0.72997	0.58583	0.31648	−0.28223	0.64354	−0.21479	0.65381	0.057712	0.33733
1.42500	1.9	−0.09489	−0.68281	0.52244	0.30249	−0.25103	0.57406	−0.20550	0.61623	0.051615	0.31374
1.50000	2.0	−0.08700	−0.64077	0.46861	0.28988	−0.22462	0.51419	−0.19718	0.58278	0.045576	0.29290

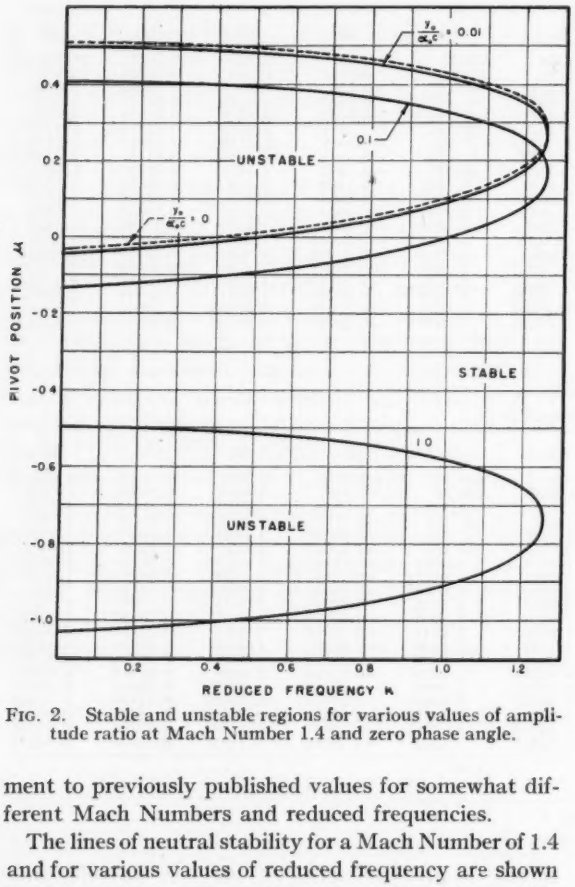

FIG. 2. Stable and unstable regions for various values of amplitude ratio at Mach Number 1.4 and zero phase angle.

ment to previously published values for somewhat different Mach Numbers and reduced frequencies.

The lines of neutral stability for a Mach Number of 1.4 and for various values of reduced frequency are shown in Figs. 2 and 3. Fig. 2 shows the stable and unstable regions in terms of the reduced frequency and pivot position for various values of the amplitude ratio and for zero phase angle. The dashed-line curve is for $y_0/\alpha_0 c = 0$, and it therefore corresponds to the single degree of freedom torsion case. It is evident that torsional instability can occur at this Mach Number for pivot positions ranging from slightly ahead of the leading edge of the wing to slightly behind the mid-chord. Increasing the magnitude of the amplitude ratio does not change the size or the shape of the unstable region but merely moves the range of pivot positions forward so that for an amplitude ratio of unity, the unstable region extends for a range of pivot positions of about one-half to a full chord ahead of the wing. It should also be noticed that the maximum value of the reduced frequency for which instability can occur does not change with the amplitude ratio for this particular phase angle and Mach Number. If the phase angle were 180° instead of zero, then a similar set of curves would result except that they would be displaced *aft* of the leading edge of the wing as the amplitude ratio is increased.

A similar set of curves for a phase angle of 270° and a Mach Number of 1.4 is shown in Fig. 3. In this case

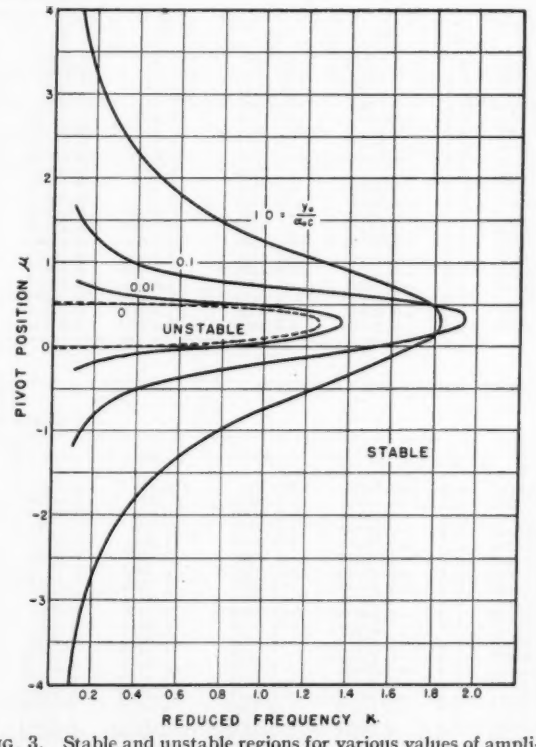

FIG. 3. Stable and unstable regions for various values of amplitude ratio at Mach Number 1.4 and 270° phase angle.

the curves separating the stable and unstable regions change size and shape with changing amplitude ratio. The unstable regions cover a large range of pivot positions for small values of the reduced frequency, and in general this range increases with an increase of amplitude ratio. The maximum value of the reduced frequency for which instability can occur is greater for every nonzero value of $y_0/\alpha_0 c$ investigated than for the case of torsional oscillations for which $y_0/\alpha_0 c = 0$.

The regions of instability for a phase angle of 90° and a Mach Number of 1.4 are of little interest. In fact, instability only occurs for extremely small values of the amplitude ratio and then the range of pivot positions is well within the limits determined for the other phase angles previously discussed.

Limiting Values of Reduced Frequency for Instability

The curves of Figs. 2 and 3 indicate that for a given Mach Number and amplitude ratio there are limits to the values the reduced frequency can have for instability regardless of the pivot position. These limiting values of the reduced frequency for a specified airfoil motion and Mach Number can be determined by making the discriminant of Eq. (7) equal to zero. Since the condition for neutral stability is a quadratic in μ, only real roots are obtained when the discriminant is positive. The values of the reduced frequency required to make the discriminant zero corresponds to the limiting high and low values of the reduced frequency for neutral stability.

The value of the discriminant, D, of Eq. (7) is

$$D = M_2^2 - 4M_1P_1 + 4\frac{y_0}{\alpha_0 c}P_1[(M_2 - M_5 - P_3)\cos\phi - (M_6 - P_4)\sin\phi] - 4\left(\frac{y_0}{\alpha_0 c}\right)^2 P_1^2 \sin^2\phi$$

It can be shown that

$$M_2 - M_5 - P_3 = 0$$

so that

$$D = M_2^2 - 4M_1P_1 - 4\frac{y_0}{\alpha_0 c}P_1(M_6 - P_4)\sin\phi - 4\left(\frac{y_0}{\alpha_0 c}\right)^2 P_1^2 \sin^2\phi \quad (8)$$

The values of the reduced frequencies necessary to make the discriminant zero for various values of amplitude ratios, phase angles, and Mach Numbers are shown in Figs. 4 and 5.

In Fig. 4 the values of k for neutral stability are plotted radially and the values of the phase angles are plotted angularly for various values of the amplitude ratio and for a Mach Number of 1.4. The dashed-line circle corresponds to the maximum value of the reduced frequency for which single degree of freedom torsional

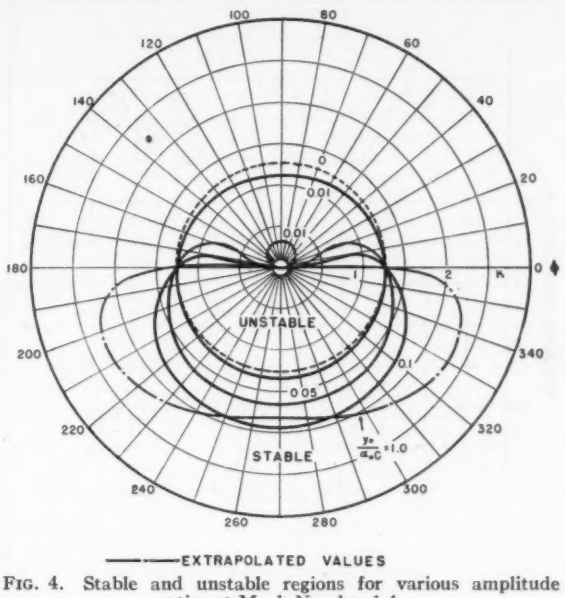

Fig. 4. Stable and unstable regions for various amplitude ratios at Mach Number 1.4.

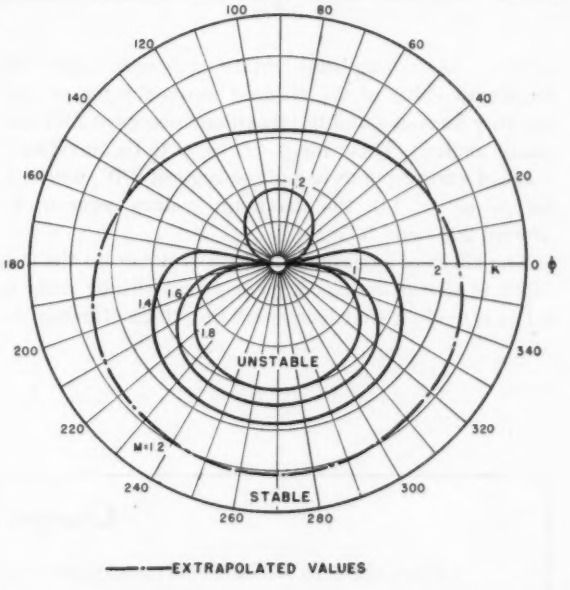

Fig. 5. Stable and unstable regions for various Mach Numbers and for an amplitude ratio of 0.1.

instability can occur. It is interesting to note that for an extremely small transverse motion such that $y_0/\alpha_0 c = 0.01$, the maximum value of k corresponding to instability does not differ much from the torsional case. However, when there is a slight transverse motion combined with the rotation, there is a minimum value of k below which instability cannot occur. These lower values of k for neutral stability are indicated by the small loop for values of phase angle in the neighborhood

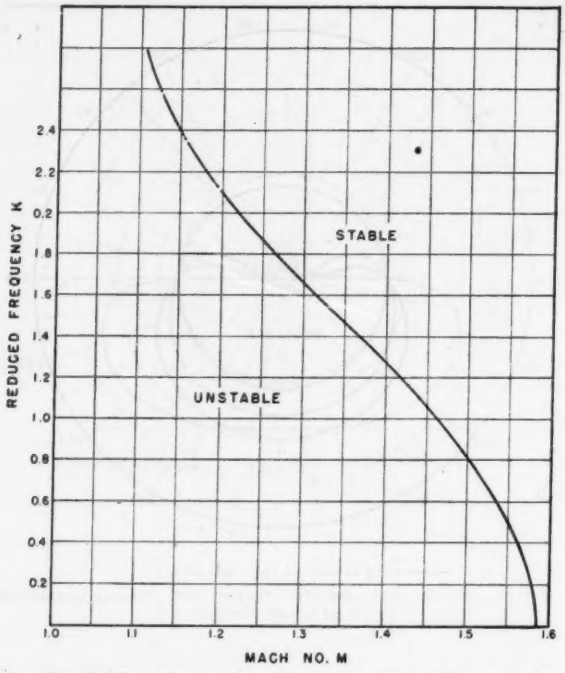

FIG. 6. Stable and unstable regions for a torsionally oscillating airfoil.

of 90°. As the amplitude ratio increases in value, the maximum value of the reduced frequency for neutral stability increases and the maximum occurs at different phase angles. Thus, for $y_0/\alpha_0 c = 0.1$, the maximum value of k corresponds to a phase angle of 270°, whereas, for $y_0/\alpha_0 c = 1.0$, the maximum values seem to be around 205° and 335°.

The effect of variation of Mach Number on the stability is shown in Fig. 5. For an amplitude ratio of 0.1 it is evident that increasing the Mach Number decreases the values of the reduced frequency for which instability can occur.

The values of the reduced frequency and Mach Number for unstable flow in the special case of only torsional oscillations is shown in Fig. 6. It should be noted that for this single degree of freedom motion, instability cannot occur at a Mach Number of over 1.58. As the Mach Number is decreased from this value, the range of reduced frequencies for instability of the system increases.

REFERENCES

[1] Possio, C., *L'azione Aerodinamica sul Profilio Oscillante alle Velocita Ultrasonic*, Acta. Pont. Acad. Sci., Vol. I, No. 11, pp. 93–105, 1937.

[2] V. Borbely, S., *Aerodynamic Forces on a Harmonically Oscillating Wing at Supersonic Velocity*, R.T.P. Translation No. 2019, British Ministry of Aircraft Production (from Z. Angew. Math. Mech., Vol. 22, No. 4, pp. 190–205, August, 1947).

[3] Miles, J. W., *The Aerodynamic Forces on an Oscillating Airfoil at Supersonic Speeds*, Journal of the Aeronautical Sciences, Vol. 14, No. 6, pp. 351–358, June, 1947.

[4] Temple, G. F., and Jahn, J. A., *Flutter at Supersonic Speeds*, Royal Aircraft Establishment Report No. SME 3314, April, 1945.

[5] Garrick, I. E., and Rubinow, S. T., *Flutter and Oscillating Air-Force Calculations for an Airfoil in a Two-Dimensional Supersonic Flow*, N.A.C.A. T.N. No. 1158, October 19, 1946.

[6] Keller, I. G., Komm, H., and Johnson, S., Curtiss-Wright Report, R46-1 February, 1946 (classified).

[7] Barton, M. V., and Poindexter, A. M., *Values of Some Aerodynamic Parameters Useful for Supersonic Flutter Studies*, University of Texas Defense Research Laboratory, Report 125, CF-720, July, 1947.

[8] Barton, M. V., *Stability of Supersonic Airflow on an Oscillating Airfoil*, University of Texas Defense Research Laboratory, Report 127, CF-753, August, 1947.

[9] Garrick, I. E., and Rubinow, S. I., *Theoretical Study of Air Forces on an Oscillating or Steady Thin Wing in a Supersonic Main Stream*, N.A.C.A. T.N. No. 1383, July, 1947.

Changes of Address

Since the Post Office Department does not as a rule forward magazines to forwarding addresses, it is important that the Institute be notified of changes in address 30 days in advance of publishing date to ensure receipt of every issue of the JOURNAL and REVIEW.

Notices should be sent directly to:

Institute of the Aeronautical Sciences, Inc.
2 East 64th Street, New York 21, New York